SECOND LAW ANALYSIS FOR HYDROMAGNETIC THIRD GRADE FLUID FLOW WITH VARIABLE PROPERTIES

by

KGOMOTSHWANA FRANS THOSAGO

THESIS
Submitted in fulfilment of the requirements for the degree of

Doctor of Philosophy

in

Applied Mathematics

in the

FACULTY OF SCIENCE AND AGRICULTURE
(School of Mathematical and Computer Science)

at the

UNIVERSITY OF LIMPOPO

Supervisor: Dr. L Rundora

Co-supervisor: Prof. SO Adesanya
(Redeemer's University, Ede, Nigeria)

2022

Declaration

I declare that the thesis hereby submitted to the University of Limpopo, for the degree of Doctor of Philosophy in Applied Mathematics has not previously been submitted by me for a degree at this or any other university; that it is my work in design and in execution, and that all material contained herein has been duly acknowledged.

Thosago KF

April 22, 2022

Date

Acknowledgements

First and foremost, I want to express my gratefulness to the Almighty God, the most merciful, caring to mankind, for enabling me to complete the work successfully.

To my supervisors Dr. Lazarus Rundora and Prof. Samuel Adesanya, I am grateful for your support and guidance throughout this project. Thank you so much for sharpening my future with evidently open and keen hearts. Through your guidance, I have learnt the research methods used in the application of mathematics in fluid flow. Your efforts in making me an independent mathematician are greatly appreciated. I also extend my appreciation to all the staff members in the Faculty for their competent guidance and advice through the administrative corridors of the university.

I would also like to thank my family for their encouragement, support and love. I am especially grateful to and for my children, who make my life full and beautiful. Above all, I wish to thank my wife. You have truly been a pillar of strength for me. I appreciate all that you do and could never thank you enough. Also, special thanks to my loving siblings, brothers, sisters and father in-law, who were of great support in deliberating over our problems and findings, as well as providing a happy distraction to rest my mind outside of my research.

Finally, I would like to thank my employer, the University of Limpopo, for funding my studies.

Dedication

The thesis dedication goes to the Lord of lords, Almighty God. And to my beloved late mother - Louisa Masekwati Raesebi Thosago who has been a great source of motivation and inspiration.

Abstract

The world is under threat from the devastating effects of the continued depletion of the Ozone layer. Increased global warming is causing catastrophic ecological damage and imbalance due to accelerated melting of glaciers, rampant runaway veld fires, widespread floods and other extreme events. The delegates to the Cop26 Climate Change Summit were reminded that the continued burning of fossil fuels is releasing carbon into the atmosphere at an unprecedented pace and scale and that the world is already in trouble. Complete substitution of fossil fuels with clean energy sources is the only solution through which the world can be saved from the deleterious effects of global warming. However, total dependence on renewable energy sources can only be possible through novel technology that enables efficient energy utilization and conservation. For instance, the evolution of advanced techniques in manufacturing processes has led to the reduction in the size of various industrial and engineering designs that consume reduced amounts of energy. Efficient energy utilization in thermo-fluid flow systems can be achieved through entropy generation minimization. Entropy is a thermodynamic quantity that represents the unavailability of a system's thermal energy for conversion into mechanical work.

In this study, thermodynamic analysis of reactive variable properties third-grade fluid flow in channels with varied geometries and subjected

to different physical effects was investigated with the second law of thermodynamics as the area of focus. Entropy generation and inherent irreversibility analysis were the main focus of the study where the sensitivities of these quantities to the embedded parameters were numerically and graphically described and analysed. The semi-analytic Adomian decomposition method, the semi-implicit finite difference scheme and the spectral quasilinearisation method were employed to solve the nonlinear differential equations modelling the flow systems. The results reveal that the effects of the parameters on flow velocity, fluid temperature, entropy generation and inherent irreversibility cannot be neglected. In particular, conditions for entropy generation minimization were successfully established and documented.

Contents

List of Figures

List of Tables

Nomenclature

β_3	third grade material coefficient
μ_0	dynamic viscosity at some reference temperature
b	viscosity variation parameter
B_o	uniform transverse magnetic field
Br	Brinkman number
C_0	reactant species initial concentration
Da	Darcy number
g	gravitational acceleration
Gr	Grashof number
K	permeability of the medium
k	thermal conductivity
l	Plancks number
Ns	dimensionless entropy generation

R the universal gas constant

T fluid temperature

t time

u fluid velocity

Be Bejan number

G pressure gradient

P fluid pressure

Q heat of the reaction

R universal gas constant

Greek Symbols

ϵ activation energy parameter

μ dynamic viscosity

ν kinematic viscosity

ρ fluid density

τ shear stress of the fluid

θ dimensionless fluid temperature

List of Publications

1. Thosago Kgomotshwana Frans, Lazarus Rundora, and Samuel Olumide Adesanya. "Thermodynamic Analysis of Magnetohydrodynamic Third Grade Fluid Flow with Variable Properties." International Journal of Engineering Research in Africa, vol. 55, pp. 28-46, 2021.

2. Thosago KF, Rundora L, and Adesanya SO."Entropy Generation Analysis in a Steady Flow of a Reactive Variable Viscosity Third Grade Fluid Through a Porous Saturated Medium with Navier-Slip and Convective Boundary Conditions" − In review - Entropy

3. Thosago KF, Rundora L, and Adesanya SO. "Inherent irreversibility analysis of an unsteady reactive hydromagnetic third grade fluid flow in a vertical channel through a porous medium with asymmetrical" convective cooling" − to be submitted

List of conferences

1. 2021: 11^{th} University of Limpopo Faculty of Science and Agriculture Postgraduate Research Conference, Bolivia Logde − "Entropy Generation Analysis in a Steady Flow of a Reactive Variable Viscosity Third Grade Fluid Through a Porous Saturated Medium with Navier-Slip and Convective Boundary Conditions."

2. 2019: 12^{th} Annual Workshop and Conference on Computational Mathematics (WOCCOM2019), UKZN −"Thermodynamic Analysis of Magnetohydrodynamic Third Grade Fluid Flow with Variable Properties"

3. 2019: 10^{th} University of Limpopo Faculty of Science and Agriculture Post-

graduate Research Conference, The Ranch Hotel – "Thermodynamic Analysis of Magnetohydrodynamic Third Grade Fluid Flow with Variable Properties"

Chapter 1

Introduction and Basic Concepts

Chapter Abstract

In this chapter, we outline the basic concepts, important definitions applicable to the study and other preliminary information. The problem statement, the aim and objectives of the study as well as the research methodology and analytical procedures are also presented in this chapter. The chapter is concluded with an outline of the structure of the thesis.

1.1 General Introduction

Fluid mechanics is concerned with understanding, predicting, and controlling the behaviour of a fluid. It deals with the study of fluids either in motion (fluid dynamics and kinematics) or at rest (fluid statics) and the subsequent effects of the fluids upon the boundaries which may be either solid surfaces or interfaces with other fluids [9]. Fluid mechanics has a wide range of applications in mechanical and chemical engineering, biological systems, and astrophysics. Fluid mechanics plays a vital role in the human body. The heart is constantly pumping blood

to and from all parts of the human body through the arteries and veins, and the lungs are the sites of airflow in alternating directions. Fluid statics embraces the study of the conditions under which fluids are at rest in stable equilibrium and is contrasted with fluid dynamics, the study of fluids flow. Fluid kinematics deals with fluids in motion, particularly the space−time relations of velocities and accelerations without considering forces associated with them.

A fluid is a substance that continually deforms (flows) under applied shear stress regardless of the magnitude of the applied stress. In contrast, a solid can resist an applied force by static deformation. Deformation is caused by shearing forces − forces that act tangentially to the surfaces to which they are applied [10].

Fluid dynamics is vital to almost all sciences and engineering and touches every aspect of human daily life. Fluid dynamics impact, in a single way or another on defence, transportation, manufacturing, environment, medicine, and energy, among others. It is also used to predict the aerodynamic behaviour of moving vehicles, the movement of biological fluids in the human body, cooling of electronic components, and performance of micro−fluidic devices. Weather predictions are also based on fluid dynamics. Due to the complexity of the field and the broadness of its applications, fluid dynamics has proven to be a highly exciting and challenging subject of modem sciences. The goal for a deeper understanding of the subject has not only inspired the development of the field itself but has also put forward the progress in the supporting areas, like, applied mathematics, numerical computing and experimental techniques [11]. Several technical and scientific applications include heating and flow control in metal processing, power generation from two-phase mixtures or seeded high-temperature gases, magnetic confinement of high-temperature plasmas and dynamos that create magnetic fields in planetary bodies [12].

Various terms have been used in reference to the broad field of electromagnetic effects in conducting fluids. Commonly used terms include magneto−fluid−mechanics, magneto−gas−dynamics, and magnetohydrodynamics (MHD). MHD devices have been in use since the early part of the 20th century. For instance, an MHD pump prototype was built as early as 1907 [13]. Heat transfer fluids such as mineral oils, water, and ethylene glycol play a significant role in numerous industrial sectors including power generation, chemical production, transportation, microelectronics, and air conditioning [14; 15; 16; 17]. Due to unresolved high demands of modern technology for process intensification and device miniaturization, new types of fluids that are more effective in terms of heat exchange performance are of more importance to be introduced.

Viscosity is the term that describes the degree of the resistance of the fluid to shear stress. There are different categories of fluids depending on properties and also the behavior within the same atmospheric conditions. These are as follows:

- Newtonian fluid - any fluid that obeys Newton's law of viscosity.
- Non-Newtonian fluid - any fluid that does not obey Newton's law of viscosity.
- Real fluids - all fluids that have viscosity.
- Ideal fluid - an imaginary fluid that is assumed to have no viscosity.

In this study, the fluid of importance is the third-grade fluid which is belongs to the class on non-Newtonian fluids.

1.1.1 Newtonian Fluid

A Newtonian fluid is best described as a fluid that exhibits a linear relationship between the shear stress and the shear rate, that is, the shear stress between

adjacent fluid layers is directly proportional to the value of the velocity gradient between two layers at constant pressure and temperature [18].
The relationship is described by

$$\tau = \mu \frac{du}{dy}, \tag{1.1}$$

where τ is shear stress and μ is fluid viscosity. Newtonian fluids are widely employed in many natural and industrial applications [19; 20; 21]. Some classic samples of fluids that show Newtonian characteristics include water, alcohol, and gasoline [22; 23].

1.1.2 Non-Newtonian Fluid

Non-Newtonian fluids exhibit a nonlinear relationship between the shear stress and the shear rate, as shown in Fig.1.1[1]. This type of fluid is more complex than the Newtonian fluid. No one relation exist that can predict the characteristics of all the non-Newtonian materials. Non-Newtonian Rheology is complex. Some classical examples of non-Newtonian fluids include biological fluids (blood, synovial fluids, saliva), dairy products (ice cream, cheese, yoghurt), pharmaceutical products, foodstuffs (sauces, marmalades, jam), etc. Depending on the complexity and the kind of constitutive relations required to explain non-Newtonian behaviour, non-Newtonian fluids could also be classified into four broad categories [24].

(i) Rheopetic: Fluids that become more viscous as they are stressed over some time. For instance, cream viscosity increases over a while.

(ii) Thixotropic: Fluids that become less viscous as they are stressed over a while. For instance, honey viscosity decreases over a while.

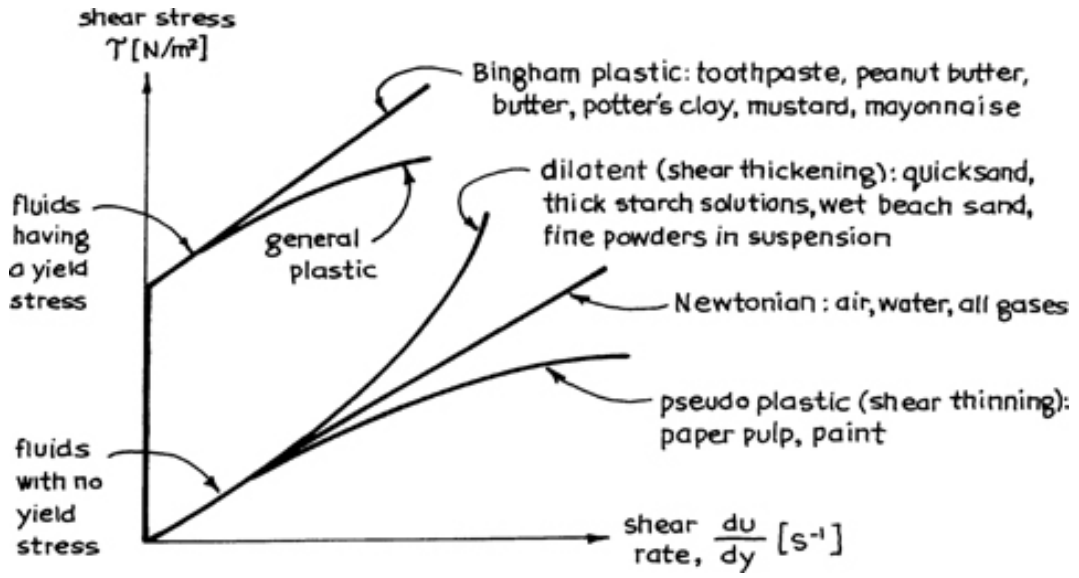

Figure 1.1: Kinds of time-independent non-Newtonian fluids (Image source: [1]).

(iii) Dilatant: These fluids become more viscous when more force is applied, as an example, wet cement viscosity increases with the increase of stress.

(iv) Pseudoplastic: Fluids become less viscous when more force is applied, as an example, tomato ketchup viscosity decreases with the increase of stress.

Although significant research has been done on both forms of fluids, in recent times more attention is being directed towards non-Newtonian fluids [25].

1.1.3 Channel Flow

Channel flow signifies a vital important class of flows in fluid mechanics due to its varied applications in biological, industrial, and engineering systems. It is important to determine the properties of this type of flow with particular interest in how the effects of changing viscosity modify the flow pattern. Channel flow is an internal flow in which the confining walls change the fluid dynamic structure of the flow from an arbitrary state at the channel inlet to a certain state at the

outlet. Channel flow is either close or open as shown in Fig.1.2 and Fig.1.3.

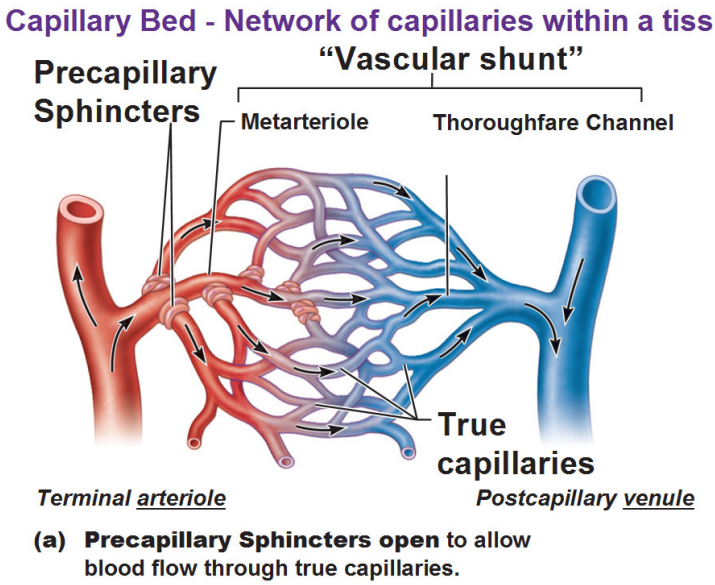

Figure 1.2: Example of closed channel flow (Image source: antranik.org/blood-vessels)

Flows in closed conduits or channels, like pipes or air ducts are completely in contact with rigid boundaries of the conduits. Almost all closed conduits in engineering applications are either circular or rectangular in cross-section. Open channel flows, on the other hand, are those whose boundaries do not seem to be entirely a solid and rigid material. The other part of the boundary of such flows could also be another fluid or nothing at all. Examples of open channel flows are rivers, irrigation canals, or sheets of water running across the ground surface after a rain. However, the most important difference is that the flow in a closed conduit is influenced by the pressure within the line, whereas flow within the open channel is influenced only by gravity. Unlike flows within an open channel,

Figure 1.3: Example of open channel flow(Image source: civiltoday.com)

flow within a closed conduit does not come in contact with the atmosphere.

1.2 Definition of Terms

1.2.1 Density

The density of a fluid is its mass per unit volume [26]. This property helps the classification of fluids as either compressible or incompressible. A fluid is termed compressible if its density varies and increases nearly proportionally to the pressure level. Otherwise, it is termed incompressible [27]. The unit of density is kgm^{-3}.

1.2.2 Temperature

Temperature is a measure of the internal energy of a fluid. If the temperature differences are strong, heat transfer may be important. The unit for temperature

is degree Celsius ($^{\circ}C$).

1.2.3 Pressure

Pressure is defined as a normal force per unit area existing in the fluid [28]. The gradient in pressure typically drives fluid flow, particularly in ducts. The unit for pressure is Nm^{-2}.

1.2.4 Buoyancy

The buoyancy or the upthrust is a force that is exerted by a fluid on an object, opposing the objects weight [29]. Buoyancy force acts upwards through the centre of gravity of the displaced volume of fluid, referred to as centre of buoyancy. When the object has a lower density than the fluid, buoyancy force will exceed weight, and the object will float. Otherwise, if the object is denser than the fluid, it will sink. Buoyancy has numerous engineering applications, some of which are in the design of boats and ships as well as in aerodynamics.

1.2.5 Internal Energy

In thermo-statics, the only energy in a substance is that which is kept in a system by molecular activity and molecular bonding forces [28]. This is commonly denoted as internal energy. An identified mass of viscous fluid may be seen as a thermodynamic system that stores various forms of energy. Whenever any form of this fluid is being deformed, it causes an irreversible transformation of mechanical energy into internal or thermal energy. The internal energy of gas includes the energies of translation, rotation, and vibration of the molecules as well as the energy of molecular dissociation and energy of electronic excitation of the molecules. The unit for internal energy is $Jmol^{-1}$.

1.2.6 Specific Heat Capacity

Specific heat capacity refers to the measure of the heat energy needed to extend the temperature of one gram of a substance by one degree Celsius [28]. Specific heat capacity is measured under two different experimental conditions. It is measured either below constant pressure conditions or under constant volume conditions. Typical values of particular heat capacities of gases are not a lot completely different from those of liquids. The unit for specific heat capacity is $Jmol^{-1}K^{-1}$.

1.2.7 Viscosity

Viscosity refers to fluid thickness. It is the resistance to the sliding motion of one fluid layer over the other [30]. Alternatively, it is defined as a fluid property that determines its resistance to shearing stresses [31]. For Newtonian fluids the relationship between the shear stress and viscosity is described by the linear relationship in equation (1.1) The viscosity property of fluids aids the classification of fluids as either Newtonian or non- Newtonian fluids.

Table 1.1: Viscosities of different materials at various temperatures

Fluid	**Viscosity (mPa.s)**	**Temperature (°C)**
Water	1.5182	5
Water	0.89	25
SAE 10W-40 Oil	37.147	60
SAE 10W-40 Oil	15.093	90
Honey	14095	20
Honey	6303.6	26
Hydrogen	0.00084	0
Hydrogen	0.00104	100
Nitrogen	0.00189	50
Yoghourt	150	40
Shampoo	3000	20
Transformer oil	75	10
Soft cheese	30000	60
Olive oil	40	40
Water varnish	900	20
Oxygen	18.1	0
Soya bean oil	60	20

Viscosity is related to collective flows that transfer momentum from one region of the fluid to another. Consider a fluid where there is, in addition to thermal tension of the molecules, a collective movement or current of the whole fluid, for example, water running in a channel under a pressure difference. Usually, viscosity is regarded as the most important material property and any practical study that requires the knowledge of fluid response would automatically turn to the basic understanding of viscosity. Overall, the Newtonian model defines the rheological behaviour of fluids. The Newtonian model is simply a special case with constant viscosity. Accurate knowledge of viscosity is very useful for the computation of the pressure, velocity, and temperature within the channels. Viscosity also helps to describe the flow behaviour of shear stress concerning the rate of deformation of the fluid.

1.2.8 Temperature Dependent Viscosity

The impact of increasing the temperature of a fluid is to decrease the cohesive forces, whereas at the same time increasing the rate of molecular interchange. The former impact tends to cause a decrease in shear stress, while the latter causes it to increase. For example, engine oil thickens appreciably on cold days and may significantly affect the performance of cars and other machinery during the cold periods. Table 1.1 shows the viscosities of some selected fluids at a given temperature. Models that describe the dependence of viscosity on temperature have been proposed, see [32; 33; 34; 35; 36]. One of the common models is the Arrhenius-type equation, [37],

$$\mu(T) = \mu_0 e^{\frac{E}{RT}}, \tag{1.2}$$

where μ_0 is the initial fluid dynamic viscosity, E is the activation energy, R is the universal gas constant, and T is the fluid temperature. The other common temperature dependent viscosity model is approximated by the Arrhenius relationship, [38],

$$\mu = \mu_0 e^{-b(T-T_0)}, \tag{1.3}$$

where T_0 is the fluid initial temperature and b is a viscosity variation parameter. There is a wide range of practical applications in the industry for heat and mass transfer problems for reacting fluids [39; 36; 40]. In Table 1.2 we list some of the most commonly used temperature dependent viscosity models.

Table 1.2: Various models of temperature dependent viscosity [7; 8]

Name	**Equation**
Power Law	$\mu = (\frac{T}{T_0})^n$
Reynolds	$\mu = be^{-aT}$
Sutherland	$\mu = \frac{\left(\frac{T}{T_0}\right)^{3/2}(T_0+C)}{T+C}$
Williams, Landel, Ferry	$log\,\frac{\mu}{\mu_0} = -\frac{C_1(T-T_0)}{C_2+T-T_0}$
Arrhenius Type	$\mu = \mu_0 \left(\frac{T}{T_0}\right)^n e^{\left(\frac{E}{RT}\right)}$
Vogel	$\mu = ae^{\frac{b}{T-C}}$
Walther	$\mu = \mu_0 + bd^{1/T^C}$

1.2.9 Porous Medium

A porous medium is defined as a material that contains a solid matrix with interconnected pores [41]. The solid material is either rigid or goes through small deformation. The interconnected pores allow the flow of single or several fluids. In a single system, the pore spaces of the porous medium are filled with a single fluid (or by several fluids completely miscible with each other). In a multiphase system, the pore spaces are filled with two or more fluids that are immiscible with each other. Some typical examples of natural porous media are sand, limestone, sandstone, wood, and human lungs [42].

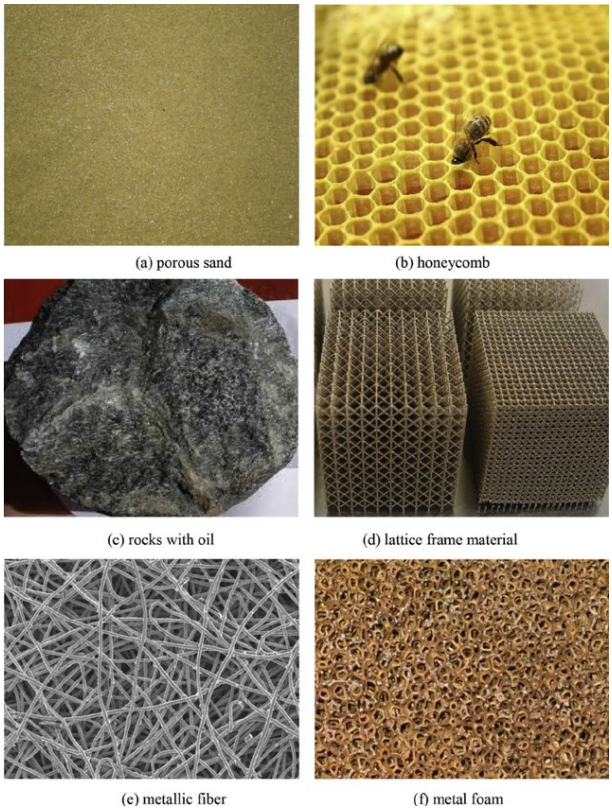

Figure 1.4: Different kinds of porous media (Image source: [2])

Porosity φ and permeability k are the most important properties of a porous medium. Porosity is the ratio of the pore volume to the total volume (matrix volume) [3]. The porosity of a porous medium is determined mathematically by the following generalized relationship that is described in Fig.1.5.

$$\varphi = \frac{\text{pore volume}}{\text{matrix volume}} = 1 - \frac{\text{grain volume}}{\text{matrix volume}},$$

where matrix volume = grain volume + pore volume. The permeability measures the capacity and the ability of the fluid to flow through the porous medium. It is a quantity that depend on the geometry of the porous medium only.

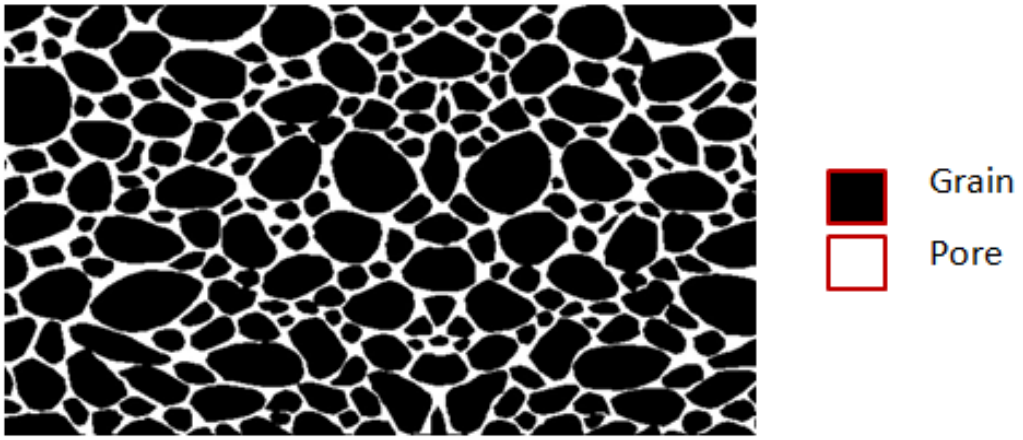

Figure 1.5: Microscopic Image of a Porous Medium (Image source: [3])

1.2.10 First Law of Thermodynamics

The first law of thermodynamics states that energy is always conserved [43]. This implies that energy can neither be formed nor destroyed, it just changes form. Schetz and Fuhs [44] further state that the amount of work done by a system equals the product of the external force acting on the system and the component of the displacement parallel to the force. The first law of thermodynamics defines internal energy as a state function and gives a formal statement of the conservation of energy. However, it gives no information about the direction wherein processes can occur, that is, the reversibility aspects of thermodynamic processes. For instance, it cannot say how cells can perform work although existing in an isothermal environment. It offers no information about the inability of any thermodynamic processes to transform heat into mechanical work with full efficiency, or any perception into why mixtures cannot spontaneously separate, or unmix themselves. An experimentally derived principle to describe the availability of energy is necessary to do this. That is precisely the role of the second law of thermodynamics to be defined subsequently.

1.2.11 Second Law of Thermodynamics.

The second law of thermodynamics points to the differences in quality between different forms of energy and describes why some processes can naturally occur, whereas others cannot. The second law of thermodynamics states that as energy is transferred or transformed, more and more of it is wasted [43]. It also states that there is a natural tendency for the entropy of a closed system to increase. Entropy generation is a thermodynamic quantity representing the unavailability of a system's thermal energy for conversion into mechanical work [45]. This is often referred to as the degree of disorder or randomness in the system.

1.3 Heat Transfer

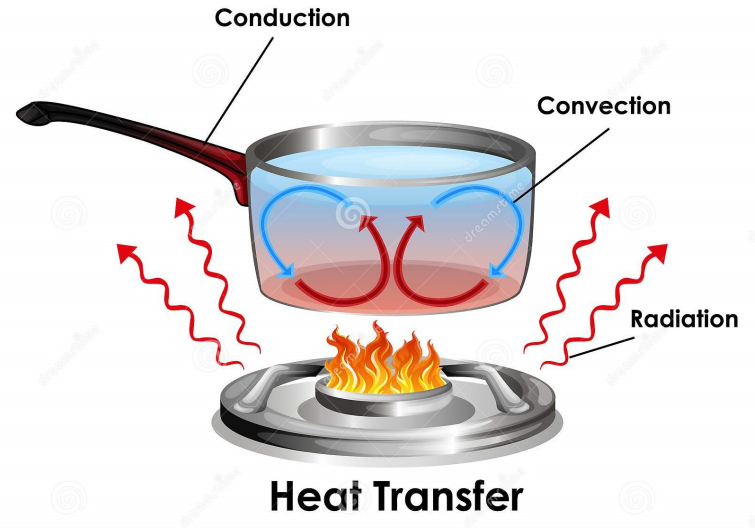

Figure 1.6: Heat transfer illustration (Image source: dreamstime.com)

Heat transfer describes the flow of heat due to temperature differences and the subsequent temperature distribution and changes [46]. The term convective heat transfer in engineering is used to describe the combined effects of heat conduction and fluid flow, and is observed as a third mechanism of heat transfer. There are

three ways in which heat is transferred in fluids, namely, conduction, convection, and radiation. Fig. 1.6 illustrates these three forms of heat transfer.

1.3.1 Conduction

On a microscopic scale, conduction happens as hot, quickly moving, or vibrating atoms and molecules interacting with neighbouring atoms and molecules, transfer a variety of their energy (heat) to the neighbouring atoms [47]. Heat is always transferred from regions of higher energy to regions of lower energy levels. This is in accordance with the second law of thermodynamics. The rate of heat transfer through conduction is a function of the temperature difference, the material concerned, and its thickness [48]. In an insulator, the heat flux is carried nearly entirely by phonon. The governing heat conduction equation along a body of length (thickness) L is

$$q = \frac{kA\Delta T}{L}, \tag{1.4}$$

where q is energy transferred per unit time, k is the thermal conductivity, A is the wall area and ΔT is the temperature difference.

1.3.2 Convection

Convection refers to the mechanism of heat transfer through a fluid in the presence of bulk fluid motion. There are three types of convection, known as free convection, forced convection, and mixed convection [49]. Irrespective of the nature of the convection, the rate of heat transfer is given by Newton's law of cooling

$$q'' = h(T_w - T_\infty), \tag{1.5}$$

where q'' is the rate at which heat is transferred, h is the convection heat transfer coefficient, T_∞ is the bulk temperature of the fluid, and T_w is the temperature of

the fluid at the wall.

1.3.2.1 Natural Convection/Free Convection

Natural convection is a mechanism of mass and heat transport in which the fluid motion is generated only by density differences in the fluid occurring due to temperature gradients, not by any external source [50]. A standard example of natural convection is the movement of smoke from a hearth. It is seen in a pot of boiling water within which the less dense heated water on the lowest part moves upwards in plumes to replace the cooler and denser water at the top of the pot that sinks, down to the bottom.

1.3.2.2 Forced Convection

Forced convection is a mechanism of transport in which fluid motion is generated by an external source such as a fan or pump [51]. Forced convection is usually used to increase the rate of heat exchange. Many types of mixing also utilise forced convection to mix one substance with another. Forced convection also appears as a by-product of other procedures, such as the action of a propeller in fluid or aerodynamic heating. Fluid radiator systems, heating and cooling of parts of the body by blood circulation are other familiar examples of forced convection [52].

1.3.2.3 Mixed Convection

Mixed convection is a combination of natural convection and forced convection [53]. In other words, mixed convection takes place when natural convection and forced convection mechanisms act together to transfer heat. The mixed convection process occurs when the effect of the buoyancy force in forced convection or the effect of forced flow in free convection becomes significant.

1.3.3 Radiation

Thermal radiation is the only form of heat transfer that can occur in the absence of any form of medium. It occurs through a vacuum. Thermal radiation is a direct result of the movement of atoms and molecules in a material. Considering the fact that those atoms and molecules are composed of charged particles (protons and electrons), their movement result in the emission of electromagnetic radiation, that emits energy away from the surface. At the same time, the surface is constantly attacked by radiation from the surroundings, resulting in the transfer of energy to the surface.

1.4 Fluids of the Differential Type

Non-Newtonian fluids cannot fit right into a single constitutive version. As such, numerous constitutive models have been proposed for different categories of non-Newtonian fluids. The flow behavior of these fluids cannot be properly defined based on the classical linearly viscous model. Numerous constitutive equations that have been suggested try to characterize the deviation of relevant non-Newtonian behavior from the classical theory. They are models that describe the relationship between shear stress and the shear rate of non-Newtonian fluids, namely, Bird-Carreau fluid, Power-law fluid, Carreau fluid, Couple stress fluid, fluids of the differential type, etc. Fluids of the differential type, also known as Rivlin-Ericksen fluids are fluids where stress is just a function of the velocity gradient and some number of its higher time derivatives as well as constitutively indeterminate pressure [54]. Fluids of the differential type fall into numerous grades depending on the constitutive structure of the fluid's Cauchy stress. Sufficiently, we have fluids of differential type of first grade, second grade , third grade, etc.

1.4.1 First Grade Fluid

First grade fluids are taken into consideration to be Newtonian fluids. The viscosity of a first grade fluid is constant and does not change with time. The Cauchy stress tensor $\mathbf{T}$ for a first grade fluid is given as [54]

$$\mathbf{T} = p\mathbf{I} + \mu\mathbf{A_1}, \tag{1.6}$$

where p denotes the pressure, $\mathbf{I}$ is the identity tensor, μ is the coefficient of viscosity and $\mathbf{A_1}$ is a Rivlin-Ericksen tensor.

1.4.2 Second Grade Fluid

One of the most popular models for non-Newtonian fluids is referred to as the second grade fluid. Second grade fluids are the most effective subclass due to the fact that exact solutions can be found for their constitutive equations. Examples of second grade fluids consist of blood, butter, starch suspension, coconut oil, shampoo, and paints. For a second grade fluid, the Cauchy stress tensors are of the form [55]

$$\mathbf{T} = -p\mathbf{I} + \mu\mathbf{A_1} + \alpha_1\mathbf{A_2} + \alpha_2\mathbf{A_1}^2, \tag{1.7}$$

where $\mathbf{T}$, p, $\mathbf{I}$ and μ are as defined earlier, α_1 and α_2 denote the elasticity and cross-viscosity, while $\mathbf{A_1}$ and $\mathbf{A_2}$ are Rivlin-Ericksen tensors defined by

$$\begin{aligned} \mathbf{A_1} &= \mathbf{L} + \mathbf{L}^T, \\ \mathbf{A_2} &= \frac{d}{dt}\mathbf{A_1} + \mathbf{A_1}\mathbf{L} + \mathbf{L}^T\mathbf{A_1}, \end{aligned} \tag{1.8}$$

where $\mathbf{L}$ is the velocity gradient, $\dfrac{d}{dt}$ denotes the material derivative and the superscript T indicates the transpose operation.

1.4.3 Third Grade Fluid

It has been observed that second grade fluids do not show the shear thinning and shear thickening behaviour. However, the model for third grade fluids is capable of describing such behavior. Polymeric-paints, DNA fluids, bio-organic solutions, and alternative synthetic materials, are examples of third grade fluids The Cauchy stress tensor $\mathbf{T}$ for a third grade fluid is given as [56]

$$\mathbf{T} = -P\mathbf{I}+\mu\mathbf{A_1}+\alpha_1\mathbf{A_2}+\alpha_2\mathbf{A_1^2}+\beta_1\mathbf{A_3}+\beta_2(\mathbf{A_1A_2}+\mathbf{A_2A_1})+\beta_3(tr\mathbf{A_1^2})\mathbf{A_1}, \quad (1.9)$$

where α_i, β_j for $i = 1, 2$ and $j = 1, 2, 3$ are the material parameters of a third grade fluid, tr is the trace operator, and A_i for $i = 1, 2, 3$ are the first three Rivlin-Ericksen tensors defined by

$$\mathbf{A_1} = (\nabla V) + (\nabla V)^T, \quad (1.10)$$

$$\mathbf{A_{n+1}} = \frac{d\mathbf{A_n}}{dt} + \mathbf{A_n}(\nabla V) + (\nabla V)^T\mathbf{A_n} \quad n = 1, 2, \quad (1.11)$$

where ∇ is the gradient operator and the other terms are as previously defined. Using the thermodynamic compatibility conditions when the fluid is locally at rest, the Clausius-Duhem inequality holds and the assumption that the Helmholtz free energy is a minimum at equilibrium provides the following restrictions [57]:

$$\mu \geq 0,\ \alpha_1 \geq 0,\ \beta_1 = \beta_2 = 0,\ \beta_3 \geq 0,\ -\sqrt{24\mu\beta_3} \leq \alpha_1 + \alpha_2 \geq \sqrt{24\mu\beta_3} \quad (1.12)$$

Thus, equation (1.9) reduces to

$$\mathbf{T} = \mu\mathbf{A_1} + \alpha_1\mathbf{A_2} + \alpha_2\mathbf{A_1^2} + \beta_1\mathbf{A_3}. \quad (1.13)$$

1.5 Magnetohydrodynamics(MHD)

The concept of magnetohydrodynamics (MHD) was first introduced by Hannes Alfven (1908-1995). Magneto refers to magnetic field, hydro refers to fluids, and dynamics refers to forces and the laws of motion. MHD is the mathematical model for the low frequency interaction that occurs between electrically conducting fluids and electromagnetic fields [58]. In other words, MHD can be described as the study of the interaction between magnetic fields and moving, electrically conducting fluids [59]. The synonyms of MHD are hydromagnetic and magneto fluid dynamics. The main work of Hartmann [60] is viewed as the origin of MHD flow in a channel. Examples of electrically conducting fluids are liquid metals (such as mercury, gallium, molten magnesium, molten antimony, liquid sodium etc.), and plasmas.

1.5.1 MHD Equations

The important concept behind MHD is that the interaction of a conducting fluid and a magnetic field causes an electromotive force to develop. This will induce electrical current with density of order $\sigma(u \times B)$, where σ is the electrical conductivity of the fluid, B is the magnetic field intensity and u is the velocity field. The current will induce another magnetic field that gets added to the original magnetic field and the fluid them flows along with magnetic field lines. The combined magnetic field (that is both the imposed and induced) then interacts with the induced current density, J, giving rise to a Lorentz force, $J \times B$ [61]. The governing equations of MHD, in differential form, are summarised as follows:

(i) Navier-Stokes equations with Lorentz force

$$\rho\left(\frac{\partial u}{\partial t}+(u\cdot\nabla)u\right)=-\nabla p+\mu\nabla^2 u+J\times B+\rho g \tag{1.14}$$

(ii) Continuity equation

$$\frac{\partial\rho}{\partial t}+\nabla\cdot\rho u=0 \tag{1.15}$$

(iii) Faraday's Law

$$\nabla\times E=\frac{\partial B}{\partial t} \tag{1.16}$$

(iv) Ampere's Law

$$\nabla\times E=\mu_m j \tag{1.17}$$

(v) Ohm's law

$$j=\sigma(U+E\times B) \tag{1.18}$$

where u is the fluid velocity, p is the fluid pressure, μ_m is the magnetic permeability, σ fluid electrical conductivity, μ is the fluid dynamic viscosity, E is the electrical field, B is the magnetic field intensity, j is the current density, and ρ is the fluid density.

1.5.2 Applications of MHD

The applications of MHD are very wide, they include metallurgically application, MHD pumps, MHD propulsion, MHD generators, and MHD flow meters, etc.

1.5.2.1 MHD Flow Meter

The idea is that a conducting fluid flowing through a magnetic field produces an electromotive force. MHD flow meter is an electromagnetic flow measurement

method that is based on exposing a flow to a magnetic field and measuring the force acting on the magnetic field generating system.

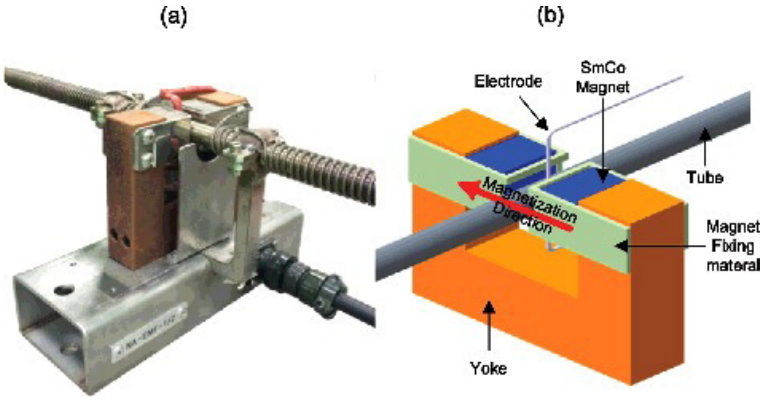

Figure 1.7: SmCo permanent magnet flowmeter: (a) photograph, (b) 3D drawing [4].

1.5.2.2 MHD Pumps and Generators

MHD generator or pump is compact and simple, and has a high power density. As such, it is notably interesting for military applications. In principle, the relationship between MHD generator and pump is related to an electrical motor being driven and operated like a generator [6]. MHD power generator or dynamo is any device that transforms electric power by means of the interaction of a moving fluid (usually an ionized gas or plasma) and a magnetic field [62]. MHD power generators are different from traditional electric generators in that they can function at high temperatures without moving parts.

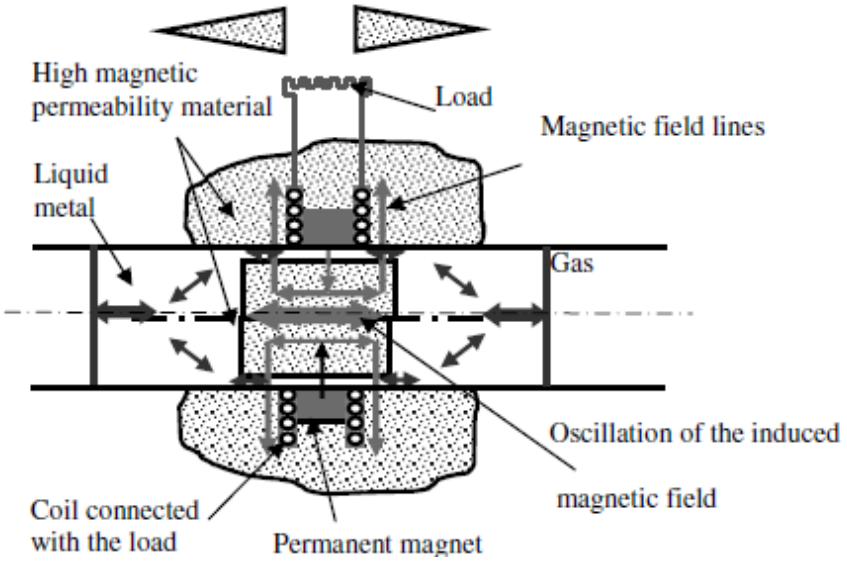

Figure 1.8: Principle of the MHD generator [5].

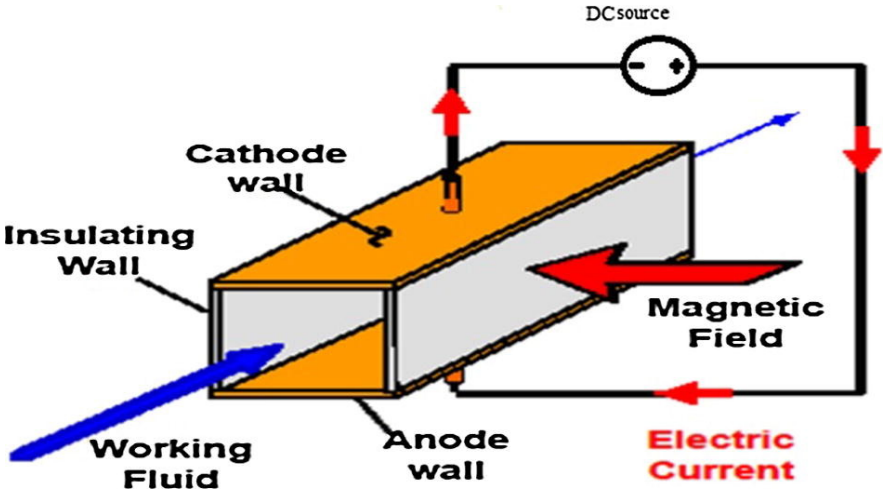

Figure 1.9: MHD pump components [6].

1.6 Entropy Generation

Entropy generation is a thermodynamic quantity representing the unavailability of a system's thermal energy for conversion into mechanical work. Entropy production determines thermal machines' performance like power plants, heat

engines, refrigerators, heat pumps, and air conditioners. It is a measure of the irreversibility that is related to the real processes. Entropy generation is usually a positive quantity or zero if the process is reversible. As entropy generation takes place, the amount of energy decreases. Thus, to preserve the quality of energy, entropy generation within the fluid flow system should be minimised.

According to Bejan [63], the general equation for the entropy generation (E_G) per unit volume is given by

$$E_G = \frac{k}{T_0^2}(\nabla T)^2 + \frac{\mu}{T_0}\Phi, \tag{1.19}$$

where k is the thermal conductivity, T_0 is the initial fluid temperature, T is the absolute temperature, μ is the temperature dependent viscosity, ∇ is the Laplacian operator, and Φ is the irreversibility ratio which is given by

$$\Phi = \frac{\text{viscous dissipation irreversibility}}{\text{Heat transfer irreversibility}}.$$

The first term in equation (1.19) is the entropy generation due to heat transfer while the second term is the viscous dissipation irreversibility.

1.7 Fluid Parameters

1.7.1 Prandtl Number

The Prandtl number (Pr) is a dimensionless number, named after the German physicist Ludwig Prandtl (1875 - 1953), defined as the ratio of momentum diffusivity to thermal diffusivity [64]. In this way, a low Prandtl number indicates strong conductive heat transfer whereas a high Prandtl number indicates strong

convective heat transfer. Mathematically, it can be stated as

$$Pr = \frac{\nu}{k}, \tag{1.20}$$

where ν is the kinematic viscosity and k is the thermal diffusivity.

1.7.2 Brinkman Number

The Brinkman number (Br) is a dimensionless number used to quantify the relationship between the heat generated by dissipation and the heat exchanged at the wall [65]. It is named after the Dutch mathematician and physicist Henri Brinkman (1908 - 1961). It is defined as

$$Br = \frac{\mu_0^3 E}{a^2 \rho^2 k R T_0^2}, \tag{1.21}$$

where μ_0 is the initial fluid viscosity, E is the activation energy, a is a channel width, T_0 is the initial fluid temperature, ρ is the fluid density, R is the universal gas constant, and k is the thermal conductivity.

1.7.3 Grashoff Number

In fluid dynamics and heat transfer, Grashof number (Gr) is a dimensionless number that approximates the ratio of the buoyancy to viscous force acting on a fluid [66]. It is named after German engineer Franz Grashof (1826 - 1893). In natural convection it plays the same role that is played by the Reynolds number in forced convection. When $Gr >> 1$, the viscous force is negligible compared to the buoyancy and inertial forces which means the fluid movement is high. The

Grashof number is defined as

$$Gr = \frac{\rho^2 g \beta a^3 R T_0^2}{\mu_0^2 E}, \tag{1.22}$$

where ρ is the fluid density, g is the gravitational acceleration, β is the thermal expansion coefficient, a is a channel width, T_0 is the initial fluid temperature, R is the universal gas constant, μ_0 is the initial fluid viscosity, and E is the activation energy.

1.7.4 Frank-Kamenetskii Number

Frank-Kamenetskii number, named after a Russian scientist, David A. Frank-Kamenetskii (1910 - 1970), explains the thermal explosion of a homogeneous mixture of reactants, kept inside a closed channel with constant temperature walls [64]. The Frank-Kamenetskii parameter (λ) is given by

$$\lambda = \frac{Q}{k} \frac{E}{R T_0^2} a^2 c \alpha e^{-\frac{E}{R T_0}} \tag{1.23}$$

where c is the concentration of the reactant, α the frequency factor and E the energy of activation of the reaction, T_0 is the initial fluid temperature, a denotes the distance measured from the centre of the configuration and R is the universal gas constant.

1.7.5 Darcy Number

In fluid dynamics, the Darcy number (Da) represents the relative impact of the porosity of the porous medium versus its cross-sectional area square [67]. Darcy number is named after French engineer Henry Darcy (1803 - 1858) and is found

from nondimensionalizing the differential form of Darcy's Law. It is defined as

$$Da = \frac{K}{a^2}, \tag{1.24}$$

where K is the permeability of the porous medium and a is the characteristic length.

1.7.6 Biot Number

The Biot number (Bi) is used in transient heat transfer calculations and provides a simple index of the ratio of the heat transfer resistances within and at the surface of a body. It is named after French physicist Jean-Baptiste Biot (1774-1862) [68]. The Biot number is used in unsteady state (transient) heat transfer conditions. It is defined as

$$Bi = \frac{hL_c}{K_b}, \tag{1.25}$$

where, h is Heat transfer coefficient characteristic dimension, which is commonly defined as the volume of the body (V_b) divided by the surface area (A_s) of the body, such that $L_c = \frac{V_b}{A_s}$ and K_b is thermal conductivity of the body.

1.8 Problem Statement

Industrial productivity, sustainability and competitiveness are all dependent on engineering solutions. On the other hand, engineering systems designs and performance are heavily reliant on mathematical models. For instance, in almost all thermo-fluid systems efficient energy utilization can be achieved through entropy generation minimization, and this falls within mathematical modelling. Entropy is a thermodynamic quantity that represents the unavailability of a systems thermal energy for conversion into mechanical work. The thermo-fluid systems ef-

ficiency is thus a function of heat irreversibilities within a flow domain under working conditions. Thus, the second law of thermodynamics can be applied to investigate the irreversibility regarding the entropy generation rate ([69]).

Ecological and economic systems that are responsible for the sustenance of life are severely threatened by the ever-increasing greenhouse gas emissions that are worsening global warming. The deleterious effects of the melting of glaciers, runaway fires, floods and other extreme events call for urgent solutions to global warming. The only workable solution to this global quagmire lies in the curtailment of the burning of fossil fuels from which energy is derived. Thus, technologies to fast pace the replacement of fossil fuels by clean energy sources like wind and solar systems must continue to be discovered and implemented. In this transition then, energy conservation and efficient utilization must be priorities as wastages will slow down the replacement processes. If ways of reducing or eliminating energy losses can be found, then complete dependence on clean energy sources can be achieved and the world can be saved from imminent demise. In particular, contemporary devices and systems are getting technologically miniaturized for many advantages, including minimal energy consumption. One other way to achieve efficiency, in thermo-fluid systems as pointed to earlier, is through systems regulation to minimize entropy generation.

In this study we carry out a thermodynamic analysis of variable properties third-grade fluid flow in channels with varied geometries and subjected to different physical effects. The rate of entropy generation and irreversibility ratio within the flow regions will be calculated using the second law of thermodynamics. The response of the fluid velocity, the temperature, the entropy generation rate and the irreversibility ratio to the various thermophysical parameters embedded in the flow systems will be analysed to inform desirable thermal regulation criteria.

1.9 Aim of the Study

The aim of this study is to analyse the flow and heat transfer characteristics of hydromagnetic third-grade fluid with variable properties.

1.10 Objectives of the Study

The objectives of the study are to:

(i) Formulate the mathematical models for third-grade fluid flow with variable properties.

(ii) Examine the combined effect of magnetic field and Joule dissipation on the entropy generation rate in a third-grade fluid flow through a horizontal channel with infinite parallel plates.

(iii) Investigate the inherent irreversibility in a hydromagnetic third-grade fluid flow through a vertical channel filled with saturated porous media and asymmetric convective boundary conditions.

(iv) Investigate the inherent irreversibility in a third-grade fluid flow through an inclined channel filled with saturated porous media and exposed to constant heat flux and convective boundary conditions.

(v) Simulate and describe the variation of important thermophysical parameters embedded in the flow systems on the fluid velocity, temperature distribution, entropy generation rate and irreversibility ratio.

1.11 Computational Approach

For nonlinear equations, numerical solutions are of specific interest because of the fact that analytical solutions might not exist in closed form. In this study, we will use analytical techniques and / or numerical methods to solve the modelling equations. The partial differential equations which will be formulated are coupled and nonlinear. We describe the methods that we anticipate to employ.

1.11.1 Adomian Decomposition Method

The Adomian decomposition method (ADM) was developed by George Adomian in 1980's. It is a semi-analytic approximation technique that achieves rapidly convergent series solution with minimal volume of computational work. It achieves solutions without any discretisation, linearization or any restrictive assumption and is mostly free from round-off errors. ADM does not require an initial guess. One other advantage of ADM is that it may be coded in symbolic computer package for successive iteration of the computation ensuring that human error is fully eliminated. Linearization bears the chance of losing the physical meaning of the problem.

Consider the generalized nonlinear differential equation of the form

$$Ly + Ry + Ny = g, \tag{1.26}$$

where L is the highest order differential operator which is invertible, R is a linear differential operator, N is the nonlinear operator and g is an inhomogeneous source term. Apply L^{-1} on both sides of equation (1.26) to obtain

$$y = h - L^{-1}(Ry) - L^{-1}(Ny), \tag{1.27}$$

where h represents the terms coming from integrating the source term g. Generally

$$L = \frac{d^n}{dx^n}(.) \tag{1.28}$$

for the n^{th} order ordinary differential equations, and thus its inverse L^{-1} follows as the n^{th} order definite integration operator from 0 to x. The decomposition method represnts the solution $y(x,t)$ as a series of the form,

$$y(x,t) = \sum_{n=o}^{\infty} y_n(x,t). \tag{1.29}$$

The nonlinear term Ny is decomposed as

$$Ny = \sum_{n=o}^{\infty} A_n, \tag{1.30}$$

where A_n's are the Adomian polynomials generated for each nonlinearity, and are obtained from the formula

$$A_n = \frac{1}{n!}\frac{d^n}{dt^n}\left(N\sum_{i=0}^{n} t^i y_i\right)_{t=0}, \quad n = 0, 1, 2, 3, 4\ldots \tag{1.31}$$

Substituting equations (1.28), (1.29) and (1.30) into equation (1.27),

$$\sum_{n=o}^{\infty} y_n(x,t) = y_0 - L^{-1}R\sum_{n=o}^{\infty} u_n - L^{-1}N\sum_{n=o}^{\infty} A_n. \tag{1.32}$$

The zeroth component is written as

$$y_0 = h \tag{1.33}$$

and the recursive relation is

$$\begin{aligned} y_1 &= -L^{-1}(Ry_0) - L^{-1}(A_0), \\ y_2 &= -L^{-1}(Ry_1) - L^{-1}(A_1), \\ y_3 &= -L^{-1}(Ry_2) - L^{-1}(A_2), \\ y_4 &= -L^{-1}(Ry_3) - L^{-1}(A_3), \\ &\vdots \\ y_{n+1} &= -L^{-1}(Ry_n) - L^{-1}(A_n). \end{aligned} \tag{1.34}$$

We write the first four Adomian polynomials as

$$\begin{aligned} A_0 &= N(y_0) \\ A_1 &= y_1 N'(y_0) \\ A_2 &= y_2 N'(y_0) + \frac{1}{2!} y_1^2 N''(y_0) \\ A_3 &= y_3 N'(y_0) + y_1 y_2 N''(y_0) + \frac{1}{3!} y_1^3 N'''(y_0) \\ &\vdots \end{aligned}$$

The solution for the $n - term$ approximation is

$$\phi_n = \sum_{i=0}^{n-1} y_i, \tag{1.35}$$

where

$$y(x,t) = \lim_{n\to\infty} \phi_n(x,t) = \sum_{i=0}^{\infty} y_i(x,t). \tag{1.36}$$

1.11.2 Finite Difference Method

The finite difference method (FDM) is a numerical approximate method for solving partial differential equations by geometry for which analytical solutions may

not exist. It can be applied to solve a wide range of problems. The problems include linear and non-linear, dependent and time-dependent problems. The FDM can be useful to problems with different boundary shapes, different kinds of boundary conditions, and for a region containing several different materials. We follow [61].

1.11.2.1 Numerical differential of functions of a single variable

Let $y = y(x)$ and $\Delta x = h$. Using the Taylor series expansion around the point $x = x_0$, and ignoring higher order terms (since they vanish to 0), we obtain the following finite difference aproximations:

- The forward difference approximation

$$y_i' = \frac{1}{h}\left(y_{i+1} - y_i\right) + \mathcal{O}(h^2). \tag{1.37}$$

- The backward difference approximation

$$y_i' = \frac{1}{h}\left(y_i - y_{i-1}\right) + \mathcal{O}(h^2). \tag{1.38}$$

- The central difference approximation

$$y_i' = \frac{1}{2h}\left(y_{i+1} - y_{i-1}\right) + \mathcal{O}(h^3). \tag{1.39}$$

- The second derivative

$$y_i' = \frac{1}{h^2}\left(y_{i+1} - 2y_i + y_{i-1}\right) + \mathcal{O}(h^3). \tag{1.40}$$

1.11.2.2 Functions of two variables

Let $u = u(x,t)$, where (x,t) belongs to some two dimensional area. Expansion in Taylor series around a point (i,j) results in the following approximations:

- The central difference approximations for the two first order partial derivatives

$$(u_x)_{i,j} = \frac{1}{2\Delta x}\left(u_{i+1,j} - u_{i-1,j}\right) + \mathcal{O}(\Delta x^3), \tag{1.41}$$

$$(u_t)_{i,j} = \frac{1}{2\Delta t}\left(u_{i+1,j} - u_{i-1,j}\right) + \mathcal{O}(\delta t^3). \tag{1.42}$$

- The approximation for the second order partial derivatives

$$(u_{xx})_{i,j} = \frac{1}{2\Delta x^2}\left(u_{i+1,j} - 2u_{i,j} + u_{i-1,j}\right) + \mathcal{O}(\Delta x^3), \tag{1.43}$$

$$(u_{tt})_{i,j} = \frac{1}{2\Delta t^2}\left(u_{i+1,j} - 2u_{i,j} + u_{i-1,j}\right) + \mathcal{O}(\delta t^3). \tag{1.44}$$

The equations that govern the flow are going to be resolved numerically using the FDM. In this study, we rely on MAPLE to simulate solutions of the nonlinear partial differential equations that govern our flow system.

1.11.3 Spectral Quasi-linearisation Method

Bellman and Kalaba [70] where the first to introduce the quasi-linearisation method (QLM) as a generalization of the Newton-Raphson method to provide lower and upper bound solutions of nonlinear differential equations. The advantage of quasi-linearisation is that the algorithm is straightforward to understand and also typically converges quickly if the initial guess is close to the actual solution. Maleknejad and Najafi [71] developed the first proof of quadratic convergence to restrictive conditions of little step size and convexity or concavity of nonlinear functions. These conditions were afterwards relaxed and the technique

was also generalised to be applied to a wider category of problems, see for example the papers by Mandelzweig [72; 73] and Lakshmikantham [74]. Tuffuor and Labadie [75] noted that the disadvantage of quasi-linearisation is the instability of the method whenever a poor initial guess is chosen. To develop the accuracy and convergence of the quasi-linearisation method for all initial guesses, Motsa and Sibanda [76] introduced the QLM algorithm at intervals of the spectral method to get a sequence of integration schemes within higher-order convergence. This method gives excellent results in terms convergence and accuracy of solutions. Motsa *et al.* [77] used the SQLM successfully to solve nonlinear equations that govern the fluid flows in bounded domains.

1.11.3.1 Quasi-linearisation

Consider a system of n^{th} order nonlinear differential equations of the form

$$\mathcal{G}(y(x)) = 0, \quad x \in [a, b], \tag{1.45}$$

subject to given boundary conditions. If we expand equation (1.45) in Taylor series about

$$\mathbf{f(x)} = \left(f(x), \frac{df(x)}{dx}, \ldots, \frac{d^{n-1}f(x)}{dx^{n-1}}, \frac{d^n f(x)}{dx^n} \right), \tag{1.46}$$

and rearranging terms upon neglecting higher order terms in equation (1.45) we get

$$\nabla \mathcal{G}(\mathbf{f}) \cdot y = \nabla \mathcal{G}(\mathbf{f}) \cdot \mathbf{f} - \mathcal{G}(\mathbf{f}), \tag{1.47}$$

which is a linear differential equation in y. If we replace $\mathbf{f}$ and y with approximations y_r and y_{r+1} of y at r and $r + 1$ iteration levels respectively, we

get

$$\nabla \mathcal{G}(y_r(x)) \cdot y_{r+1}(x) = \nabla \mathcal{G}(y_r(x)) \cdot y_r(x) - \mathcal{G}(y_r(x)), \tag{1.48}$$

which expands to

$$\sum_{k=0}^{n} \frac{d^k y_{r+1}}{dx^k} \frac{\partial \mathcal{G}(y_r)}{\partial y_r^{(k)}} = \sum_{k=0}^{n} \frac{d^k y_r}{dx^k} \frac{\partial \mathcal{G}(y_r)}{\partial y_r^{(k)}} - \mathcal{G}(y_r), \quad r = 0, 1, 2, 3, 4, \ldots \tag{1.49}$$

Provided $y_0(r)$ is known, solving equation (1.49) for each $r = 0, 1, 2, 3, 4, \ldots$ yields a sequence

$$\{y_1(x), y_2(x), y_3(x) \ldots\}, \tag{1.50}$$

of approximations to actual solution $y(x)$ of a system of differential equations (1.45). We expect that $y_r(x) \to y(x)$ as $r \to \infty$ at each $x \in [a, b]$. The basic idea behind SQLM is the introduction of a Chebyshev differenatial matrix which is used to approximate the deivatives of the unknown variables at the collocation points as the matrix vector.

1.11.3.2 Chebyshev Differenatial

It is convenient to use the linear transformation

$$x(\eta) = \frac{1 - \eta}{2} a + \frac{1 + \eta}{2} b, \quad -1 \leq \eta \leq 1, \tag{1.51}$$

to migrate from the physical domain $[a, b]$ on the x-axis to the computational domain $[-1, 1]$ on the η-axis. Consequently, equation (1.49) becomes

$$\sum_{k=0}^{n} \frac{d^k y_{r+1}(\eta)}{d\eta^k} \left(\frac{2}{b-a}\right)^k \frac{\partial \mathcal{G}(y_r)}{\partial y_r^{(k)}} = \sum_{k=0}^{n} \frac{d^k y_r(\eta)}{d\eta^k} \left(\frac{2}{b-a}\right)^k \frac{\partial \mathcal{G}(y_r)}{\partial y_r^{(k)}} - \mathcal{G}(y_r(\eta)), \quad r = 0, 1, 2, 3, 4, \ldots \tag{1.52}$$

We let

$$-1 = \eta_N < \eta_{N-1} < \cdots < \eta_1 < \eta_0 = 1$$

where $\eta_i = cos(\frac{\pi i}{N})$ with $i = 0, 1, 2, 3, 4, \ldots, N$ are Gauss-Lobatto collocation points. We approximate the derivatives of the unknown $y(\eta)$ at the collocation points using the formula

$$\frac{d^p}{d\eta^p} y_r(\eta_i) = \sum_{j=0}^{N} [\mathbf{D}^p]_{ij} y_r(\eta_j), \quad i = 0, 1, 2, 3, 4, \ldots, N, \tag{1.53}$$

where the $(N+1) \times (N+1)$ matrix $\mathbf{D}$ is called the Chebyshev differential matrix given by the following theorem [78].

Theorem 1.11.1 *For each $N \geq 1$, let the rows and columns of each $(N+1) \times (N+1)$ Chebyshev spectral differention matrix $\boldsymbol{D}_N$ be indexed from 0 to N. The entries of the matrix are:*

$$(\boldsymbol{D}_{NN})_{00} = \frac{2N^2+1}{6}, (\boldsymbol{D}_N)_{NN} = -\frac{2N^2+1}{6},$$
$$(\boldsymbol{D}_{NN})_{ij} = \frac{-x_j}{2(1-x_j^2)}, j = 1, 2, \ldots, N-1,$$
$$(\boldsymbol{D}_N)_{ij} = \frac{c_j(-1)^{i+j}}{c_j(x_i - x_j)}, i \neq j, j = 1, 2, \ldots, N-1,$$

where

$$c_i = \begin{cases} 2, & i = 0 \ or \ N, \\ 0 & otherwise \end{cases}$$

This process is called Chebyshev differentiation.

Evaluating equation (1.52) at $\eta = \eta_i$, $(i = 0, 1, 2, 3, 4, \ldots, N)$ and applying formula (1.53) gives the linear system

$$\left[\mathbf{b_{n,r}}\mathbf{D}^n + \mathbf{b_{n-1,r}}\mathbf{D}^{n-1} + ... + \mathbf{b_{1,r}}\mathbf{D} + \mathbf{b_{0,r}}\mathbf{I}\right]\mathbf{y}_{r+1} = \mathbf{R_r}, \tag{1.54}$$

where

$$\begin{aligned} \mathbf{b_{n,r}} &= diag\{b_{n,r}(\eta_0), b_{n,r}(\eta_1), b_{n,r}(\eta_2), \ldots, b_{n,r}(\eta_N)\} \\ &= \begin{bmatrix} b_{n,r}(\eta_0) & & \\ & \ddots & \\ & & b_{n,r}(\eta_N) \end{bmatrix}, \end{aligned}$$

is an $(N+1) \times (N+1)$ diagonal matrix,

$$\mathbf{y}_{r+1} = \left[y_{r+1}(\eta_0), y_{r+1}(\eta_1), y_{r+1}(\eta_2), \ldots, y_{r+1}(\eta_E)\right]^T,$$

$\mathbf{I}$ is $(N+1) \times (N+1)$ identity matrix,

and

$$\mathbf{R_r} = \left[\mathbf{b_{n,r}}\mathbf{D}^n + \mathbf{b_{n-1,r}}\mathbf{D}^{n-1} + ... + \mathbf{b_{1,r}}\mathbf{D} + \mathbf{b_{0,r}}\mathbf{I}\right]\mathbf{y}_r - F(y_r),$$

is a residual error. We can write equation (1.54) as

$$A\mathbf{y}_{r+1} = \mathbf{R_r} \tag{1.55}$$

where

$$A = \mathbf{b_{n,r}}\mathbf{D}^n + \mathbf{b_{n-1,r}}\mathbf{D}^{n-1} + ... + \mathbf{b_{1,r}}\mathbf{D} + \mathbf{b_{0,r}}\mathbf{I}$$

Note that before we solve the linear system (1.55), we need to specify initial guess $y_0(\eta)$. We choose it so that it satisfies the boundary conditions as prescribed.

1.12 Thesis Outline

The organization of the thesis is as follows:

Chapter One

In chapter one, the focus is on the introduction and the basic concepts of fluid mechanics. We defined and elaborated the most important terminology and expressions used in the study. The problem statement, the aim and objectives of the study, and the research methodology are also presented in this chapter.

Chapter Two

In this chapter, we present the literature review, motivation of the study and significance of the study.

Chapter Three

In this chapter, we investigate combined effects of applied transverse magnetic field, variable linear viscosity and thermal conductivity on the entropy generation rate in a steady third-grade fluid flow in a horizontal channel with infinite parallel plates. Objectives (i), (ii) and (v) are achieved in this chapter.

Chapter Four

In this chapter, a steady incompressible reactive third grade fluid flow in an inclined channel filled with porous media with Navier-slip and convective bound-

ary conditions is investigated. The numerical solution is obtained using SQLM. Specific research objectives (i), (iv) and (v) are achieved in this chapter.

Chapter Five

This chapter investigates combined effects of magnetic field, buoyancy, porous media, variable viscosity and asymmetric convective boundary conditions on entropy generation in an unsteady incompressible third-grade fluid flow with variable properties. Objectives (i), (ii) and (v) are achieved in this chapter.

Chapter Six

General discussion, conclusions, recommendations and envisaged future work are presented in chapter six.

Chapter 2

Literature Review

Chapter Abstract

An overarching literature review, a statement of motivation for the study and the significance of the study are presented in this chapter.

2.1 Literature Review

In recent times, studies related to the flow of electrically conducting fluid have attracted the attention of many researchers due to its numerous applications in thermal sciences, engineering and technology. For instance, Abro and Khan [79] investigated the double convection MHD flow of a Casson fluid using the Fabrizio Caputo derivatives. Khan *et al.* [80] introduced the new chemical reaction model in MHD using the Homotopy analysis method. Their results show that the velocity distribution decreases for higher estimation of magnetic parameter whereas the temperature distribution increases. Ramandevi *et al.* [81] studied the MHD flow and heat transfer of two distinct non-Newtonian fluids using the Cattaneo Christov heat flux model. Ullah *et al.* [82] investigated the impact of slip condi-

tion on MHD free convective flow of non-Newtonian fluid over a stretching sheet saturated in a porous medium.

In all the studies cited above and indeed in most other related studies, variations of some important fluid properties with temperature were neglected. In reality, fluid thermal conductivity and viscosity are very sensitive to temperature changes, and more accurate and useful results could be obtained by taking these variations into consideration. For instance, it is well known that the viscosity of engine oil decreases by 24 times when the fluid temperature is increased from 200 C to 800 C, the viscosity of water reduces by 2.7 times and the viscosity of air drops by 1.4 times in the same temperature range. Based on these facts, several studies have been conducted on fluid flow and heat transfer by taking variable fluid properties into consideration. Alam *et al.* [83] examined the impact of variable fluid properties and thermophoresis on unsteady forced convective permeable stretching/shrinking boundary layer. Mosayebidorcheh *et al.* [84] studied the hybrid approach to unsteady Couette flow and heat transfer. Siddiga *et al.* [85] analyzed the variable parameters for the natural convection flow along a vertical wavy cone in a thermally radiating fluid via the finite difference method. Latif *et al.* [86] studied the impact of temperature-dependent viscosity on MHD third order peristaltic fluid flow in a channel. Rashidi *et al.* [87] studied the convective non-Newtonian third grade fluid flow over a linearly stretching sheet. Imtiaz *et al.* [88] investigated third-grade fluid flow with Cattaneo Christov heat flux. Hayat *et al.* [89] analyzed MHD mixed convection flow of a third grade fluid over an exponentially stretching sheet.

Meanwhile, entropy generation minimization is important as it informs thermomechanical designs that have optimal energy utilization efficiency. In such designs, as thermal energy is converted into useful mechanical work, irreversibilities that result in loss of energy are minimized. For this reason, the research

community has continued focus on inherent irreversibility analysis on thermo-fluid flows. Such studies are important as they have a direct desirable impact on contemporary technology and modernity. For instance, the transition from reliance on energy derived from fossil fuels to clean energy sources like wind and solar power requires technology that conserves and optimizes energy utilization. If this is not done, cleaner energy sources may not be able to sustain the worlds energy demand. On the other hand, continued increased burning of fossil fuels is releasing carbon into the atmosphere at a rate that has reached unprecedented levels. Because of the exacerbation of global warming, the world is witnessing the melting of glaciers, uncontrolled runaway fires, devastating floods and other extreme events that are negatively impacting on natural and artificial ecosystems from which life depends on.

Through the advancement of technology in industrial and manufacturing processes, we are witnessing increased miniaturization of devices and processes that require less energy to power them. For thermo-fluid flow systems, entropy generation minimization, as already referred to, also helps in optimizing the use of energy. Entropy generation in a third-grade fluid flow with variable properties was studied by Adesanya [90]. Adesanya and Falade [91] analyzed the entropy generation rate of MHD third grade fluid flow and heat transfer between horizontal parallel plates saturated with porous materials. Kareem *et al.* [92] investigated the magnetic field and Ohmic heating effects on the entropy generation rate of couple stress fluid flow through a porous channel. Mansour *et al.* [93] studied entropy generation analysis for unsteady MHD Casson fluid flow and heat transfer over a stretching sheet.

Inherent irreversibility analysis and entropy generation studies in thermo-fluid flow systems with variable properties have not been fully exhausted. As mentioned, studies have tended to concentrate on unrealistic assumptions of constant

fluid properties. This study contributes to ongoing scientific debates and literature on inherent irreversibility analysis and entropy generation in non-Newtonian fluid flows by investigating third grade fluid flow in channels of varied configurations subjected to various physical effects. On the one hand, we analyse the combined effects of buoyancy, porous media, Navier slip, constant heat flux and convective boundary conditions on entropy generation and irreversibility ratio in a steady incompressible flow of third grade fluid in an inclined channel. On the other hand we carry out a thermodynamic analysis on a steady MHD third-grade fluid flow with variable properties in a horizontal channel with infinite parallel plates. Combined effects of an applied transverse magnetic field and variable linear viscosity and thermal conductivity on entropy generation and irreversibility are investigated. On the third modification, combined effects of buoyancy, porous media, variable viscosity, magnetic field and convective boundary conditions are investigated in an unsteady flow of the same working fluid in a vertical channel filled with saturated porous media. Succinct analysis of the effects of the embedded thermophysical parameters on the flow variables, entropy generation and irreversibility ratio will be carried out with the aid of a graphical approach, quantitative and qualitative descriptions. The analysis may influence parameter regulation criteria that are useful for designs that optimize energy consumption.

The relationships in the problems to be studied in the following chapters are clear, and the problems are deliberately formulated as such to constitute a smooth flowing study. The inclusion of one non-MHD problem is so that MHD effects can be compared and contrasted with non-MHD effects. Each problem is preceded by an introduction that carries a focused literature review directly related to that problem. In this way, a comprehensive systematic study of each problem is achieved.

2.2 Motivation for the Study

While several numerical methods can be applied to solve nonlinear ordinary and partial differential equations, in this study ADM, FDM and SQLM were chosen because of their desirable attributes that have been documented in the previous chapter. It is only through the application of the methods that refinement of solution techniques can be achieved. This is a significant part of the focus of researchers because ultimately it is efficient numerical methods that give rise to reliable solutions. The focus on non-Newtonian fluid is informed by the fact that non-Newtonian fluids dominate industrial applications. The novelty of this study mainly stems from the realistic assumptions of fluid variable properties. Examples of industrial fluid flow systems with engineering relevance and on which MHD analysis is applicable are a flow of molten steel, iron ore, volcanic eruptions, combustible fluids, crude oil at refineries and much more. The significance of Lorentz forces in a moving fluid coupled with the magnetic field is well documented [94]. For instance, this phenomenon is encountered in the following industrial applications: MHD generators, pumps, cooling of nuclear reactors, geothermal energy extractors, thermal insulators, nuclear waste disposal, heat exchangers, petroleum and polymer technology, and heat transfers involving metallurgical processes and many more. With such wide applications, our proposed study is justifiable. Further motivation stems from the contemporary energy dynamics that we cited in the literature survey. A survey of literature revealed that the scope of our study herein has not been fully accounted for in the previous models.

2.3 Significance of the Study

There is a growing demand for economical and maintainable systems across the globe. Most industrial and engineering flow processes and thermal systems are

unable to work at an optimal level due to entropy generation. The determination of entropy generation (EG) is thus extremely vital for upgrading the system performance since EG is the measure of the destruction of accessible work of the system. Through our research study, the factors (or parameters) that contribute to entropy generation can be identified so that their effects can be minimized through intelligent regulation and that the flow system efficiency can be maximised. Moreover, with the global technological advancements on non-Newtonian fluids, the results from the study will help in improving, conserving and upgrading several designs in industrial thermo-fluid systems.

Chapter 3

Thermodynamic Analysis of Magnetohydrodynamic Third Grade Fluid Flow with Variable Properties

Chapter Abstract

In this chapter we computationally study entropy generation in a MHD third grade fluid flow in a horizontal channel with impermeable walls. The fluids viscosity and thermal conductivity are assumed to be dependent on temperature. The flow is driven by an applied uniform axial pressure gradient between infinite parallel plates and is considered to be incompressible, steady and fully developed. ADM is used to obtain series solutions of the nonlinear governing equations. Thermodynamic analysis is done by computing the entropy generation rate and the irreversibility ratio (Bejan number). The effects of the various pertinent embedded parameters on the velocity field, temperature field, entropy generation rate and Bejan number

are analysed through vivid graphical manipulations. The analysis shows that an appropriate combination of thermophysical parameters efficiently achieves entropy generation minimization in the thermomechanical system.The analysis shows that entropy generation minimization is achieved by increasing the magnetic field and the third grade material parameters, and therefore designs and processes incorporating MHD third grade fluid flow systems are far more likely to give optimum and efficient performance.

3.1 Introduction

Behavioural features and characteristics of industrial fluids such as hydrocarbon oils, synthetic esters, polyphenylethers, oil and greases, clay coating and suspensions, paper products, some food stuffs and slurries cannot be modelled by the classical Navier-Stokes constitutive model [95; 96; 97; 98] . These fluids belong to a larger class of non-Newtonian fluids whose complex rheological properties cannot be adequately described by any single constitutive model. They find a diversity of applications in geothermal engineering, petrochemical engineering, lubricants, polymer technology, pharmaceutical applications and many others. This, and their inherent complexity is stimulus to the apparent interest of researchers in the sphere of non-Newtonian fluid flow. One model that describes non-Newtonian character is the fluids of the differential type that was observed to have the ability to represent shear thickening and shear thinning properties of such fluids. The third grade fluid model that is under consideration herein is an example of the fluids of the differential type. In [99] and [100], the mechanics of the fluids of the differential type are described in detail. To date, several investigations on third grade fluid flow in varied flow configurations and conditions have been carried out. Makinde *et al.* [98] examined thermal effects in an

unsteady flow of a reactive variable viscosity third grade fluid in porous saturated medium with asymmetrical convective boundary conditions. Rundora and Makinde [101; 102] investigated the effects of suction/injection and the effects of Navier slip, respectively, on the same type of flow as in [98]. An increase in the suction/injection Reynolds number was observed to retard the velocity and temperature fields, increase the wall shear stress, diminish the wall heat transfer rate and increase the thermal criticality values of the Frank-Kamenetskii parameter. On the other hand, increasing the slip parameters was observed to enhance heat production in the reactive flow. More recently, Chinyoka and Makinde [103] investigated the unsteady, non-isothermal, pressure driven channel flow of a variable viscosity third grade liquid subjected to convective cooling. Other recent studies are in [104; 105; 106; 107].

Meanwhile analysis of electrically conducting fluids in channels in the presence of externally applied magnetic field has also dominated the research landscape. This is owing to pertinent applications of such flows in thermo-electrical systems like heat exchangers, cooling of electronic devices, electromagnetic processing of materials, metal purification and astrophysics applications [108]. When an external magnetic field is imposed onto a moving electrically conducting fluid, current is induced into the fluid, which in turn polarizes the fluid and a drag-like force (Lorentz force) is formed. This MHD phenomenon, following the ground breaking work of Hartmann [60], has contributed to research that continues to improve technological advancement. Hayat *et al.* [109] studied Soret and Dufour effects on MHD flow of a Cason fluid. Unsteady MHD Poiseuille flow between two infinite parallel plates in an inclined magnetic field with heat transfer was investigated by Idowu and Olabode [110]. Bolarin *et al.* [111] investigated the natural convection of a one-dimensional heat generation and viscous dissipation model of a MHD third grade fluid in an inclined cylindrical pipe with radiation.

Other recent MHD investigations are in [112] and [113].

Apart from heat and mass transfer, it is beneficial to optimize the efficiency of thermal devices, thermomechanical systems and processes. This is achieved through entropy generation minimization. Entropy is a thermodynamic quantity representing the unavailability of a systems thermal energy for conversion into mechanical work, often interpreted as the degree of disorder or randomness in the system [114]. Flow and heat transfer processes inevitably undergo changes over time due to energy loses, and such changes are irreversible. This, in a nutshell, is the second law of thermodynamics. Since these changes (processes) increase entropy, entropy generation rate is thus a standard metric used to study the irreversibility effects [115; 116]. In this way, the work lost, usually due to heat transfer, viscous dissipation and conduction, is determined by entropy generation [117]. In a parametric study, a combination of geometrical and physical parameters must be chosen in order to minimize entropy generation. Pursuit, by researchers, for entropy generation minimization conditions in devices and processes is ongoing. Ibáñez [118] studied the combined effects of hydrodynamic slip, magnetic field, suction/injection and convective boundary conditions on the global entropy generation in steady flow of an incompressible electrically conducting fluid through a channel with permeable plates. The results indicated that an appropriate combination of geometrical and physical parameters in the system achieves entropy generation minimization. Adesanya and Falade [91] investigated entropy generation rate in the flow and heat transfer of hydromagnetic third grade fluid in a horizontal channel saturated with porous materials. They obtained their solution using a regular perturbation method. Eegunjobi and Makinde [119] investigated the combined effects of buoyancy and Navier slip on the entropy generation rate in a vertical porous channel with wall suction/injection. Entropy generation analysis for a reactive couple stress fluid flow through a channel saturated with porous

materials was carried out by Adesanya [120]. Analysis of entropy generation for MHD flow of third grade nanofluid over a nonlinear stretching surface embedded in a porous medium was investigated by Hayat *et al.* [121]. Ijaz Khan *et al.* [122] studied entropy optimization in MHD flow of a third grade nanofluid with viscous dissipation and chemical reaction.

To date, only a few authors have investigated third grade fluid flow with variable fluid properties. For instance, constant fluid viscosity and thermal conductivity is a simplification that may produce results that may be divorced from reality. It is a practical reality that viscosity and thermal conductivity are affected by fluid temperature. Flow models where fluid viscosity and thermal conductivity are dependent on temperature can adequately mimic real life models. In the studies [98; 101; 102] referred to earlier, the third grade fluid viscosity was assumed to vary exponentially with temperature. There are not many studies on entropy generation for third grade fluid with variable properties. Adesanya [90] studied the entropy generation rate in a third grade fluid with viscosity and thermal conductivity depending linearly on temperature. The present study is a computational analysis of entropy generation in an MHD third grade fluid where the fluid viscosity and thermal conductivity have a linear dependence on fluid temperature as in [90]. To the best of the author's knowledge, combined effects of magnetic field, variable linear viscosity and thermal conductivity on third grade fluid flow has not been studied. In the sections to follow we present the physics of the problem, entropy generation analysis, the Adomian decomposition method of solution (ADM) and results and discussion of the results.

3.2 Mathematical Model Formulation

We consider a steady fully developed flow of an incompressible third-grade fluid in a channel with infinite plates placed at y=-h and y=h as shown in Fig. 3.1. The fluid is assumed to have variable viscosity and thermal conductivity.

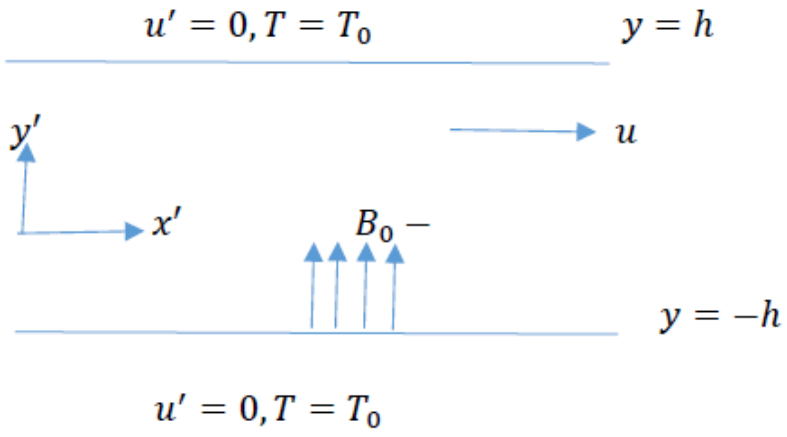

Figure 3.1: Schematic diagram of the problem

We further assume that the fluid is reactive and internal heat generation of the fluid is a linear function of temperature. The independent variables x', y' and h denote the horizontal distance along the plates, the vertical distance and the half of the channel width, respectively. The plates are considered to be impermeable and the no-slip condition applies at the plates. A uniform transverse magnetic field B_0 is imposed externally onto the channel plates. Following [123] and [124], the momentum and energy balance equations for the fully developed flow can be written as

$$\frac{du'}{dx'} + \frac{dv'}{dy'} = 0 \tag{3.1}$$

$$0 = -\frac{dP}{dx'} + \frac{d}{dy'}\left(\mu'(T)\frac{du'}{dy'}\right) + 6\beta_3 \frac{d^2u'}{dy'^2}\left(\frac{du'}{dy'}\right)^2 - \sigma_e B_0^2 u', \tag{3.2}$$

$$0 = \frac{d}{dy'}\left(k'(T)\frac{dT}{dy'}\right) + \mu'(T)\left(\frac{du'}{dy'}\right)^2 + 2\beta_3\left(\frac{du'}{dy'}\right)^4 + Q_0(T - T_0) + \sigma_e B_0^2 u'^2, \tag{3.3}$$

with appropriate boundary conditions

$$\begin{aligned} &u' = 0,\ T = T_0,\ \text{on } y' = \pm h, \\ &\frac{du'}{dy'} = 0,\ \frac{dT}{dy'} = 0,\ \text{on } y' = 0. \end{aligned} \tag{3.4}$$

The temperature dependent viscosity and thermal conductivity take the form [90]

$$\begin{aligned} \mu'(T) &= \mu - \eta_0(T - T_0), \\ k'(T) &= k + \eta_1(T - T_0), \end{aligned} \tag{3.5}$$

where P is the fluid pressure, u' is the fluid velocity, T is the fluid temperature, β_3 is the material coefficient, k' is the thermal conductivity, μ' is the dynamic viscosity, η_0, η_1 are the viscosity and thermal conductivity variation parameters, Q_0 is the heat generated internally, σ_e is the electrical conductivity, B_0 is the magnectic field, T_0 and T_1 are the referenced fluid temperatures. Here, we introduce the following dimensionless variables, wherein the prime letters designate the dimensional physical quantities and the lowercase letters as the corresponding non-dimensional quantities:

$$\begin{aligned} &x = \frac{x'}{h}, y = \frac{y'}{h}, u = \frac{u'}{U}, v = \frac{v'}{U}, \gamma = \frac{\beta_3 U^2}{h^2\mu}, \theta = \frac{T - T_0}{T_1 - T_0}, \alpha = \frac{\eta_0(T_1 - T_0)}{\mu}, \\ &\Omega = \frac{T_1 - T_0}{T_0}, G = -\frac{h^2}{\mu U}\frac{dP}{dx}, \delta = \frac{Q_0 h^2}{k}, B_r = \frac{\mu U^2}{k(T_1 - T_0)}, \lambda = \frac{\eta_1(T_1 - T_0)}{k}, \\ &H^2 = \frac{\sigma_e B_0^2 h^2}{\mu}, \end{aligned} \tag{3.6}$$

where α is a viscosity variation parameter, γ is the third grade material parameter, G is the pressure gradient, θ is the dimensionless fluid temperature, λ is the thermal conductivity variation parameter, B_r is the Brinkman number, H^2 is the

Hartman number, δ is the internal heat generation parameter, Ω is the parameter that measures the temperature difference between the two heat reservoiors, and U represents characteristic velocity. The following non-dimensional nonlinear equations arise:

$$\frac{du}{dx} + \frac{dv}{dy} = 0, \tag{3.7}$$

$$\frac{d^2u}{dy^2} = \alpha\left(\theta\frac{d^2u}{dy^2} + \frac{d\theta}{dy}\frac{du}{dy}\right) - 6\gamma\frac{d^2u}{dy^2}\left(\frac{du}{dy}\right)^2 + H^2u - G, \tag{3.8}$$

$$\frac{d^2\theta}{dy^2} = -\lambda\left(\theta\frac{d^2\theta}{dy^2} + \left(\frac{d\theta}{dy}\right)^2\right) - B_r\left(\frac{d\theta}{dy}\right)^2\left(1 - \alpha\theta + 2\lambda\left(\frac{du}{dy}\right)^2\right) - \delta\theta - B_rH^2u^2. \tag{3.9}$$

The related boundary conditions of the governing equations with dimensionless variables are expressed as

$$\begin{aligned} u &= 0 \text{ on } y = \pm 1, \\ \theta &= 0 \text{ on } y = \pm 1. \end{aligned} \tag{3.10}$$

3.3 Entropy Generation Analysis

As stated earlier, in a thermomechanical system of the nature studied herein, energy loses due to entropy generation arising from heat transfer and viscous dissipation are inevitable. Entropy generation minimization should thus be an important objective of the study, since it is through this that the efficiency of the thermodynamic system is enhanced. Consequently, the local volumetric rate of entropy generation for a viscous incompressible conducting third grade fluid in the presence of magnetic field will be expressed as [125]:

$$E_G = \frac{k'}{T_0^2}\left(\frac{dT}{dy'}\right)^2 + \frac{1}{T_0}\left(\frac{du'}{dy'}\right)^2\left(\mu' + 2\beta_3\left(\frac{du'}{dy'}\right)^2\right) + \frac{\sigma_e B_0^2 u'^2}{T_0}. \tag{3.11}$$

Here,

$$N'_H = \frac{k'}{T_0^2}\left(\frac{dT}{dy'}\right)^2$$

is irreversibility due to heat transfer,

$$N'_F = \frac{1}{T_0}\left(\frac{du'}{dy'}\right)^2\left(\mu' + 2\beta_3\left(\frac{du'}{dy'}\right)^2\right)$$

is entropy generation from viscous dissipation for a third grade fluid and

$$N'_M = \frac{\sigma_e B_0^2 u'^2}{T_0}$$

is local entropy generation owing to the effect of the externally applied magnetic field. Using the non-dimensional variables in equation (3.6) and the non-dimensional entropy generation rate, N_s, defined as

$$N_s = \frac{T_0^2 h^2 E_G}{k(T_1 - T_0)^2},$$

the non-dimensional form of the entropy generation rate (equation (3.11)) becomes

$$N_s = (1 + \lambda\theta)\left(\frac{d\theta}{dy}\right)^2 + \frac{B_r}{\Omega}\left[\left(\frac{du}{dy}\right)^2\left(1 - \alpha\theta + 2\gamma\left(\frac{du}{dy})^2\right) + H^2u^2\right)\right]. \quad (3.12)$$

The corresponding components of equation (3.12) are N_H-entropy generation due to heat transfer, N_F-entropy generation due to fluid friction and N_M-entropy

generation due to magnetic field, and they are given by:

$$\begin{aligned} N_H &= (1+\lambda\theta)\left(\frac{d\theta}{dy}\right)^2, \\ N_F &= \frac{B_r}{\Omega}\left(\frac{du}{dy}\right)^2\left(1-\alpha\theta+2\gamma\left(\frac{du}{dy}\right)^2\right), \\ N_M &= \frac{B_r}{\Omega}\left(H^2u^2\right). \end{aligned} \tag{3.13}$$

The irreversibility ratio parameter denoted by the Bejan number (Be) can be written as [115; 116]:

$$\begin{aligned} Be &= \frac{\text{entropy generation due to heat transfer}}{\text{entropy generation rate}} \\ &= \frac{N_H}{N_S} \\ &= \frac{N_H}{N_H+N_F+N_M} \\ &= \frac{1}{1+\Phi}, \\ \Phi &= \frac{N_F+N_M}{N_H} \end{aligned}$$

3.4 Adomian Decomposition Method of Solution

ADM consists of splitting the equation into linear and nonlinear parts.Writing equation (3.8) and (3.9) in integral form and imposing initial conditions yields:

$$\begin{aligned} u(y) = a_0 &- \int_0^y\int_0^y G dY dY + \int_0^y\int_0^y \alpha\left(\theta\frac{d^2u}{dY^2}+\frac{d\theta}{dY}\frac{du}{dY}\right)dYdY \\ &- \int_0^y\int_0^y 6\gamma\frac{d^2u}{dY^2}\left(\frac{du}{dY}\right)^2 dYdY + \int_0^y\int_0^y H^2u dYdY, \end{aligned} \tag{3.14}$$

$$\theta(y) = b_0 - \int_0^y \int_0^y \lambda \left(\theta \frac{d^2\theta}{dY^2} + \left(\frac{d\theta}{dY} \right)^2 \right) dY dY - \int_0^y \int_0^y \delta\theta dY dY - \int_0^y \int_0^y B_r H^2 u^2 dY dY$$
$$- \int_0^y \int_0^y B_r \left(\frac{d\theta}{dY} \right)^2 \left(1 - \alpha\theta + 2\gamma \left(\frac{du}{dY} \right)^2 \right) dY dY, \tag{3.15}$$

where the constants a_0 and b_0 are to be determined later. The decomposition method represents the solutions of equation (3.14) and (3.15) as a series form [126]:

$$\begin{aligned} u(y) &= \sum_{n=0}^{\infty} u_n, \\ \theta(y) &= \sum_{n=0}^{\infty} \theta_n, \end{aligned} \tag{3.16}$$

where the components $u_n(y)$,$n \geq 0$ and $\theta_n(y)$,$n \geq 0$ are determined recursively. Substituting equation (3.16) into equation (3.14) and (3.15) yields the following algorithm,

$$u_n = a_0 - \int_0^y \int_0^y G dY dY + \int_0^y \int_0^y \alpha A_n dY dY - \int_0^y \int_0^y 6\gamma B_n dY dY + \int_0^y \int_0^y H^2 u_n dY dY, \tag{3.17}$$

$$\theta_n = b_0 - \int_0^y \int_0^y \lambda C_n dY dY - \int_0^y \int_0^y B_r D_n \left(1 - \alpha\theta + 2\gamma F_n \right) dY dY - \int_0^y \int_0^y \delta\theta dY dY$$
$$- \int_0^y \int_0^y B_r H^2 I_n dY dY, \tag{3.18}$$

where A_n, B_n, C_n, D_n, F_n and I_n are the nonlinear terms represented by,

$$\begin{aligned} A_n &= \theta \frac{d^2u}{dY^2} + \frac{d\theta}{dY}\frac{du}{dY}, \\ B_n &= 6\gamma \frac{d^2u}{dY^2}\left(\frac{du}{dY}\right)^2, \\ C_n &= \theta_n \frac{d^2\theta_n}{dy^2} + \left(\frac{d\theta_n}{dy}\right)^2, \\ D_n &= \left(\frac{d\theta_n}{dy}\right)^2, \\ F_n &= \left(\frac{d\ u_n}{dy}\right)^2, \\ I_n &= (u_n)^2. \end{aligned} \tag{3.19}$$

Equations (3.17) and (3.18) can be expressed recursively as:

$$\begin{aligned} u_0 &= a_0 - \int_0^y \int_0^y G dY dY, \\ u_{n+1} &= \int_0^y \int_0^y \left(\alpha A_n - 6\gamma B_n + H^2 u_n\right) dY dY, \end{aligned} \tag{3.20}$$

$$\begin{aligned} \theta_0 &= b_0, \\ \theta_{n+1} &= \int_0^y \int_0^y (-\lambda C_n - B_r D_n \left(1 - \alpha\theta + 2\gamma F_n\right) - \delta\theta - B_r H^2 I_n) dY dY. \end{aligned} \tag{3.21}$$

The nonlinear terms in (3.17) and (3.18) are decomposed into Adomian polynomials as follows:

$$\left.\begin{aligned} A_0 &= \theta_0 \frac{d^2u_0}{dy^2} - \frac{d\theta_0}{dy}\frac{du_0}{dy} \\ A_1 &= \theta_0 \frac{d^2u_1}{dy^2} + \theta_1 \frac{d^2u_0}{dy^2} - \left(\frac{d\theta_0}{dy}\frac{du_1}{dy} + \frac{d\theta_1}{dy}\frac{du_0}{dy}\right) \\ A_2 &= \theta_0 \frac{d^2u_2}{dy^2} + \theta_1 \frac{d^2u_1}{dy^2} + \theta_2 \frac{d^2u_0}{dy^2} - \left(\frac{d\theta_0}{dy}\frac{du_2}{dy} + \frac{d\theta_1}{dy}\frac{du_1}{dy} + \frac{d\theta_2}{dy}\frac{du_0}{dy}\right) \\ &\vdots \end{aligned}\right\} \tag{3.22}$$

$$\left.\begin{aligned} B_0 &= \frac{d^2u_0}{dy^2}\left(\frac{du_0}{dy}\right)^2 \\ B_1 &= 2\frac{d^2u_0}{dy^2}\frac{du_1}{dy}\frac{du_0}{dy} + \frac{d^2u_1}{dy^2}\left(\frac{du_0}{dy}\right)^2 \\ B_2 &= 2\frac{d^2u_0}{dy^2}\frac{du_2}{dy}\frac{du_0}{dy} + \frac{d^2u_0}{dy^2}\left(\frac{du_1}{dy}\right)^2 + 2\frac{d^2u_1}{dy^2}\frac{du_1}{dy}\frac{du_0}{dy} + \frac{d^2u_2}{dy^2}\left(\frac{du_0}{dy}\right)^2 \\ &\vdots \end{aligned}\right\} \tag{3.23}$$

$$\left.\begin{aligned} C_0 &= \theta_0\frac{d^2\theta_0}{dy^2} + \left(\frac{d\theta_0}{dy}\right)^2 \\ C_1 &= \theta_0\frac{d^2\theta_1}{dy^2} + \theta_1\frac{d^2\theta_0}{dy^2} \\ C_2 &= \theta_0\frac{d^2\theta_2}{dy^2} + \theta_2\frac{d^2\theta_0}{dy^2} + \left(\frac{d\theta_1}{dy}\right)^2 \\ &\vdots \end{aligned}\right\} \tag{3.24}$$

$$\left.\begin{aligned} D_0 &= \left(\frac{d\theta_0}{dy}\right)^2 \\ D_1 &= 2\frac{d\theta_0}{dy}\frac{d\theta_1}{dy} \\ D_2 &= \frac{d\theta_0}{dy}\frac{d\theta_2}{dy} + \left(\frac{d\theta_1}{dy}\right)^2 \\ &\vdots \end{aligned}\right\} \tag{3.25}$$

$$\left.\begin{aligned} F_0 &= \left(\frac{du_0}{dy}\right)^2 \\ F_1 &= 2\frac{du_0}{dy}\frac{du_1}{dy} \\ F_2 &= \frac{du_0}{dy}\frac{du_2}{dy} + \left(\frac{du_1}{dy}\right)^2 \\ &\vdots \end{aligned}\right\} \tag{3.26}$$

$$\left.\begin{aligned} I_0 &= u_0^2 \\ I_1 &= 2u_0u_1 \\ I_=&2u_0u_2 + u_1^2 \\ &\vdots \end{aligned}\right\} \tag{3.27}$$

By truncating the solutions, we have the approximate solutions as:

$$u(y) = \sum_{n=0}^{m} u_n, \tag{3.28}$$

$$\theta(y) = \sum_{n=0}^{m} \theta_n. \tag{3.29}$$

3.5 Validation of Results

In the absence of magnetic field ($B_0 = 0$), the results obtained are consistent with the results reported by Adesanya [90].

3.6 Results and Discussion

In the ensuing discussion, we study the hydromagnetic third grade fluid flow in a horizontal channel with impermeable walls. The fully developed flow is driven by an applied uniform axial pressure gradient. A succinct theoretical analysis of the effects of the thermophysical parameters on the flow velocity and temperature field is carried out with the aid of vivid graphical simulations. The influence of the embedded parameters on entropy generation is also analysed similarly. Unless a parameter is being varied, we employ the default values: $\alpha = 0.1$, $\gamma = 0.1$, $G = 1$, $\lambda = 0.1$, $B_r = 0.5$, $H^2 = 0.1$, $\delta = 0.5$, and $\Omega = 1$.

3.6.1 Velocity Profiles

Figures 3.2 to 3.6 show the response of the fluid velocity profile to changes in the values of the pertinent parameters embedded in the flow system. In Fig.3.2 the velocity profile is observed to increase with an increase in the variable vis-

cosity parameter. This phenomenon is explained by the fact that as the variable viscosity parameter α increases, the fluid viscosity decreases and the fluids resistance to flow is diminished. An increase in the third grade material parameter γ significantly decreases the velocity profile (Fig.3.3). Increasing γ means that the non-Newtonian properties of the fluid are enhanced and the fluid gets thickened in the processes. The thickened fluid inevitably has increased resistance to flow. The effects of the magnetic field on the fluid velocity profiles is displayed in Fig.3.4. As pointed out earlier, the magnetic field induces current that polarizes the fluid and a drag-like force (Lorentz force) is formed. This force tends to agglomerate the fluid particles making them heavier leading to reduced velocity as depicted in the figure. The Brinkmann number, $B_r = \frac{\mu U^2}{k(T_1 - T_0)}$, is a measure of heat flux from the channel plates to the viscous fluid. It is the ratio between heat produced by the viscous dissipation and heat transported by molecular conduction from the plates. Higher values of the Brinkmann number therefore signify slower conduction of heat produced by viscous dissipation and hence the larger the temperature rise. As the fluid temperature rises, the fluid viscosity decreases and the fluid particles are thus freer to move faster. This explains the increasing velocity profile (Fig.3.5) with an increase in the Brinkmann number. In Fig.3.6, an increase in the pressure gradient parameter leads to an increase in the fluid velocity. This is indeed not surprising since the fluid motion is driven by pressure gradient. The fluid velocity profile is largely unaltered by the internal heat generation parameter σ and the thermal conductivity variation parameter, λ. These parameters only enter the velocity equation implicitly through the temperature field and thus their effects on the fluid velocity are expected to be not as noticeable as those on the temperature profile.

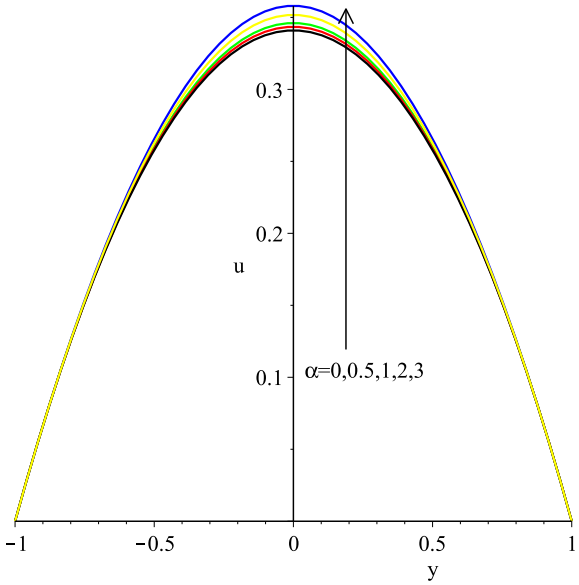

Figure 3.2: Variation of the velocity profile with the variable viscosity parameter

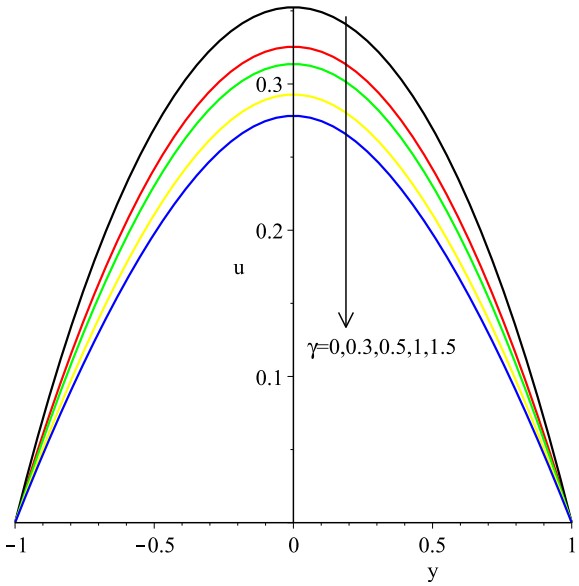

Figure 3.3: Variation of the velocity profile with the third grade material parameter

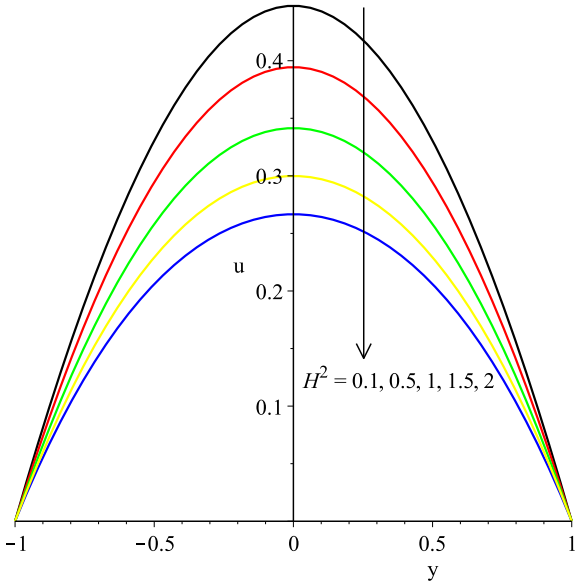

Figure 3.4: Variation of the velocity profile with the magnetic field parameter

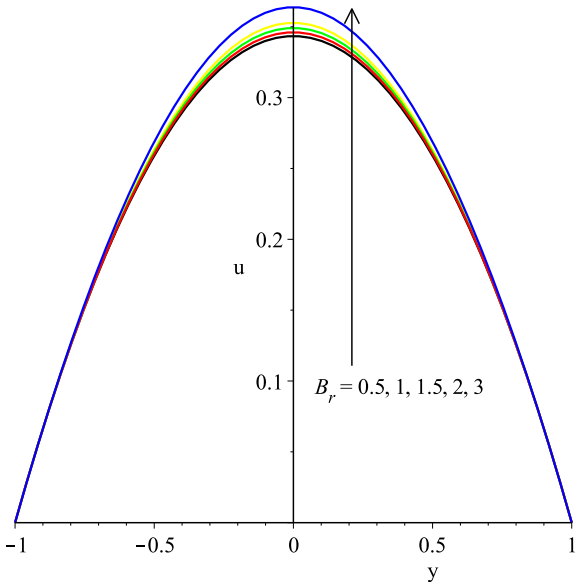

Figure 3.5: Variation of the velocity profile with the Brinkmann number

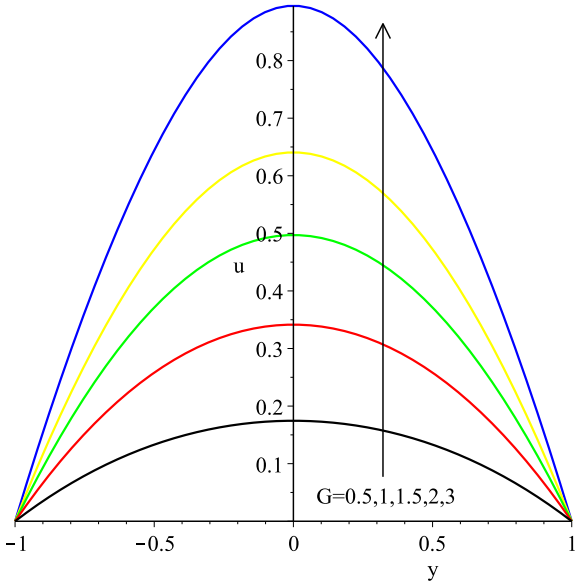

Figure 3.6: Variation of the velocity profile with the pressure gradient parameter

3.6.2 Temperature Profiles

Figure 3.7 shows that an increase in variable viscosity parameter α increases the fluid temperature due to rise in the temperature difference. As explained earlier, the variable viscosity parameter increases the fluid velocity. Now, the increased velocity in turn increases the viscous heating source terms in the energy equation resulting in increased temperature. The effect of the third grade material parameter γ on the fluid temperature is illustrated in Fig.3.8 and shows a significant decrease of temperature with increasing values of the parameter. This can be explained by the coupling effect since the fluid velocity was also seen to decrease with the increasing non-Newtonian parameter. In Fig.3.9 and Fig.3.10, the internal heat generation parameter δ and the Hartmann number are observed to significantly increase the fluid temperature. The phenomenon in Fig.3.9 is not surprising as increasing δ means that more heat is being generated in the bulk of the fluid. In Fig.3.10, larger values of the Hartmann number correspond to

an increase in the drag-like Lorentz force (resistive force) that has already been referred to. This force is caused by the current that the magnetic field induces into the conducting fluid and the passage of current produces heat through Joule heating (Ohmic heating), also known as resistive heating. It is thus inevitable that the fluid temperature rises with increasing magnitude of the magnetic field. In Fig.3.11, higher values of the Brinkmann number causes significant increase in the fluid temperature. This phenomenon has already been explained in attempt to describe the variation seen in Fig.3.5 under section 3.6.1 In Fig.3.12 an increase in the pressure gradient parameter increases the fluid temperature as it does to fluid velocity. The fluid temperature profile was also observed to be marginally decreased by an increase in the thermal conductivity variation parameter .

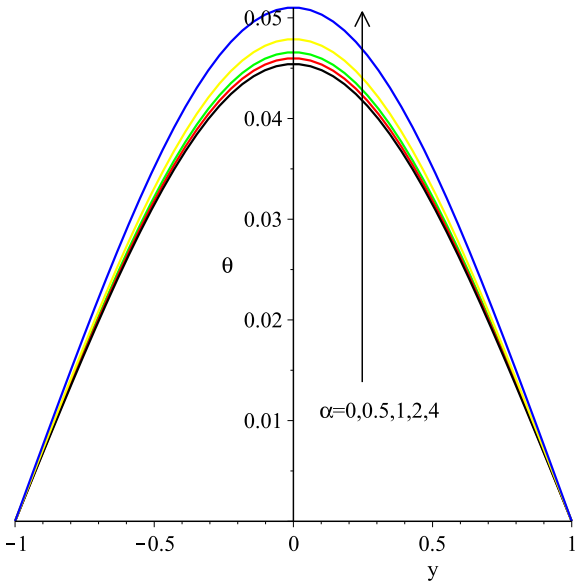

Figure 3.7: Effects of the variable viscosity parameter on fluid temperature

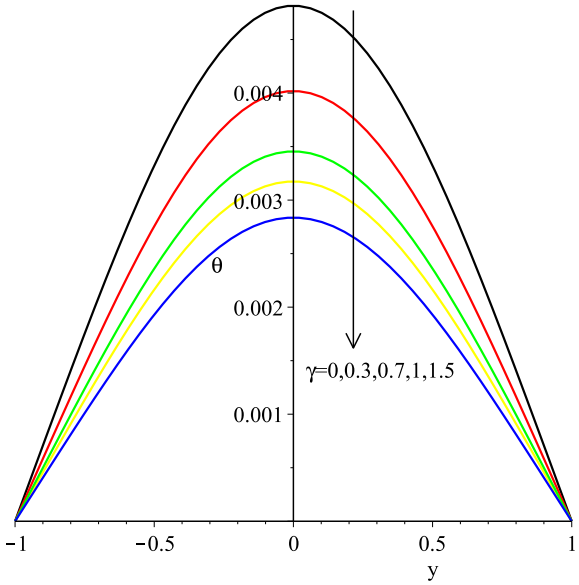

Figure 3.8: Effects of the third grade material parameter on fluid temperature

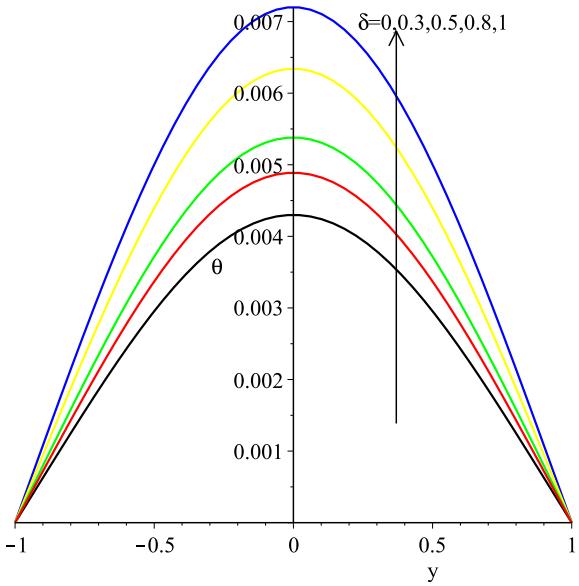

Figure 3.9: Effects of the internal heat generation parameter on fluid temperature

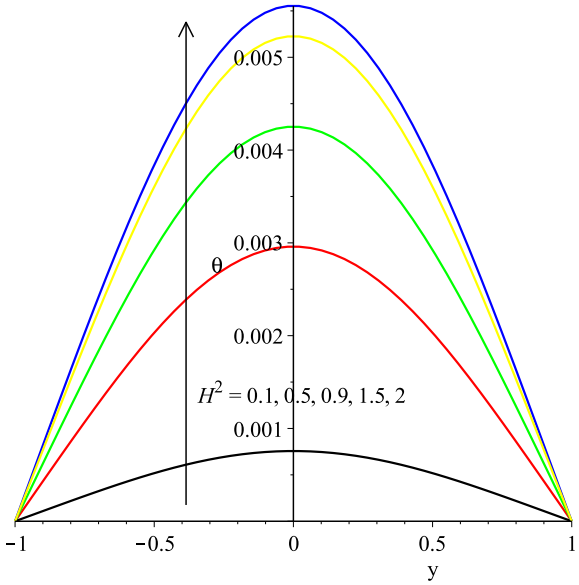

Figure 3.10: Effects of the magnectic field on fluid temperature

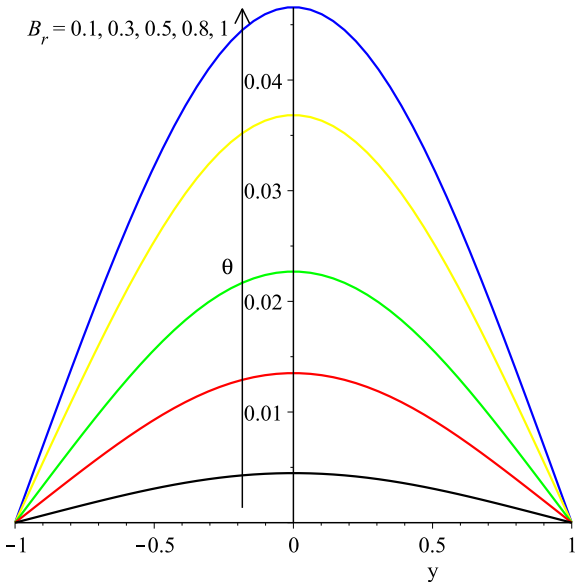

Figure 3.11: Effects of the Brinkmann number on fluid temperature

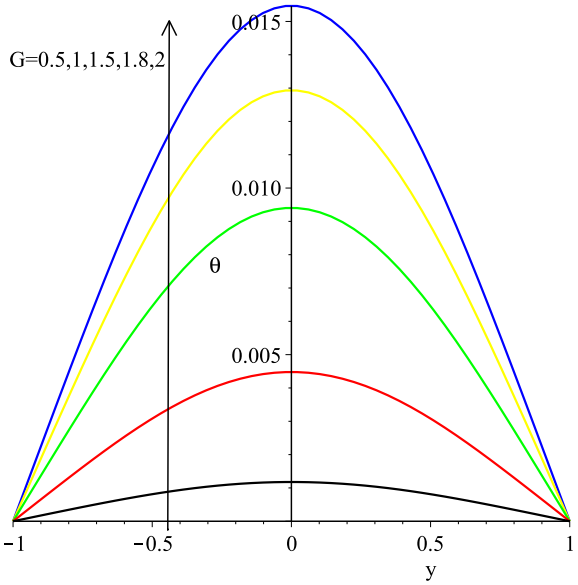

Figure 3.12: Effects of the pressure gradient parameter on fluid temperature

3.6.3 Entropy Generation Profile

Figures 3.13 to 3.16 illustrate the variation of the entropy generation rate profile as influenced by increasing values of the Brinkmann number, the Hartmann number, the third grade material parameter and the pressure gradient parameter. Fig.3.13 shows the entropy generation rate increasing with increasing values of the Brinkmann number. In Fig.3.14, as we move closer to the walls of the channel ($0.4 \leq \mid y \mid \leq 1$), the entropy generation rate decreases with increasing intensity of the magnetic field. Closer to the centre of the channel, as the magnetic field intensity increases, the entropy generation rate initially increases before stabilizing. This phenomenon can be explained by the fact that the externally applied magnetic field damps the fluid flow more closer to the channel walls than at the core region. In this way, the entropy generation rate closer to the channel walls is bound to be mostly diminished near the walls than at the channel core region where fluid velocity is maximum. Increasing the values of the third grade ma-

terial parameter (non-Newtonian parameter) diminishes the entropy generation rate within the channel (see Fig.3.15), while in Fig.3.16 the effect of the pressure gradient parameter almost mirrors that of the Brinkmann number. It was also observed that the internal heat generation parameter has a marginal effect on entropy generation and both the thermal conductivity variation parameter and the variable viscosity parameter showed no influence on the rate of entropy generation

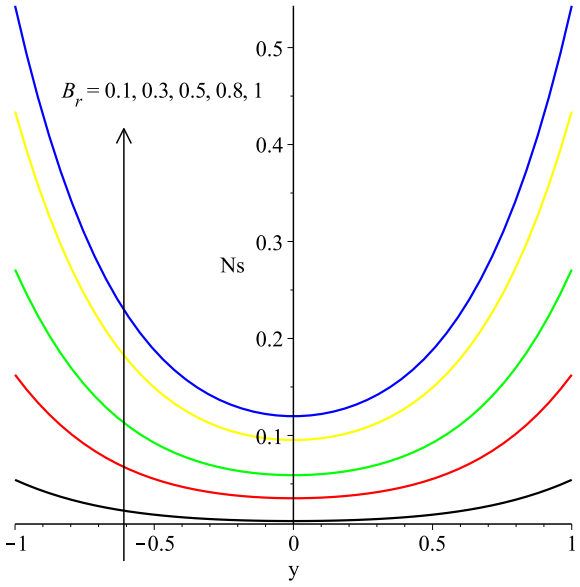

Figure 3.13: Effects of the Brinkmann number on entropy generation rate

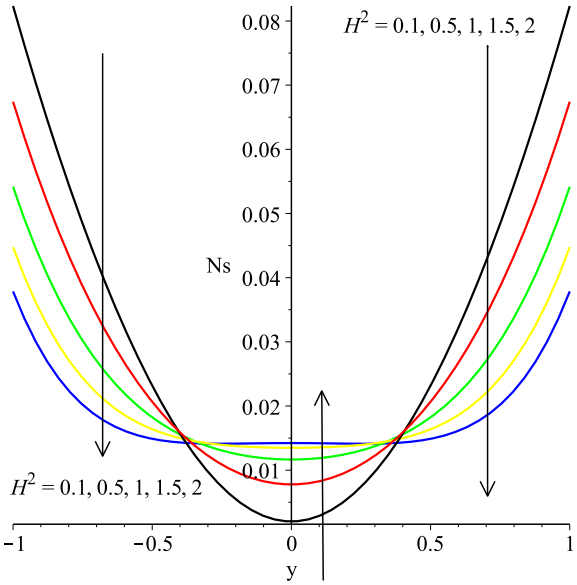

Figure 3.14: Effects of the Hartmann number on entropy generation rate

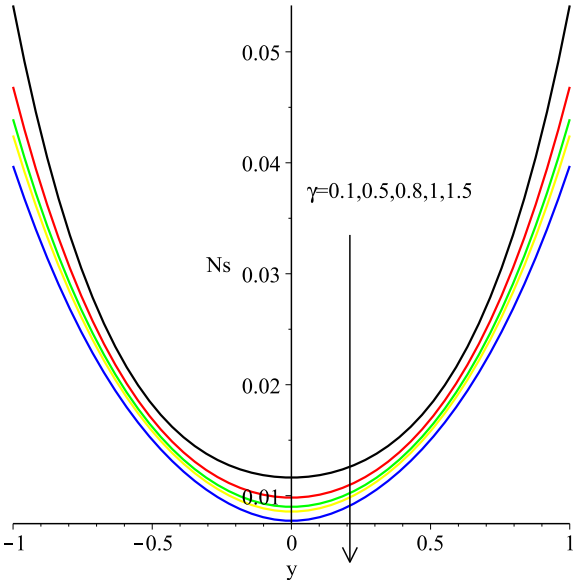

Figure 3.15: Effects of the third grade material parameter on entropy generation rate

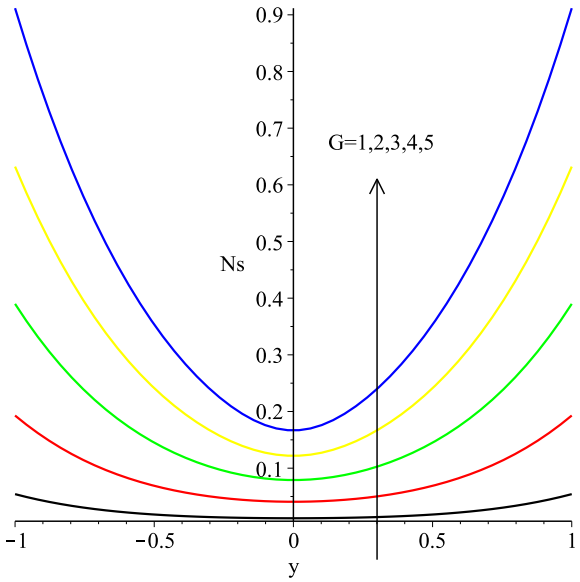

Figure 3.16: Effects of the pressure gradient parameter on entropy generation rate

3.6.4 Bejan Number Profile

The Bejan number profile in response to the various parameters is displayed in Figures 3.17 to 3.21. What comes out prominently within the figures is the observation that the irreversibility ratio at the centre of the channel is stable at value *Be=0*. This shows that at the centre of the channel the irreversibilities due to fluid friction effects and magnetic field dominate. Elsewhere within the channel and towards the channel walls, the figures show that heat transfer irreversibilities are dorminant. Figs. 3.17, 3.18, 3.19 and 3.21 show the dominance effects of heat transfer irreversibility increasing with increasing values of the Brinkmann number, the Hartmann number, the internal heat generation parameter and the pressure gradient parameter respectively. In Fig.3.20 the third grade material parameter has the opposite effect. The irreversibility ratio was also observed to be marginally affected by variable viscosity parameter.

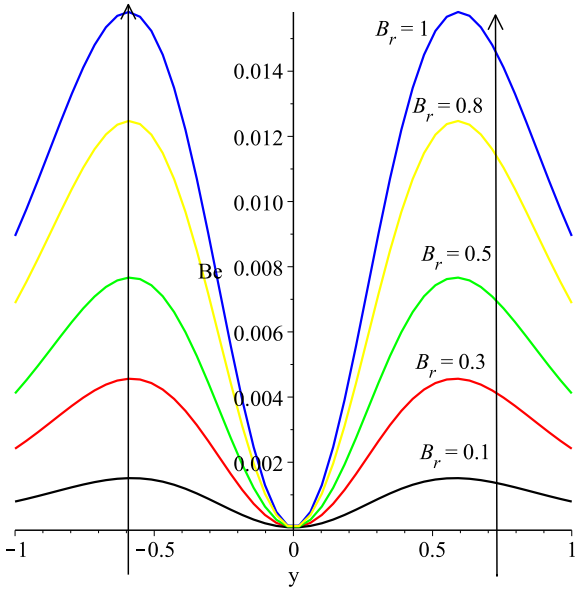

Figure 3.17: Effects of the Brinkmann number on irreversibility ratio

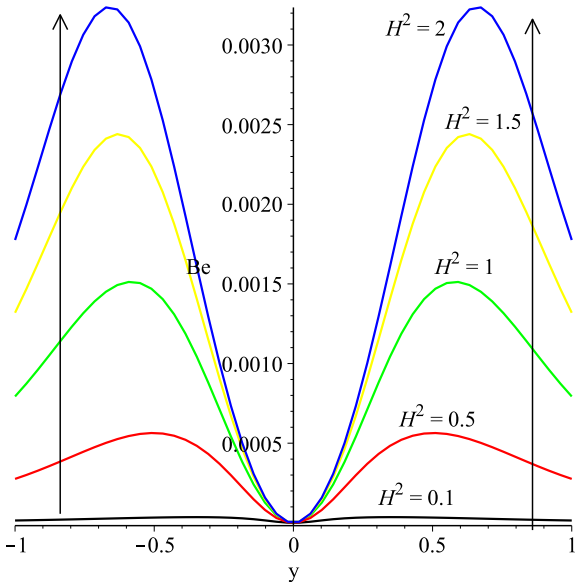

Figure 3.18: Effects of the Hartmann number on irreversibility ratio

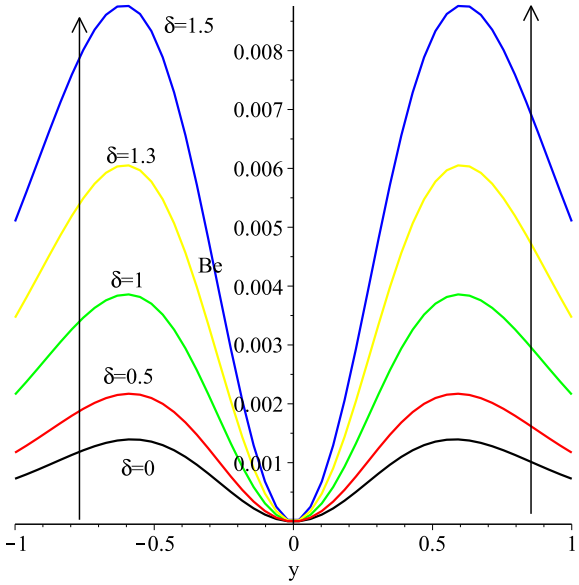

Figure 3.19: Effects of the internal heat generation parameter on irreversibility ratio

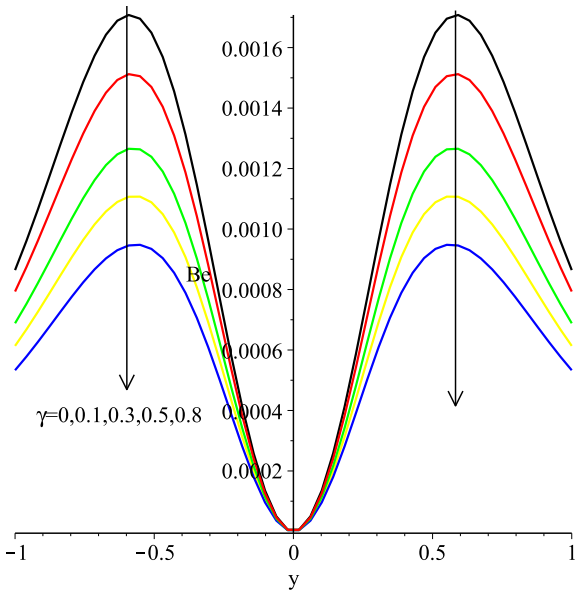

Figure 3.20: Effects of the third grade material parameter on irreversibility ratio

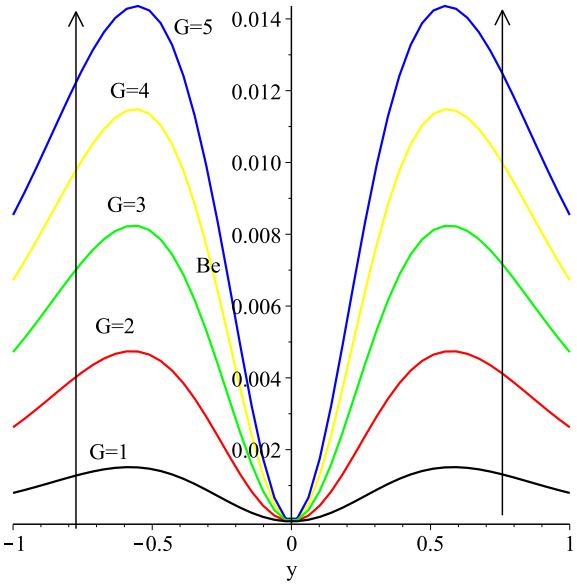

Figure 3.21: Effects of the pressure gradient parameter on irreversibility ratio

3.7 Conclusion

In this chapter, a computational study of entropy generation in a fully developed incompressible variable properties MHD third grade fluid flow in a horizontal channel with impermeable walls has been achieved. The Adomian decomposition method was used to compute series solutions of the fluid velocity and temperature profiles. The influence of the various parameters embedded in the flow system on the velocity, temperature, entropy generation rate and Bejan number were analysed through the use of graphical simulations. The following findings manifested:

- The fluid velocity profile is enhanced by the viscosity variation parameter and Brinkmann number, while the third grade material parameter and the magnetic field have a flow dampening effect.

- The viscosity variation parameter, the internal heat generation parameter,

the magnetic field and the Brinkmann number increase fluid temperature but the third grade material parameter has the opposite effect.

- Towards the channel walls, the magnetic field reduces the entropy generation rate, while at the centre of the channel it increases it before stabilizing.

- The Brinkmann number increases the entropy generation rate, while the third grade material parameter has a diminishing effect.

- At the center of the channel, the irreversibility ratio is stable at value $Be=0$ signifying dominance of irreversibilities due to fluid friction effects and magnetic field. Towards the channel walls heat transfer irreversibilities dominate.

- The Brinkmann number, the magnetic field and the internal heat generation parameter increase the dominance effect of the heat transfer irreversibility but the third grade material parameter has the opposite effect.

- Since entropy generation minimization is achieved by increasing the magnetic field and the third grade material parameters, designs and processes incorporating MHD third grade fluid flow systems are far more likely to give optimum and efficient performance.

Chapter 4

Entropy Generation Analysis in a Steady Flow of a Reactive Variable Viscosity Third Grade Fluid Through a Porous Saturated Medium with Navier-Slip and Convective Boundary Conditions

Chapter Abstract

This chapter investigates the combined effects of Navier slip, convective boundary conditions, porous medium permeability and variable viscosity on a reactive third-grade fluid flow through an inclined channel filled with a saturated porous

medium. The flow is assumed to be driven by combined effects of an applied axial constant pressure gradient and buoyancy. The lower plate is subjected to convective heat exchange with the ambient while the upper plate is kept at a constant heat flux. We employ the SQLM to numerically solve the coupled nonlinear flow governing equations. Fluid velocity and temperature profiles, entropy generation rate and irreversibility ratio are computed graphically and analysed quantitatively and qualitatively regarding the effects of the parameters embedded in the flow system. A residual error analysis demonstrated high accuracy and convergence of the numerical method. The results on flow velocity and temperature distribution, entropy generation rate and Bejan number revealed fascinating manifestations that have profound implications in designing of thermomechanical systems. In particular, the results on entropy generation and irreversibility ratio computations are pertinent to optimal designs of systems that achieve efficient energy utilization.

4.1 Introduction

In recent years, many researchers have paid renewed interest and attention to the flow of reactive fluids because of the evolution of advanced techniques in manufacturing processes, which has led to the reduction in the size of various industrial and engineering designs. In particular, energy transfer and variable viscosity property of a fluid have been of vast interest among researchers [98; 127; 128; 129; 130; 131; 132; 133]. Industrial and technological applications are found in areas such as atmospheric flows, thermal regulation, cooling of electronic devices, nuclear reactors, thermal hydraulics and many others. Flow devices that involve the manipulation of fluid flow in various geometries have proliferated owing to improvements in science and technological innovation.

Meanwhile, entropy generation minimization in thermo-fluid flows is critically

important in improving efficiency of machines and processes. Bejan [115] defines entropy as a thermodynamic quantity that represents the unavailability of a systems thermal energy for conversion into mechanical work. Efficient energy utilization during the convection in any fluid flow system is one of the fundamental problems in engineering. In the industry, issues like productivity, sustainability and competitiveness require engineering solutions, and such solutions are heavily reliant on mathematical models. Modern economies are being urged to curtail their energy dependence on fossil fuels in order to mitigate the continuous depletion of the ozone layer that is causing the acceleration of global warming. The deleterious consequences of global warming like runaway fires, rising sea levels and melting of glaciers are occurring at unsustainable rates in the present day. As more clean renewable energy forms are being sought to replace fossil fuels, it has become more and more urgent for economic systems to conserve more and more energy for continued sustainability. Thus, the need for continued research on entropy generation minimization cannot be over-emphasized.

The problem of the slip flow regime is very important in this era of modern science and rapid industrialization. In many practical applications, the fluid adjacent to a solid surface does not take the velocity of the surface. The fluid at the surface has a finite tangential velocity, it slips along the surface. The assumption of the no-slip boundary condition has been the norm in most studies despite the fact that the no-slip boundary condition is a hypothesis rather than a condition deduced from any principle. Evidences of slip of a fluid on a solid surface were reported by several authors including Mathews and Hill [134] and Zhu and Granick [135]. Rundora and Makinde [102; 136] reported on the computational effects of Navier slip on unsteady flow of a reactive variable viscosity third-grade fluid through a porous saturated medium with asymmetric convective boundary conditions. Das *et al.* [137] studied the combined effects of magnetic field, Navier

slip and convective cooling on the entropy generation in an unsteady MHD flow through a channel. This chapter aims to investigate the combined effects of Navier slip, variable viscosity, porous medium permeability and convective boundary conditions on entropy generation in a steady flow of a reactive third-grade fluid through an inclined channel filled with a porous saturated medium.

4.2 Mathematical Formulation

Consider a steady flow of an incompressible variable viscosity, reactive third grade fluid through an inclined channel filled with a homogeneous and isotropic porous medium as shown in Fig.4.1

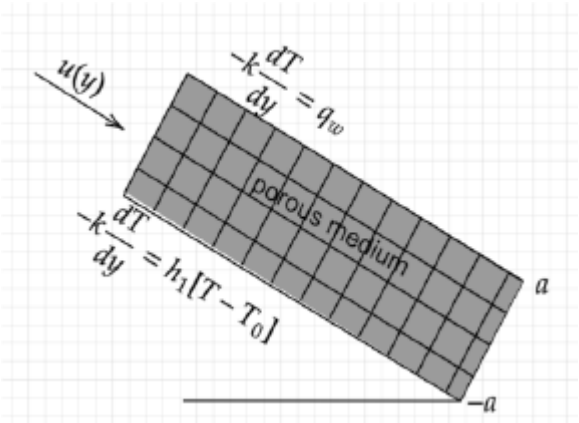

Figure 4.1: Schematic diagram of the problem

The lower wall of the channel is subjected to convective heat exchange with the surrounding medium, while the upper wall is subjected to a constant heat flux. It is assumed that the convective heat exchange with the ambient follows Newton's law of cooling. The flow is assumed to be induced by an applied axial constant pressure gradient and buoyancy force. Neglecting the reacting viscous fluid consumption, the model equations emanating from the momentum and heat

balance can be written as [138; 139; 102]:

$$0 = -\frac{d\bar{P}}{d\bar{x}} + \frac{d}{d\bar{y}}\left(\bar{\mu}(T)\frac{d\bar{u}}{d\bar{y}}\right) + 6\beta_3\frac{d^2\bar{u}}{d\bar{y}^2}\left(\frac{d\bar{u}}{d\bar{y}}\right)^2 - \frac{\bar{\mu}(T)\bar{u}}{K} + \rho g\beta(T - T_0)sin(\omega), \quad (4.1)$$

$$0 = k\frac{d^2T}{d\bar{y}^2} + \left(\frac{d\bar{u}}{d\bar{y}}\right)^2\left[\bar{\mu}(T) + 2\beta_3\left(\frac{d\bar{u}}{d\bar{y}}\right)^2\right] + \frac{\bar{\mu}(T)\bar{u}^2}{K} + QC_0A\left(\frac{hT}{vl}\right)^m e^{-\frac{E}{RT}}, \quad (4.2)$$

with appropriate boundary conditions

$$\begin{aligned} \bar{y} = -a: \quad \lambda_1\bar{u} = \bar{\mu}(T)\frac{d\bar{u}}{d\bar{y}}, \quad -k\frac{dT}{d\bar{y}} = h_1[T - T_0], \\ \bar{y} = a: \quad \lambda_2\bar{u} = \bar{\mu}(T)\frac{d\bar{u}}{d\bar{y}}, \quad -k\frac{dT}{d\bar{y}} = q_w. \end{aligned} \quad (4.3)$$

$\bar{P}$ is the modified fluid pressure, $\bar{x}$ and $\bar{y}$ are the axial and normal coordinates to the inclined channel, $\bar{u}$ is the fluid velocity, h_1 is the heat transfer coefficient at the lower plate, T_0 is the fluid initial temperature, T is the fluid temperature, g is the acceleration due to gravity, ω is the angle of inclination, β_3 is the third-grade material coefficient, k is the thermal conductivity, K is the Porous medium permeability, $\bar{\mu}$ is the fluid dynamic viscosity, ρ is the density, Q is the heat generated internally, C_0 is the initial concentration of the reactant species, A is the reaction rate constant, λ_1 and λ_2 are the slip coefficients at the lower and upper channel walls respectively, q_w is the constant heat flux, E is the activation energy, h is the Boltzmann's constant, l is the Planck's number, R is the universal gas constant, v is the vibration frequency, β is the volumetric thermal expansion coefficient, m is the numerical exponent such that the three values represent numerical exponents for sensitised, Arrhenius and biomolecular kinetics respectively as $m \in \{-2, 0, 0.5\}$[140; 141]. The temperature dependent viscosity $\bar{\mu}(T)$ can be expressed as

$$\bar{\mu}(T) = \mu_0 e^{-b(T - T_0)} \quad (4.4)$$

where μ_0 is the initial fluid viscosity at temperature T_0 and b is the viscosity variation parameter. Introducing the following non-dimensional variables into equations (4.1) - (4.4),

$$y = \frac{\bar{y}}{a}, \quad x = \frac{\bar{x}}{a}, \quad f = \frac{\bar{u}\rho a}{\mu_0}, \quad \alpha = \frac{bRT_0^2}{E}, \quad G = -\frac{dP}{dx}, \quad \Omega = \frac{\beta_3\mu_0}{\rho^2 a^4}, \quad Da = \frac{K}{a^2},$$
$$P = \frac{a^2\rho\bar{P}}{\mu_0^2}, \quad \epsilon = \frac{RT_0}{E}, \quad \theta = \frac{E(T-T_0)}{RT_0^2}, \quad Gr = \frac{\rho^2 g\beta a^3 RT_0^2}{\mu_0^2 E}, \quad Br = \frac{\mu_0^3 E}{a^2\rho^2 kRT_0^2},$$
$$\delta^2 = \frac{1}{Da}, \quad \beta_1 = \frac{\mu_0}{\lambda_1 a}, \quad \beta_2 = \frac{\mu_0}{\lambda_2 a}, \quad Bi = \frac{ah_1}{k}, \quad \lambda = \frac{QEAa^2C_0}{kRT_0^2}\left(\frac{hT_0}{\nu l}\right)^m e^{-\frac{E}{RT_0}}, \tag{4.5}$$

we obtain the non-dimensional governing equations

$$e^{-\alpha\theta}f'' + 6\Omega f''f'^2 - \alpha e^{-\alpha\theta}f'\theta' - \delta e^{-\alpha\theta}f + Gr\theta Sin(\omega) + G = 0, \tag{4.6}$$

$$\theta'' + Brf'^2(e^{-\alpha\theta} + 2\Omega f'^2) + \delta Bre^{-\alpha\theta}f^2 + \lambda(1+\epsilon\theta)^m exp\left(\frac{\theta}{1+\epsilon\theta}\right) = 0, \tag{4.7}$$

with corresponding non-dimensional boundary equations

$$\begin{aligned} y = -1: \quad & f = \beta_1 e^{-\alpha\theta}f', \quad \theta' = -Bi\theta, \\ y = 1: \quad & f = \beta_2 e^{-\alpha\theta}f', \quad \theta' = -Bi\theta, \end{aligned} \tag{4.8}$$

where Ω is the third grade fluid material parameter, P is the fluid pressure, G is the pressure gradient, α is the variable viscosity parameter, ϵ is the activation energy parameter, Gr is the Grashof number, Br is the Brinkman number, β_1, β_2 are the lower and upper wall slip parameters respectively, Bi is the Biot number, Da is the Darcy number, δ is the porous medium shape parameter, λ is the Frank-Kamenetsikii parameter, θ is the non-dimensional fluid temperature, x and y are the non-dimensional axial and normal coordinates to the inclined channel and f is the non-dimensional fluid velocity.

4.3 Entropy Generation Analysis

The local volumetric rate of entropy generation for a viscous incompressible third grade fluid in the presence of porous media will be expressed as

$$E_G = \frac{k}{T_0}\frac{d^2T}{d\bar{y}^2} + \frac{\bar{\mu}(T)}{T_0}\left(\frac{d\bar{u}}{d\bar{y}}\right)^2\left(1 + \frac{2\beta_3}{\bar{\mu}(T)}\left(\frac{d\bar{u}}{d\bar{y}}\right)^2\right) + \frac{\bar{\mu}(T)\bar{u}^2}{KT_0}, \tag{4.9}$$

where the first term is the heat transfer irreversibility, the second term is the entropy generation due to third grade fluid viscous dissipation, and the last term is the irreversibility due to the presence of porous media. Using the non−dimensional parameters and variables (4.5), we get the equation for the non−dimensional entropy generation rate as

$$N_s = \theta'' + Bre^{-\alpha\theta}\left[f'^2(1 + 2\Omega e^{\alpha\theta}f'^2) + \delta^2 f^2\right]. \tag{4.10}$$

The non-dimensional entropy generation rate, $N_s = \frac{E_G a^2 E}{kRT_0}$, is the ratio of the volumetric entropy generation rate to the characteristic entropy generation rate. Equation (4.10) can be broken down into

$$\begin{aligned} N_s &= N_h + N_f, \\ N_h &= \theta'', \\ N_f &= Bre^{-\alpha\theta}\left[f'^2(1 + 2\Omega e^{\alpha\theta}f'^2) + \delta^2 f^2\right], \end{aligned} \tag{4.11}$$

where N_h is the entropy generation due to heat transfer irreversibility and N_f is the entropy generation due to the combined fluid viscous dissipation and porosity of the porous medium. The Bejan number (Be) is used to evaluate the irreversibil-

ity distribution and defined as

$$Be = \frac{N_h}{N_h + N_f}. \tag{4.12}$$

According to Bejan [63], the Bejan number varies from 0 to 1, where $Be = 0$ tells us that the irreversibility due fluid viscous dissipation and porosity dominate, $Be = \frac{1}{2}$ indicates that the irreversibility due fluid viscous dissipation and porosity is equal to irreversibility due heat transfer in the entropy production, and $Be = 1$ reveals that irreversibility due to heat transfer dominates.

4.4 Method of Solution

The system of nonlinear ordinary differential equations (4.6) - (4.7), with boundary conditions (4.8) is solved numerically by the SQLM. Firstly, quasilinearisation iteration scheme is applied to linearize the system. Bellman and Kalaba [70] introduced this QLM which is a generalisation of the Newton-Raphson method for solving nonlinear boundary value problems. The quasilinearisation technique is utilised to linearise the equations before they are solved using the SQLM. We let

$$F = e^{-\alpha\theta} f'' + 6\Omega f'' f'^2 - \alpha e^{-\alpha\theta} f'\theta' - \delta e^{-\alpha\theta} f + Gr\theta Sin(\omega) + G = 0, \tag{4.13}$$

$$H = \theta'' + Br f'^2(e^{-\alpha\theta} + 2\Omega f'^2) + \delta Br e^{-\alpha\theta} f^2 + \lambda(1+\epsilon\theta)^m exp\left(\frac{\theta}{1+\epsilon\theta}\right) = 0. \tag{4.14}$$

Reducing the non-linear equations (4.13) and (4.14) to linear equations using QLM, we let f_r, θ_r be an approximate current solution and f_{r+1}, θ_{r+1} be an improved solution of the system of equations. Assuming $|f_{r+1} - f_r| \ll 1$ and $|\theta_{r+1} - \theta_r| \ll 1$, we linearise the equations by expanding F and H using Taylor

series expansion. We have

$$a_{2,r}f''_{r+1} + a_{1,r}f'_{r+1} + a_{0,r}f + b_{1,r}\theta'_{r+1} + b_{0,r}\theta_{r+1} = R_{1,r}, \tag{4.15}$$

$$c_{2,r}\theta''_{r+1} + c_{1,r}\theta'_{r+1} + c_{0,r}\theta + d_{1,r}f'_{r+1} + d_{0,r}f_{r+1} = R_{2,r}, \tag{4.16}$$

with new non−dimensional boundary conditions

$$\begin{aligned} y = -1: \quad & f_{r+1} = \beta_1 e^{-\alpha\theta_r} f'_r, \quad \theta'_{r+1} = -Bi\theta_r, \\ y = 1: \quad & f_{r+1} = \beta_2 e^{-\alpha\theta_r} f'_r, \quad \theta'_{r+1} = -Bi\theta_r, \end{aligned} \tag{4.17}$$

where

$$\begin{aligned}
a_{2,r} &= \frac{\partial F}{\partial f''_r} = e^{-\alpha\theta_r} + 6\Omega f'^2_r, \\
a_{1,r} &= \frac{\partial F}{\partial f'_r} = -\alpha e^{-\alpha\theta_r}\theta'_r + 12\Omega f''_r f'_r, \\
a_{0,r} &= \frac{\partial F}{\partial f_r} = -\delta e^{-\alpha\theta_r}, \\
b_{1,r} &= \frac{\partial F}{\partial \theta'_r} = -\alpha e^{-\alpha\theta_r} f'_r, \\
b_{0,r} &= \frac{\partial F}{\partial \theta_r} = -\alpha e^{-\alpha\theta_r} f''_r + \alpha^2 e^{-\alpha\theta_r} f'_r\theta'_r - \alpha\delta e^{-\alpha\theta_r} f_r + GrSin(\omega), \\
c_{2,r} &= \frac{\partial H}{\partial \theta''_r} = 1, \\
c_{1,r} &= \frac{\partial H}{\partial \theta'_r} = 0, \\
c_{0,r} &= \frac{\partial H}{\partial \theta_r} = -\alpha Bre^{-\alpha\theta_r} f'^2_r - \alpha\delta Bre^{-\alpha\theta_r} f^2_r + \lambda(1+\epsilon\theta)^{m-2} exp\left(\frac{\theta}{1+\epsilon\theta}\right)(m\epsilon(1+\epsilon\theta)+1), \\
d_{1,r} &= \frac{\partial H}{\partial f'_r} = 2Bre^{-\alpha\theta_r} f'_r + 8Br\Omega f'^3_r, \\
d_{0,r} &= \frac{\partial H}{\partial f'_r} = 2\delta Bre^{-\alpha\theta_r} f_r,
\end{aligned}$$

$$R_{1,r} = e^{-\alpha\theta_r} f_r'' - \alpha e^{-\alpha\theta_r}\theta_r' f_r' + 6\Omega f_r'' f_r'^2 - \delta e^{-\alpha\theta_r} f_r,$$
$$R_{2,r} = Br f_r'^2(e^{-\alpha\theta_r} + 2\Omega f_r'^2) + \delta Br e^{-\alpha\theta_r} f_r^2 + \lambda(1+\epsilon\theta_r)^m exp\left(\frac{\theta}{1+\epsilon\theta_r}\right). \tag{4.18}$$

The QLM iteration scheme (4.15) and (4.16) is solved using the Chebyshev spectral collocation method. The approximations for the unknown functions are done by using Chebyshev interpolating polynomials in such a way that they are collocated at the Gauss-Lobatto points defined as

$$\tau_i = cos\left(\frac{\pi i}{N}\right), \quad i = 0, 1, 2, ..., N, \tag{4.19}$$

where N is the number of collocation points. The functions f_{r+1} and θ_{r+1} at the collocation points are represented by

$$\begin{aligned} f_{r+1}(\tau) &= \sum_{k=0}^{N} f_{r+1}(\tau_k) T_k(\tau_i), \\ \theta_{r+1}(\tau) &= \sum_{k=0}^{N} \theta_{r+1}(\tau_k) T_k(\tau_i), \quad i = 0, 1, 2, ..., N, \end{aligned} \tag{4.20}$$

where T_k is the k^{th} Chebyshev polynomial defined by

$$T_k(\tau) = cos(kcos^{-1}\tau). \tag{4.21}$$

The derivatives of f_{r+1} and θ_{r+1} at the collocation points are represented as

$$\begin{aligned}\frac{d^p f_{r+1}}{dy^p} &= \sum_{k=0}^{N} \mathbf{D}_{ki}^p f_{r+1}(\tau_k),\\ \frac{d^p \theta_{r+1}}{dy^p} &= \sum_{k=0}^{N} \mathbf{D}_{ki}^p \theta_{r+1}(\tau_k),\end{aligned} \tag{4.22}$$

where p is the order of differentiation and $\mathbf{D}$ is the Chebyshev spectral differential matrix of order $(N+1)\times(N+1)$. We substitute equations (4.19) - (4.22) into equations (4.15) - (4.16) to obtain

$$\left[a_{2,r}\mathbf{D}^2 + a_{1,r}\mathbf{D} + a_{0,r}\mathbf{I}\right]\mathbf{F_{r+1}} + \left[b_{1,r}\mathbf{D} + b_{0,r}\mathbf{I}\right]\mathbf{\Theta_{r+1}} = \mathbf{R_{1,r}}, \tag{4.23}$$

$$\left[d_{1,r}\mathbf{D} + d_{0,r}\mathbf{I}\right]\mathbf{F_{r+1}} + \left[c_{2,r}\mathbf{D}^2 + c_{1,r}\mathbf{D} + c_{0,r}\mathbf{I}\right]\mathbf{\Theta_{r+1}} = \mathbf{R_{2,r}}, \tag{4.24}$$

where $\mathbf{I}$ is $(N+1)\times(N+1)$ identity matrix.
Putting equations (4.23) and (4.24) in a matrix form we get

$$\begin{bmatrix} A_{11} & A_{12} \\ A_{21} & A_{22} \end{bmatrix}\begin{bmatrix} \mathbf{F_{r+1}} \\ \mathbf{\Theta_{r+1}} \end{bmatrix} = \begin{bmatrix} \mathbf{R_{1,r}} \\ \mathbf{R_{2,r}}, \end{bmatrix} \tag{4.25}$$

where

$$\begin{aligned} A_{11} &= a_{2,r}\mathbf{D}^2 + a_{1,r}\mathbf{D} + a_{0,r}\mathbf{I},\\ A_{12} &= b_{1,r}\mathbf{D} + b_{0,r}\mathbf{I},\\ A_{21} &= d_{1,r}\mathbf{D} + d_{0,r}\mathbf{I},\\ A_{22} &= c_{2,r}\mathbf{D}^2 + c_{1,r}\mathbf{D} + c_{0,r}\mathbf{I},\\ \mathbf{F_{r+1}} &= [f_{r+1}(\tau_0), f_{r+1}(\tau_1), f_{r+1}(\tau_0), ..., f_{r+1}(\tau_{i-1}), f_{r+1}(\tau_i)]^T,\\ \mathbf{\Theta_{r+1}} &= [\theta_{r+1}(\tau_0), \theta_{r+1}(\tau_1), \theta_{r+1}(\tau_0), ..., \theta_{r+1}(\tau_{i-1}), \theta_{r+1}(\tau_i)]^T. \end{aligned} \tag{4.26}$$

The approximate solutions for $\mathbf{F}$ and $\mathbf{\Theta}$ are obtained by solving the matrix system (4.25),

$$\begin{bmatrix} \mathbf{F_{r+1}} \\ \mathbf{\Theta_{r+1}} \end{bmatrix} = \begin{bmatrix} A_{11} & A_{12} \\ A_{21} & A_{22} \end{bmatrix}^{-1} \begin{bmatrix} \mathbf{R_{1,r}} \\ \mathbf{R_{2,r}} \end{bmatrix} \tag{4.27}$$

and we use a suitable initial approximation that satisfies the boundary conditions of equations (4.6) and (4.7) as

$$f_0(y) = -\frac{1}{2}Gy^2 - \frac{G(\beta_1+\beta_2)y}{\beta_1-\beta_2+2} - \frac{1}{2}\frac{G(4\beta_1\beta_2-3\beta_1+3\beta_2-2)}{\beta_1-\beta_2+2}, \tag{4.28}$$

$$\theta_0(y) = 0. \tag{4.29}$$

4.5 Results and Discussion

Combined effects of temperature-dependent viscosity, porous media permeability, Navier slip and convective boundary conditions on the flow of a reactive third grade fluid in an inclined channel have been studied. In the following discussion, we carry out a detailed thermodynamic analysis of the dependence of the fluid velocity and temperature profiles, the entropy generation and the irreversibility ratio on the various thermophysical parameters embedded in the flow system. We present the SQLM graphical solutions and provide a qualitative description of the simulated variations. Unless otherwise stated, the following parameter values are employed: $\alpha = 0.1$, $\Omega = 0.1$, $\delta = 0.1$, $Gr = 0.8$, $\omega = \pi/4$, $G = 1$, $Br = 0.5$, $\lambda = 0.1$, $\epsilon = 0.1$, $\beta_1 = 0.1$, $\beta_2 = 0.1$, $Bi = 5.0$, and $m = 0.5$. Where a parameter is not varied, these will be the default values used.

4.5.1 Residual Analysis

The accuracy and convergence of the SQLM were validated by performing a residual error analysis. The residual errors were calculated to gain understanding of the accuracy, as defined by

$$||Res(f)||_\infty = ||e^{-\alpha\theta}f'' + 6\Omega f''f'^2 - \alpha e^{-\alpha\theta}f'\theta' - \delta e^{-\alpha\theta}f + Gr\theta Sin(\omega) + G||,$$

$$||Res(\theta)||_\infty = ||\theta'' + Brf'^2(e^{-\alpha\theta} + 2\Omega f'^2) + \delta Bre^{-\alpha\theta}f^2 + \lambda(1+\epsilon\theta)^m exp\left(\frac{\theta}{1+\epsilon\theta}\right)||.$$

The error infinity norms, which are used to confirm the convergence of the SQLM approximations are defined by

$$\text{Error(f)} = \max_{0\leq i\leq N} \parallel \mathbf{F_{r+1,i}} - \mathbf{F_{r,i}} \parallel_\infty,$$

$$Error(\theta) = \max_{0\leq i\leq N} \parallel \mathbf{\Theta_{r+1,i}} - \mathbf{\Theta_{r,i}} \parallel_\infty .$$

We note that the accuracy of order 10^{-5} for residual errors were attained after two iterations for $f(y)$ and $\theta(y)$ as shown in Table 4.1, and this shows that the method is highly accurate with a good convergence rate. To have a clearer picture of the convergence rates, we plot the residual errors against the number of iterations in Fig.4.2. Figure 4.2 shows that an increase in the number of iterations results in a decrease in the error infinity norm and the method converges after two iterations.

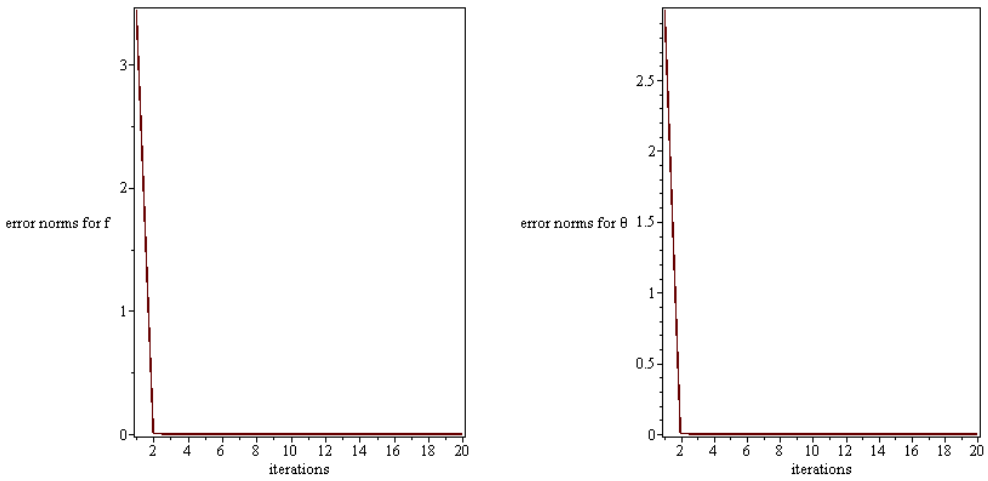

((a)) ((b))

Figure 4.2: (a) Error infinity norm for $f(y)$ and (b) Error infinity norm for $\theta(y)$

4.5.2 Velocity Profile

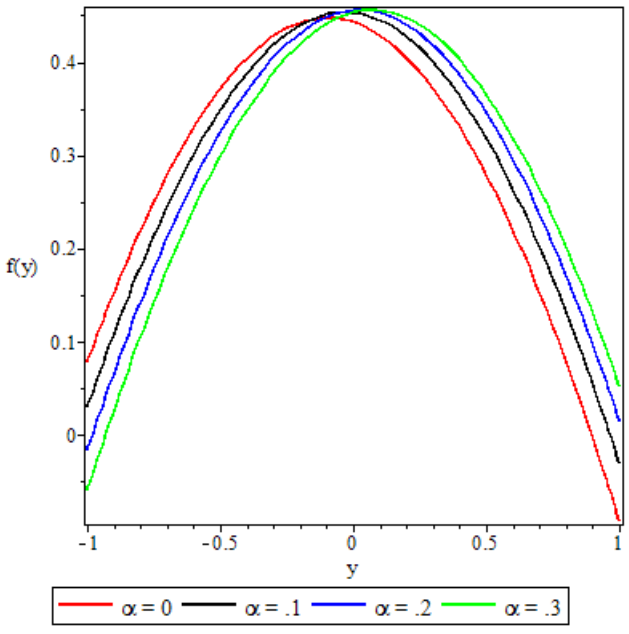

Figure 4.3: Variation of the velocity profile with the variable viscosity parameter

Table 4.1: Residual errors when $\alpha = 0.1$, $\Omega = 0.1$, $\delta = 0.1$, $Gr = 0.8$, $Br = 0.5$, $\lambda = 0.1$, $\omega = (\pi/4)$, $G = 1$,$\epsilon = 0.1$, $\beta_1 = 1$, $\beta_2 = 0.1$, $Bi = 5.0$, $m = 0.5$

Iterations (i)	**Error norm for** $f(y)$	**Error norm for** $\theta(y)$
1.0000	3.4440509	2.9974374
2.0000	0.0029493302	0.0045507285
3.0000	$7.4336997 \times 10^{-06}$	$4.5201419 \times 10^{-06}$
4.0000	$6.3871925 \times 10^{-10}$	$7.9216664 \times 10^{-11}$
5.0000	$1.2640627 \times 10^{-14}$	$6.8049385 \times 10^{-16}$
6.0000	3.977×10^{-20}	$4.9541979 \times 10^{-21}$
7.000	$2.5233673 \times 10^{-25}$	$3.4350721 \times 10^{-26}$
8.0000	4.63×10^{-30}	4.332×10^{-30}
9.0000	1.01×10^{-30}	2.85×10^{-30}
10.0000	1.87×10^{-30}	1.52×10^{-30}
11.0000	1.60×10^{-30}	2.993×10^{-30}
12.0000	2.21×10^{-30}	2.25×10^{-30}
13.0000l	1.25×10^{-30}	8.91×10^{-30}
14.0000	1.38×10^{-30}	4.777×10^{-30}
15.0000	3.83×10^{-30}	2.637×10^{-30}
16.0000	2.40×10^{-30}	5.093×10^{-30}
17.0000	1.10×10^{-30}	6.264×10^{-30}
18.0000	1.91×10^{-30}	4.164×10^{-30}
29.0000	3.54×10^{-30}	5.028×10^{-30}
20.0000	3.72×10^{-30}	6.960×10^{-30}

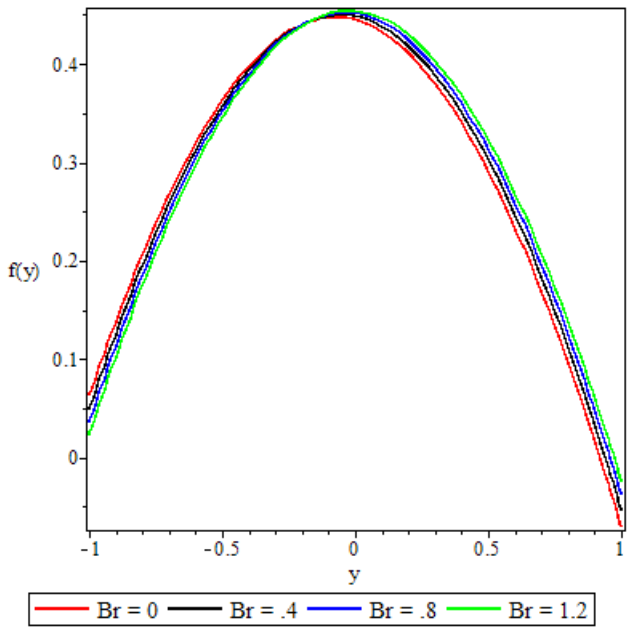

Figure 4.4: Variation of the velocity profile with the Brinkman number

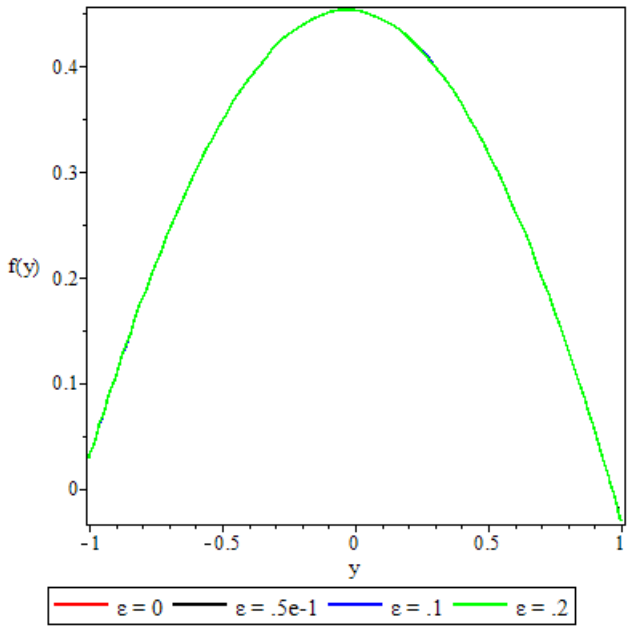

Figure 4.5: Variation of the velocity profile with the activation energy parameter

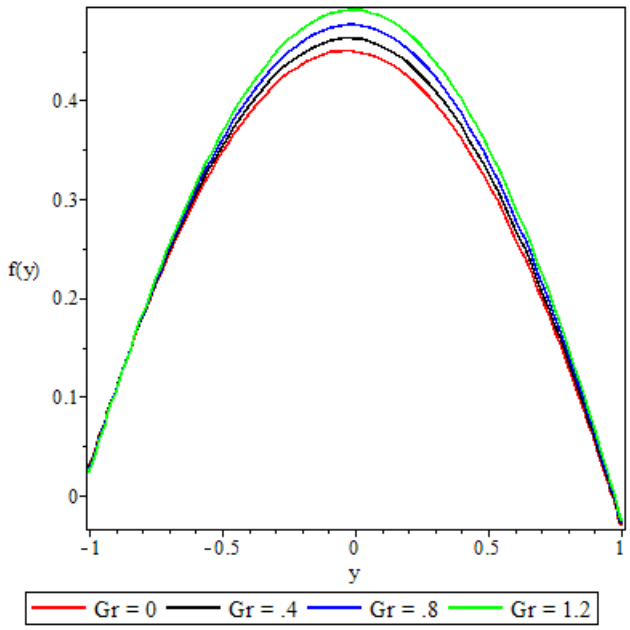

Figure 4.6: Variation of the velocity profile with the Grashof number

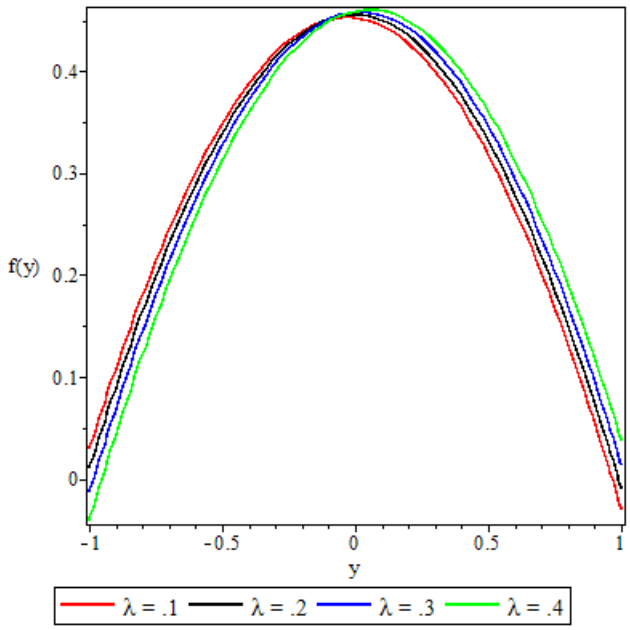

Figure 4.7: Variation of the velocity profile with the Frank-Kamenetsikii parameter

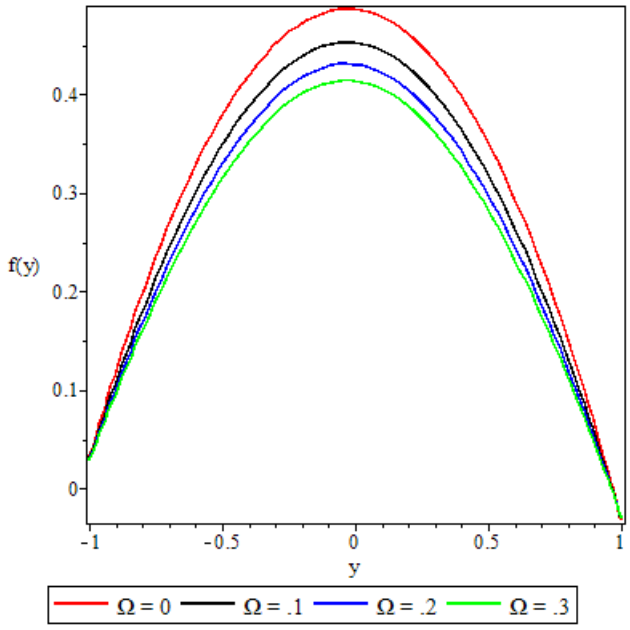

Figure 4.8: Variation of the velocity profile with the third grade material parameter

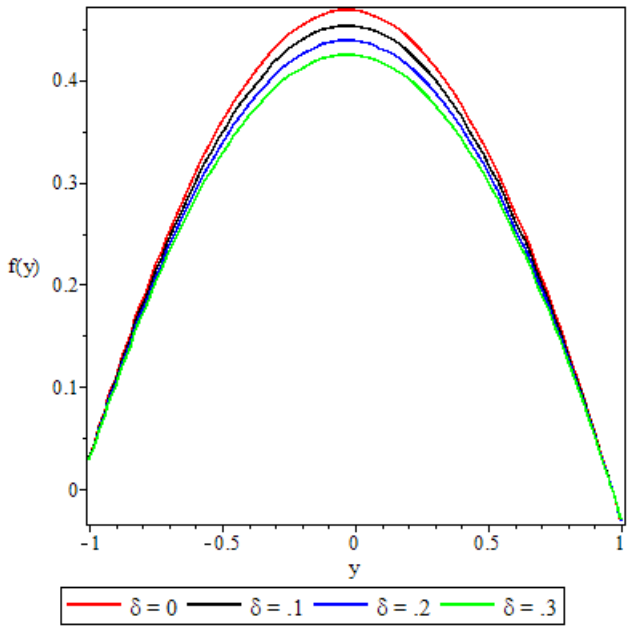

Figure 4.9: Variation of the velocity profile with porous medium shape factor parameter

The response of the fluid velocity profile to the various flow parameters is displayed in Figs. $4.3 - 4.9$. The figures reveal parabolic velocity profiles where the maximum velocity is recorded at the centre of the channel. Figure 4.3 reveals that from the centre of the channel towards the lower wall, the velocity profile decreases with increasing values of the variable viscosity parameter α. On the other hand, towards the upper channel wall, the figure shows the profile increasing with the variable viscosity parameter. Bearing in mind that increasing values of the variable viscosity parameter means that the fluid viscosity is reduced, this observation is to be expected since the lower wall is subjected to convective heat exchange with the ambient and on the upper wall there is a constant heat flux. As the fluid emits heat into the ambient the fluid viscosity increases resulting in velocity retardation. In Fig.4.4 the Brinkmann number Br is observed to affect the fluid velocity in a way similar to the variable viscosity parameter, although

its effect is less pronounced as compared to the effect of the variable viscosity parameter. Since the Brinkmann number is a measure of heat flux from the channel plates to the viscous fluid, the observed similarity is to be expected.

In Fig.4.5 we see that the activation energy parameter ϵ has no significant effect on the fluid velocity. This is explained by the fact that the activation energy parameter only enters the velocity equation implicitly through the temperature/viscosity coupling. In this way, its effects on the velocity can at best be marginal. An increase in the Grashof number Gr, Fig.4.6, is observed to increase the fluid velocity. Variations in the Grashof number explain the buoyancy effects on the flow. Higher Grashof numbers point to increased buoyancy source terms that result in the corresponding increase in the fluid velocity as illustrated in Fig.4.6. The variation of the fluid velocity in response to increasing values of the Frank-Kamenetsikii parameter (chemical reaction parameter λ) is displayed in Fig.4.7. An increase in the chemical reaction parameter means that the rate of chemical reaction increases, and so are the heating source terms. Fig.4.7 shows that towards the lower channel wall, the reaction parameter retards the velocity, whereas towards the upper wall the velocity is enhanced. At the lower wall, as explained earlier, convective heat emitted out into the ambient means that the reaction rate is suppressed and so the fluid particles have less energy to move. At the upper wall, a constant heat flux into the fluid boosts the rate of chemical reaction that results in increased excitation of the fluid particles.

Figures 4.8 and 4.9 show the flow damping effects of the third grade material parameter and the porous medium shape parameter δ, respectively. An increase in the third grade material parameter Ω results in corresponding increases in the non-Newtonian properties of the fluid, like the visco-elastic effects and others, that induce increased resistance to flow. On the other hand, increasing the porous medium shape parameter means that the pore spaces in the porous matrix are

reduced, resulting in reduced porosity and hence damping the flow.

4.5.3 Fluid Temperature Distribution

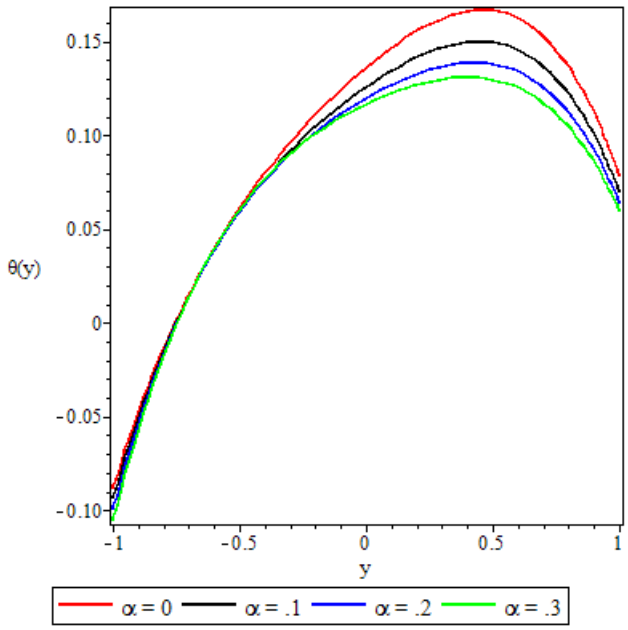

Figure 4.10: Variation of the temperature distribution with the variable viscosity parameter

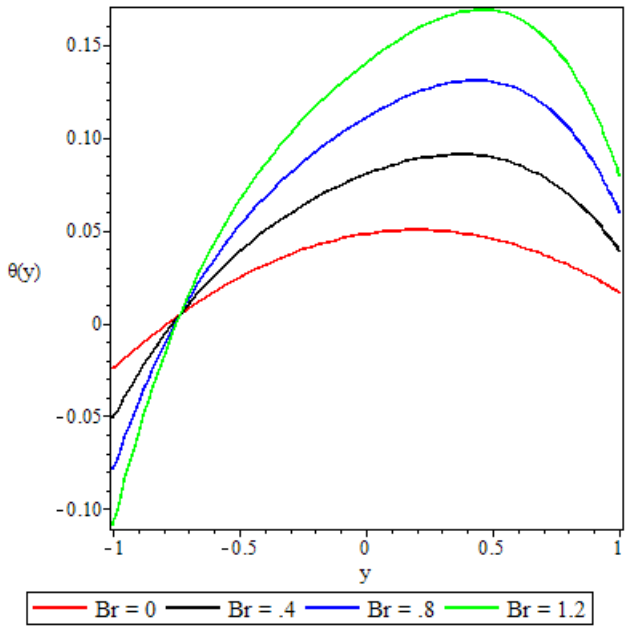

Figure 4.11: Variation of the temperature distribution with the Brinkmann number

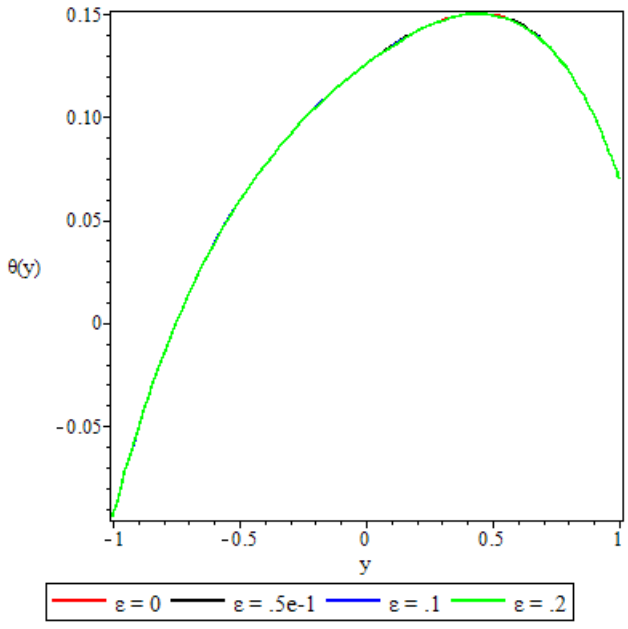

Figure 4.12: Variation of the temperature distribution with the activation energy parameter

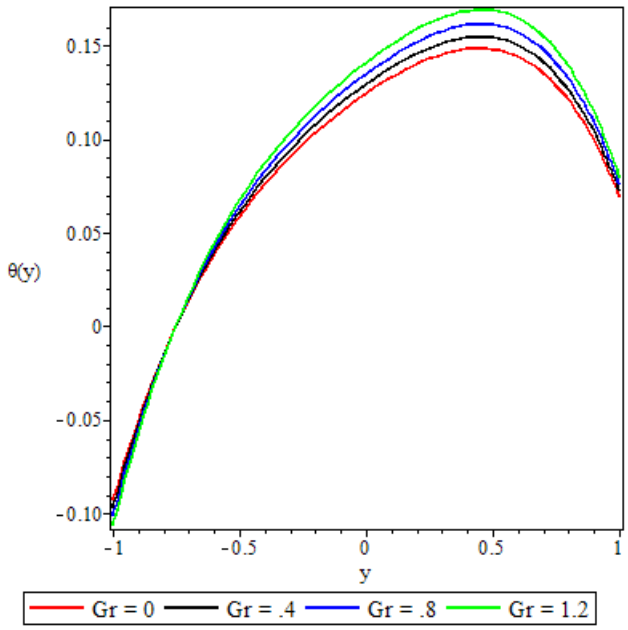

Figure 4.13: Variation of the temperature distribution with the Grashof number

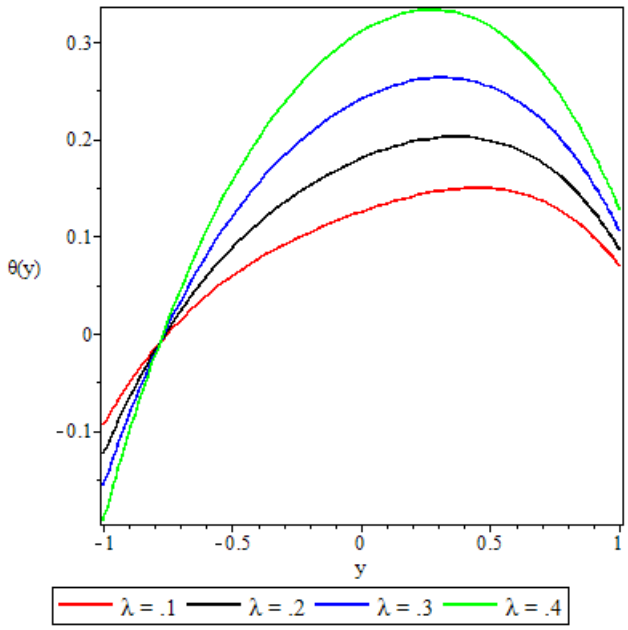

Figure 4.14: Variation of the temperature distribution with the Frank-Kamenetsikii parameter

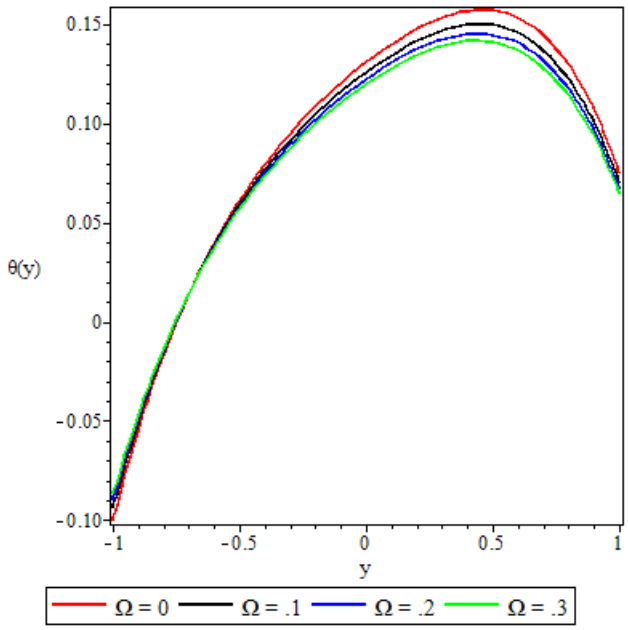

Figure 4.15: Variation of the temperature distribution with the third grade material parameter

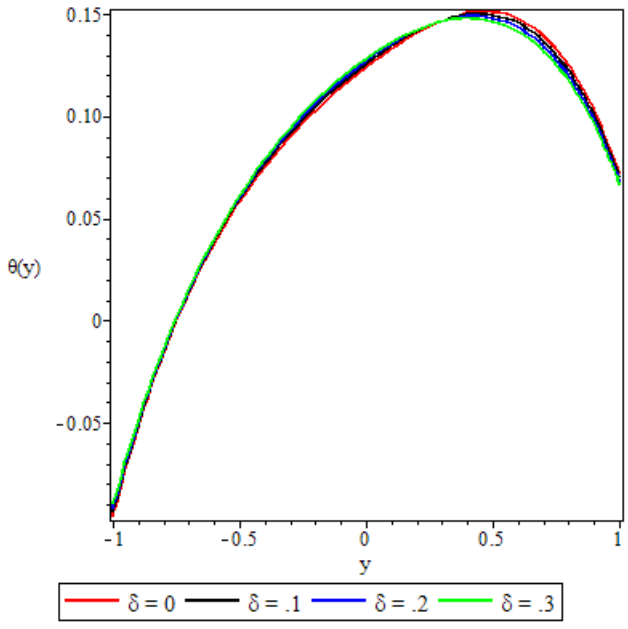

Figure 4.16: Variation of the temperature distribution with the porous medium shape parameter

Figures $4.10 - 4.16$ display variations of the fluid temperature profile in response to various flow governing parameters. A common feature that is revealed by all these graphs is the dipping of the fluid temperature to very low levels as we move closer to and at the lower channel wall. This is attributed to the high Biot number ($Bi = 5.0$) at the lower channel wall that was set as the default value in all the computations. In general, high values of the Biot number render increased convective heat loss from the wall to the ambient, leading to a decrease in the wall temperature. Higher degrees of convective cooling at the lower wall induces a significant temperature drop in the bulk of the fluid closer to the wall.

Except for Fig.4.12, where the activation energy parameter shows only marginal effects on the fluid temperature, and Fig.4.15, where the third grade material parameter retards the fluid temperature, all the other figures show the fluid temperature increasing with an increase in the values of the variable viscosity parameter, the Brinkmann number, the Grashof number, the chemical reaction parameter, and the porous medium shape parameter. The Brinkmann number and the chemical reaction parameter are observed to cause the most significant increase in fluid temperature. As alluded to earlier in the discussion, increasing values of the variable viscosity parameter means that the fluid viscosity is reduced, and this diminishes the fluids resistance to flow. The resultant increased fluid velocity increases the viscous heating source terms in the temperature equation, leading to the elevation of fluid temperature as depicted in Fig.4.10. In Fig.4.11, the Brinkmann number, a measure of heat flux from the channel wall into the fluid, is observed to increase the fluid temperature significantly as pointed to earlier. In Fig.4.13, increasing buoyancy forces lead to an increase in fluid temperature. The heat flux from the upper channel wall into the fluid leads to a volumetric thermal expansion of the fluid which induces some overturning instability in the fluid that causes the fluid particles to move faster. Due to coupling, the increased veloc-

ity increases the heating source terms in the temperature equation, resulting in enhanced fluid temperature. Figure 4.14 shows the fluid temperature increasing significantly with an increase in the values of the chemical reaction parameter. This phenomenon has been explained earlier in section 4.5.2

In section 4.5.2, we explained the reduction of fluid velocity due to increasing non-Newtonian character as measured by the third grade material parameter. The reduced velocity in turn decreases the viscous heating source terms in the temperature equation which leads to a drop in fluid temperature as shown in Fig.4.15. In Fig.4.16, except very close to the upper wall, elsewhere in the channel an increase in the porous medium shape parameter values cause a slight increase in the fluid temperature. This can be attributed to the frictional forces caused by the fluid particles as they force their way into reduced pore spaces. Close to the upper wall, reduced porosity is seen to decrease the fluid temperature. This, again, can be explained by the coupling effect via damped velocity.

4.5.4 Entropy Generation

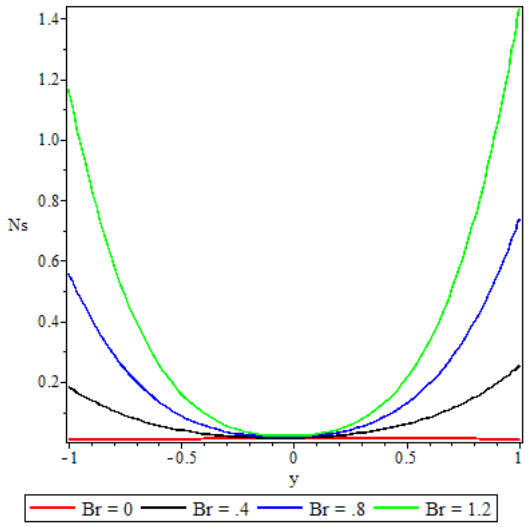

Figure 4.17: Variation of the entropy generation with the Brinkmann number

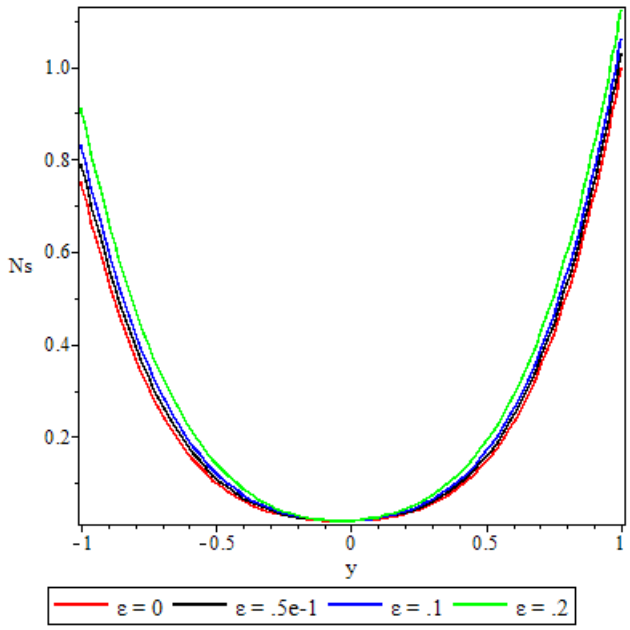

Figure 4.18: Variation of the entropy generation with the activation energy parameter

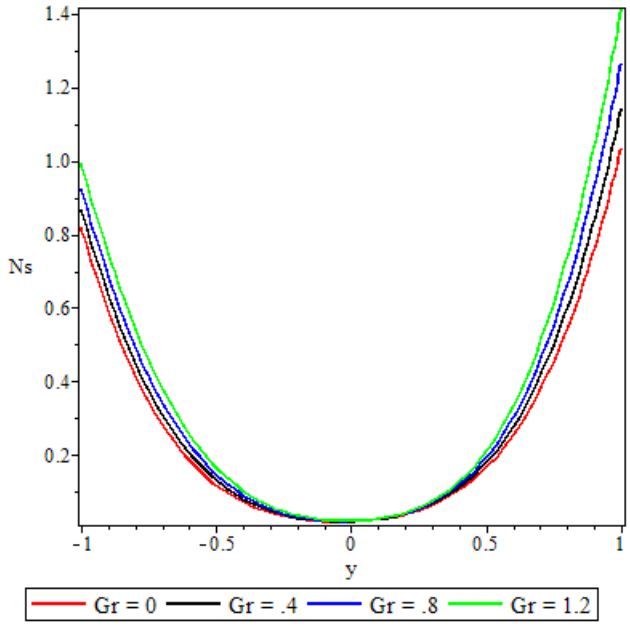

Figure 4.19: Variation of the entropy generation with the Grashof number

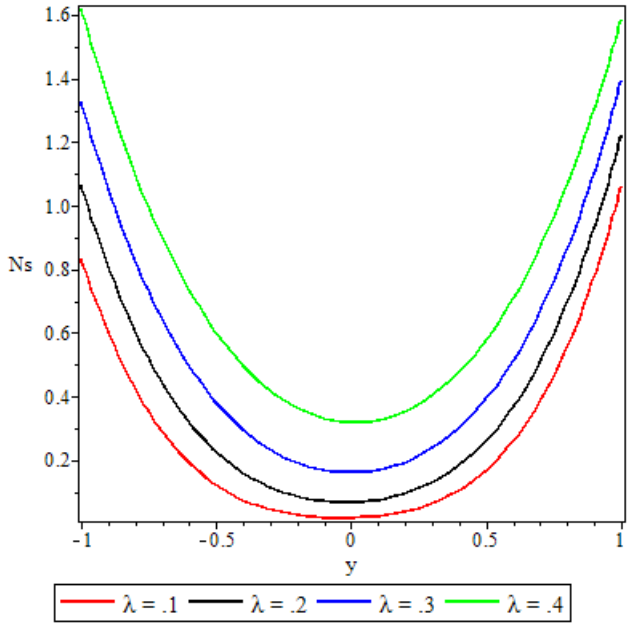

Figure 4.20: Variation of the entropy generation with the Frank-Kamenetsikii parameter

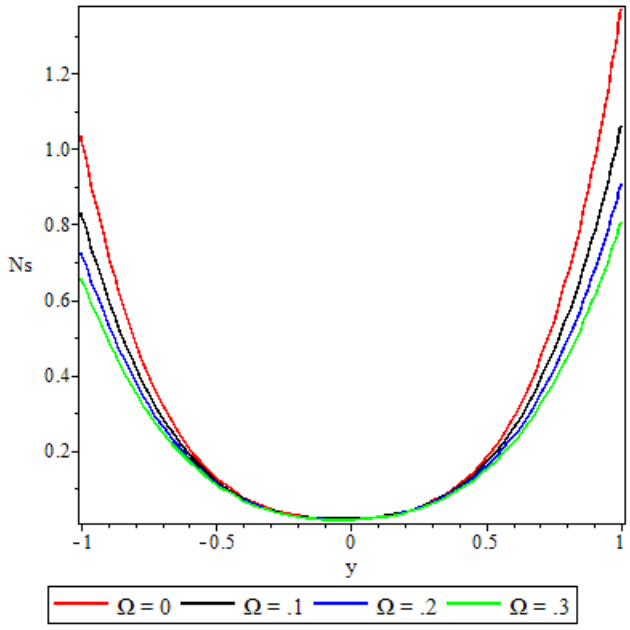

Figure 4.21: Variation of the entropy generation with the third grade material parameter

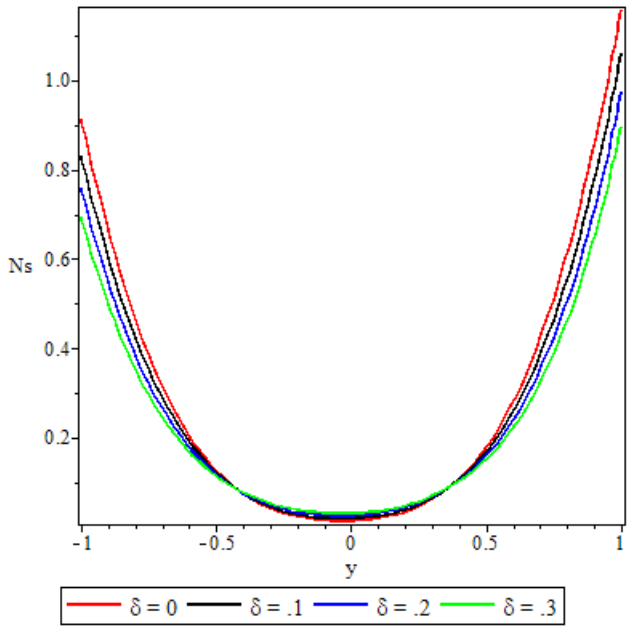

Figure 4.22: Variation of the entropy generation with the porous medium shape parameter

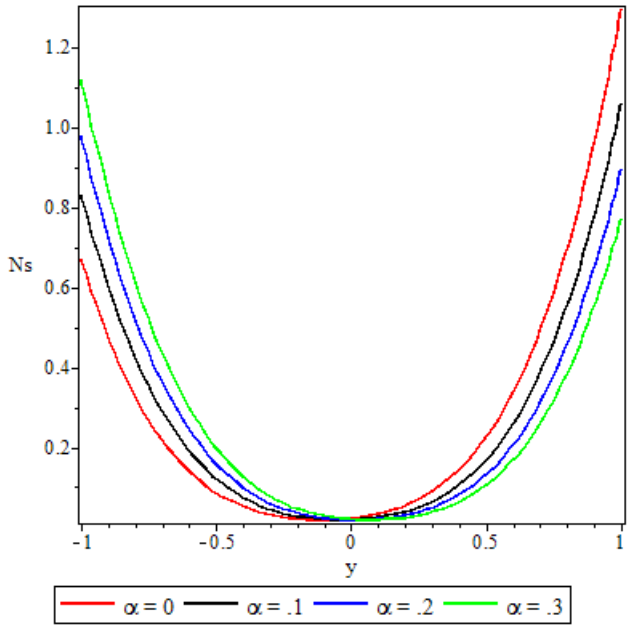

Figure 4.23: Variation of the entropy generation with the variable viscosity parameter

Analysis of the entropy generated in the flow is carried out with the aid of Figs.4.17 to 4.23. The figures depict parabolic entropy profiles with minimum entropy rate $Ns = 0$ at the channel core region. Except for Fig.4.20, all the other figures show that the entropy generation at the channel core region remains unaffected by the parameter variations. Figures $4.17 - 4.20$ show the entropy generation rate increasing with increasing values of the Brinkmann number, the activation energy parameter, the Grashof number and the chemical reaction parameter, respectively. The most significant effects are in Figs 4.17 and 4.20, due to the Brinkmann number and the chemical reaction parameter. In Fig.4.20, the rate of entropy generation is increased throughout the entire channel including the core region. In Figs. 4.21 and 4.22 the third grade material parameter and the porous medium shape parameter have a retardation effect on the entropy generation rate. In the lower half of the channel, Fig.4.23, an increase in the variable viscosity parameter enhances the entropy generation rate, while in the upper half of the channel the variable viscosity parameter has the opposite effect. Comparing Fig.4.23 and Fig.4.3, we observe that in the region where the variable viscosity parameter decreases the fluid velocity, it enhances the rate of entropy generation. In the region where the variable viscosity parameter increases the fluid velocity, it retards the entropy generation rate.

4.5.5 Bejan Number

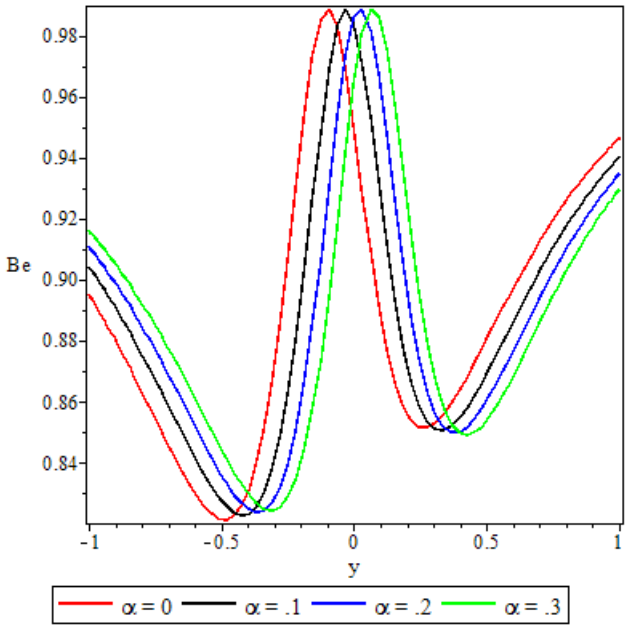

Figure 4.24: Variation of the Bejan number with the variable viscosity parameter

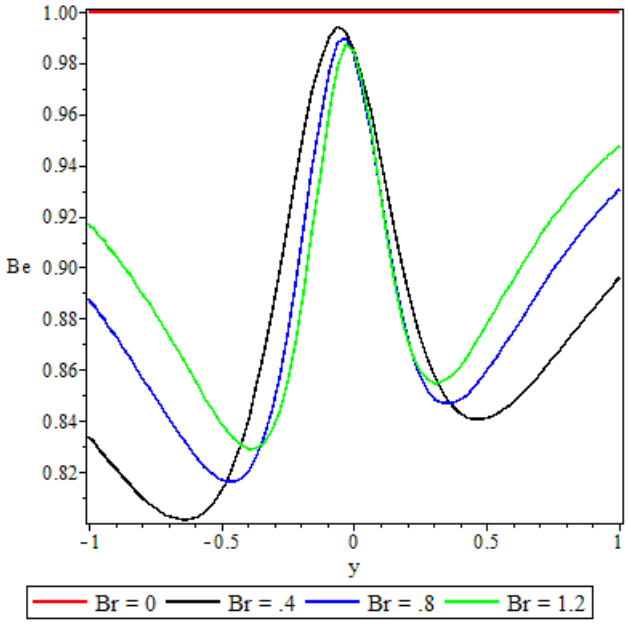

Figure 4.25: Variation of the Bejan number with the Brinkmann number

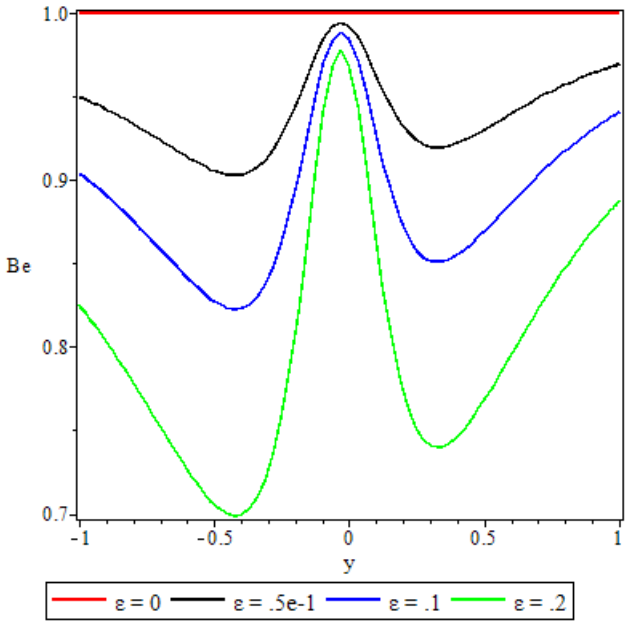

Figure 4.26: Variation of the Bejan number with the activation energy parameter

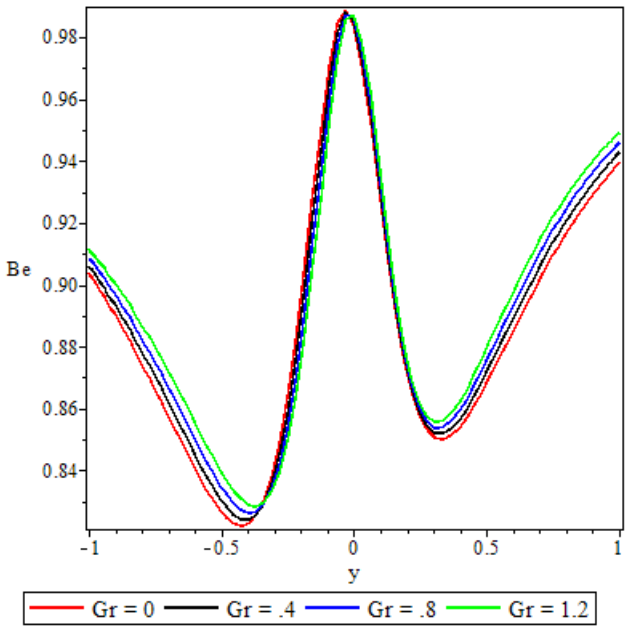

Figure 4.27: Variation of the Bejan number with the Grashof number

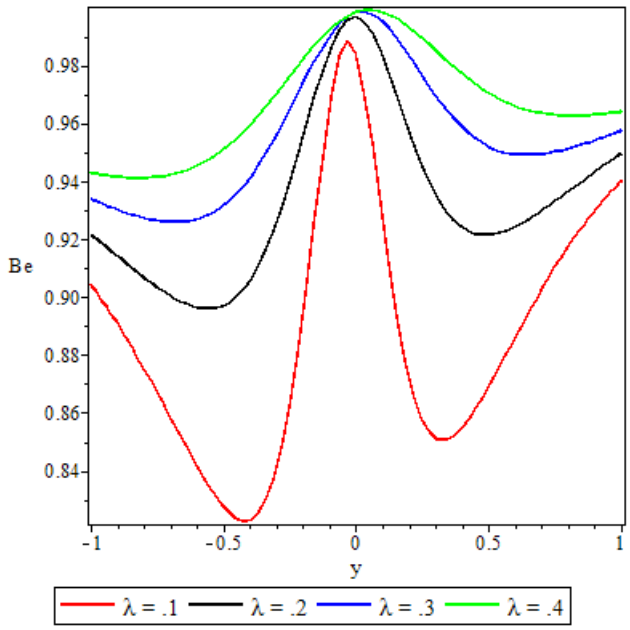

Figure 4.28: Variation of the Bejan number with the Frank−Kamenetsikii parameter

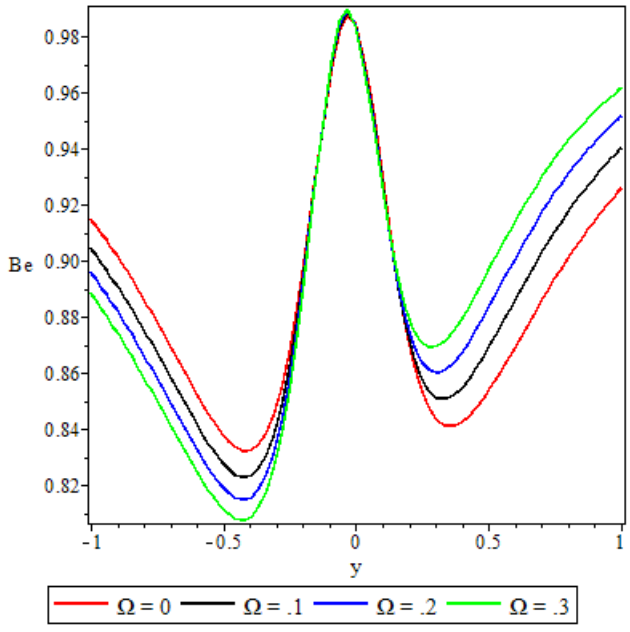

Figure 4.29: Variation of the Bejan number with the third grade material parameter

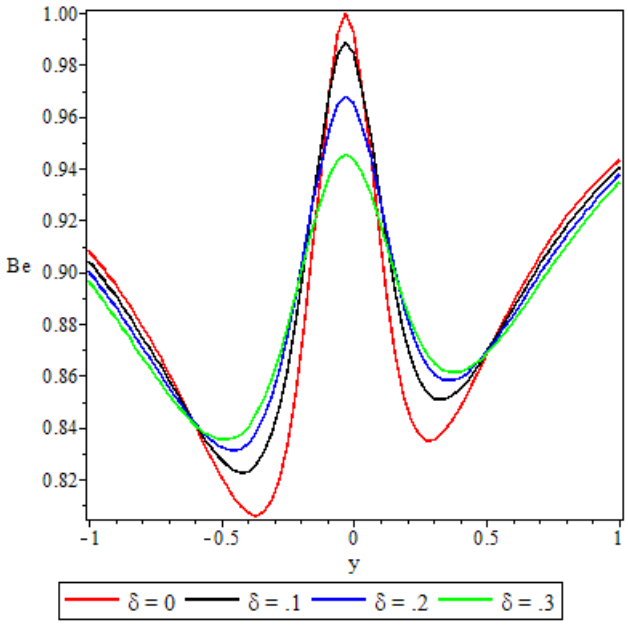

Figure 4.30: Variation of the Bejan number with the porous medium shape factor parameter

Figures 4.24 − 4.30 demonstrate the irreversibility ratio trends in response to variation of the flow governing parameters. A striking feature displayed by all these 7 graphs is that the irreversibility ratio is maximum at the channel core region. This shows that in this flow, irreversibility due to heat transfer dominates in the core region. Elsewhere within the channel, the graphs reveal the combined irreversibility due to viscous dissipation and porous medium porosity dominating the heat transfer irreversibility at the centre of the lower half of the channel (at $y = -0.5$) and the centre of the upper half (at $y = 0.5$). Figure 4.24 shows that as the variable viscosity parameter is increased, from $y = -1$ to $y = -0.5$ the Bejan number increases and in the next quarter of the channel the opposite effect happens. From the centre of the channel to $y = 0.5$ the Bejan number increases and in the last quarter of the channel it is retarded. An interesting observation in Fig.4.25 is that the irreversibility ratio is constant at Be=1 throughout the

channel when $Br = 0$. The same observation is made in Fig.4.26 when $\epsilon = 0$. As the Brinkmann number increases, the Bejan number increases in the lower quarter of the channel in Fig.4.25. In the same graph, from $y = -0.5$ to $y = 0.5$, the Bejan number decreases with the Brinkmann number, and in the upper quarter, it is enhanced. In Fig.4.26, increasing values of the activation energy parameter diminishes the Bejan number in both the lower half and the upper half of the channel.

The effects of the Grashof number on the irreversibility ratio, Fig.4.27, mirrors those of the Brinkmann number, albeit at a less pronounced intensity. In Fig.4.28, an increase in the chemical reaction parameter reveals effects that are exactly opposite of the effects of the activation energy parameter described in Fig.4.26. In Fig.4.29, an increase in the non-Newtonian properties of the fluid decreases the Bejan number in the lower half of the channel, whereas in the upper half of the channel it is enhanced. Figure 4.30 shows that increasing the porous medium shape parameter retards the Bejan number at the centre of the channel, enhances it at the centre of both halves of the channel and retards it again as we approach the channel walls.

4.6 Conclusions

In this article, entropy generation analysis of a steady flow of a reactive variable viscosity third grade fluid through a porous saturated medium with Navier slip and convective boundary conditions was successfully carried out with the aid of SQLM. The numerical method was found to be highly accurate and convergent. Graphical analysis of the response of the velocity and temperature distributions, entropy generation rate and irreversibility ratio to the various parameters embedded in the flow system revealed that:

- The temperature-dependent viscosity, the Brinkmann number and the chemical reaction parameter have a retardation effect on the fluid velocity in the lower half of the channel that is subjected to convective heat exchange with the ambient, while the opposite effect is observed in the upper half of the channel that is subjected to a constant heat flux.

- The non-Newtonian properties of the fluid and the porous medium shape factor parameter were observed to have a damping effect on the fluid velocity, while the buoyancy forces were observed to have the opposite effect.

- The fluid temperature profile was observed to increase with an increase in the Brinkmann number, the buoyancy force, and the chemical reaction parameter, whereas the variable viscosity parameter and the third grade material parameter had a retardation effect.

- A parabolic entropy generation rate profile was observed with minimum entropy $N_s = 0$ at the centre of the channel.

- Parameters either increase or decrease the entropy generation rate elsewhere in the channel but at the centre of the channel it remained unaffected by all the parameters except the chemical reaction parameter.

- The irreversibility ratio was observed to be maximum at the centre of the channel indicating the dominance of heat transfer irreversibility over the combined viscous dissipation and porosity irreversibility.

- Elsewhere in the channel parameters revealed varied effects on the Bejan number but in general irreversibility due to viscous dissipation and porosity was found to dominate heat transfer irreversibility at the middle of either half of the channel.

These observed interesting manifestations will no doubt inform optimal designs of thermomechanical systems to achieve energy utilization efficiency.

Chapter 5

Inherent Irreversibility Analysis of an Unsteady Reactive Hydromagnetic Third Grade Fluid Flow in a Vertical Channel through a Porous medium with Asymmetrical Convective Cooling

Chapter Abstract

This chapter numerically investigates the inherent irreversibility of unsteady MHD reactive flow of a third grade fluid through a porous saturated medium with asymmetric convective boundary conditions. The convective heat transfer between the

walls of the channel and the immediate surrounding follows Newton's law of cooling. To approximate the entropy generation rate and the Bejan number, the non-dimensional governing equations are solved numerically by utilizing the finite difference method. The effects of the Brinkmann number, the Frank-Kamenetskii parameter, the Hartman number and other flow parameters on velocity, temperature, entropy generation rate and Bejan number are analyzed graphically and discussed qualitatively and quantitatively.

5.1 Introduction

The hydromagnetic flow in a channel is a classical problem whose solutions have drawn the attention of many researchers because of its applications in engineering and industrial processes exemplified by mechanical designing processes, atomic control engineering, astrophysical plasmas, aerodynamic heating, and MHD pumps and generators. VeeraKrishna and Reddy [142] presented a transient unsteady MHD reactive flow of a second-grade fluid through a porous medium in a rotating parallel plate channel. Reza-E-Rabbi *et al.* [143] and Das *et al.* [144] studied the heat and mass transfer analysis of MHD flow with thermal radiation and chemical reaction effects. In the work of [145], the heat transfer and entropy generation characteristics of an unsteady MHD flow of a viscous incompressible electrically conducting Casson nano-fluid over a moving infinite vertical plate was investigated. There is plenty of literature available on the flow and heat transfer of MHD non-Newtonian fluid in channels with different configurations. Additionally, recent discoveries on fluid flow in channels subjected to symmetrical or asymmetrical convective cooling cannot be neglected. Examples of such studies are found in [146; 147; 148; 131].

The foremost priority of the research community in the current time is to

find techniques for controlling the wastage of useful energy in thermomechanical processes. Energy loses result in productivity inefficiency that leads to wastage of resources. As defined in chapters 3 and 4, entropy is a thermodynamic quantity representing the unavailability of a system's thermal energy for conversion into mechanical work, often interpreted as the degree of disorder or randomness in the system. When the rate of entropy generation enhances in any thermal system, it can destroy the useful work and reduce the efficiency of the system. Physically, entropy generation is associated with thermodynamical irreversibility, which is a common phenomenon in all kinds of heat and mass transfer systems. Therefore, it is necessary to minimize the entropy generation to prevent any irreversibility losses that can affect system performance. The first and second law of thermodynamics are used to characterize and optimize a system [115]. Bejan [115; 149] was the first researcher to undertake theoretical work on thermodynamic irreversibility in fluid flow and heat transfer. He demonstrated that the efficiency of a thermal system could be improved by minimizing entropy generation. Following his ground breaking work, several authors [150; 151; 152; 153; 138; 154; 155; 156; 157], mentioning a few, have analyzed aspects of the irreversibility problems under different flow conditions. Adesanya *et al.* [120] investigated the inherent irreversibility in a couple stress fluid flow through a horizontal channel. Salawu and Fatunmbi [138] investigated inherent irreversibility of a reactive incompressible third-grade fluid poiseuille flow with variable viscosity and convective cooling under the influence of an externally applied magnectic field.

Meanwhile, fluid flow through porous saturated media plays an important role in various engineering and industrial processes. Examples include transpiration cooling processes, material drying, porous coatings, fuel cells and textiles. There are many different technologies that depend on porous media. Among the im-

portant technology that depend on the properties of porous media is hydrology, which relates to water movement in the earth and sand structures. Researchers who have shown interest in porous media flow include [91; 136; 158; 159; 160; 161].

The analysis of a reactive hydromagnetic fluid flow in a channel filled with a porous medium subjected to convective boundary conditions was investigated by Hassan and Maritz [162]. Rundora and Makinde [102] and Makinde *et al.* [98] examined the thermal effects in an unsteady MHD third grade fluid flow through a porous saturated medium with asymmetrical convective boundary conditions. In this work, we extend the work of [163] by examining entropy generation of an unsteady hydromagnetic flow of a reactive variable viscosity, electrically conducting third grade fluid through a porous saturated medium with asymmetrical convective boundary conditions.

5.2 Mathematical Formulation

Consider an unsteady flow of an incompressible electrically conducting, variable viscosity, reactive third grade fluid through a vertical channel filled with a homogeneous and isotropic porous medium. The flow is assumed to be induced by the action of an applied axial pressure gradient and buoyancy force and is subjected to the influence of an externally applied homogeneous magnetic field as shown in Fig. 4.1.

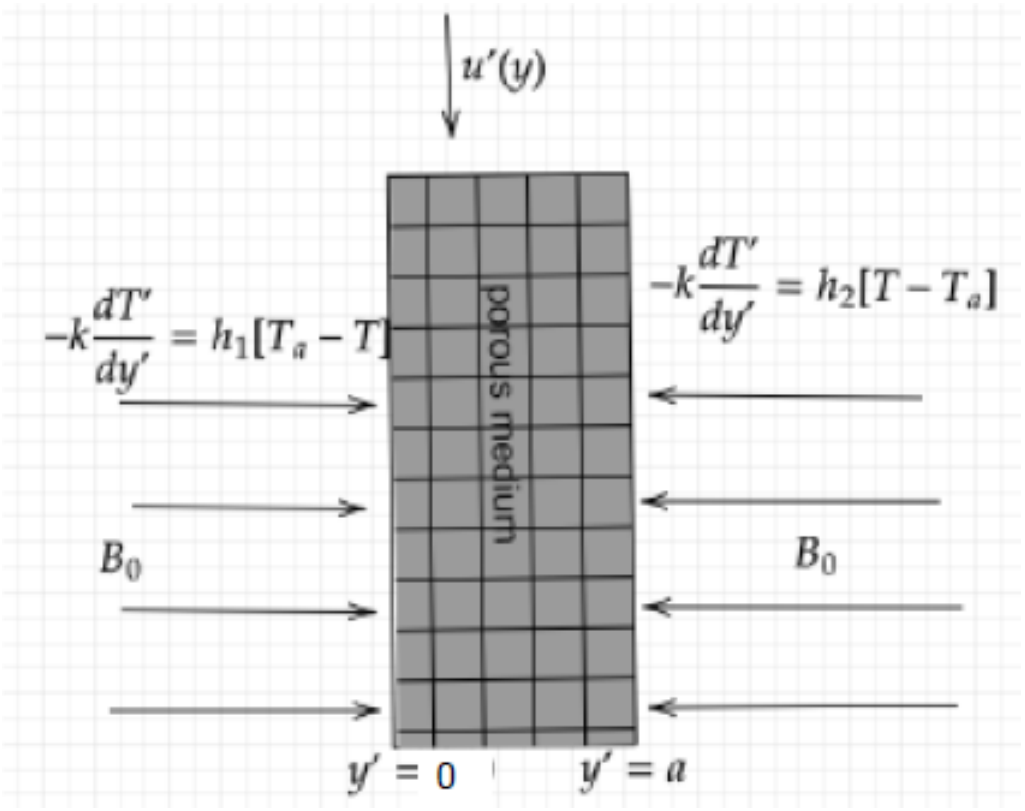

Figure 5.1: Schematic diagram of the problem

The fluid is assumed to have small electrical conductivity so that the electromagnetic force produced is very minimal. The channel walls are subjected to asymmetric convective heat exchange with the ambient due to unequal heat transfer. The x-axis is parallel to the gravitational acceleration g but in the opposite direction while the y-axis is perpendicular to the vertical parallel plates. Following Rundora and Makinde [163], and taking into account the buoyancy effects in a vertical channel, the governing equations for the momentum and heat balance can be written as

$$\begin{aligned}\rho\frac{\partial u'}{\partial t'} = &-\frac{\partial P}{\partial x'} + \frac{\partial}{\partial y'}\left(\mu'(T)\frac{\partial u'}{\partial y'}\right) + \alpha_1\frac{\partial^3 u'}{\partial y'^2\partial t} + 6\beta_3\frac{\partial^2 u'}{\partial y'^2}\left(\frac{\partial u'}{\partial y'}\right)^2 \\ &- \frac{\mu'(T)u'}{\rho K} - \sigma_0 B_0^2 u' + \rho g\beta(T - T_0),\end{aligned} \tag{5.1}$$

$$\rho c_p \frac{\partial T}{\partial t'} = k\frac{\partial^2 T'}{\partial y'^2} + \left(\frac{\partial u'}{\partial y'}\right)^2 \left[\mu'(T) + 2\beta_3 \left(\frac{\partial u'}{\partial y'}\right)^2\right] + \frac{\mu'(T)u'^2}{K} + \sigma_0 B_0^2 u' + QC_0 A \left(\frac{hT}{vl}\right)^m e^{-\frac{E}{RT}}. \tag{5.2}$$

The corresponding boundary conditions are given as

$$\begin{aligned} u'(y',0) = 0, \quad T(y',0) = T_0, \\ u'(0,t') = 0, \quad -k\frac{\partial T'}{\partial y'}(0,t') = h_1[T_a - T(0,t')], \\ u'(a,t') = 0, \quad -k\frac{\partial T'}{\partial y'}(a,t') = h_2[T(a,t') - T_a], \end{aligned} \tag{5.3}$$

where c_p is the specific heat at constant pressure, T is the fluid temperature, A is the reaction rate constant, P is pressure, ρ is the fluid density, α_1, β_3 are the material coefficients, k is the thermal conductivity, K is the Porous medium permeability, Q is the heat of the reaction, B_0 is the uniform transverse magnetic field, C_0 is the initial concentration of the reactant species, $m \in \{-2, 0, 0.5\}$ are the numerical exponents for sensitized, Arrhenius and bimolecular kinetics respectively, E is the activation energy, h is the Boltzmann's constant, l is the Planck's number, R is the universal gas constant, σ_0 is the fluid electrical conductivity, v is the vibration frequency, and h_1, h_2 are the heat transfer coefficients at the lower and upper plates, respectively. The temperature dependent viscosity, μ', can be expressed as

$$\mu'(T) = \mu_0 e^{-b(T-T_0)}, \tag{5.4}$$

where b is a viscosity variation parameter, μ_0 is the initial fluid dynamic viscosity and T_0 is the fluid initial temperature. Introducing the following dimensionless

variables

$$x=\frac{x'}{a}, y=\frac{y'}{a}, u=\frac{u'\rho a}{\mu_0}, t=\frac{t'\mu_0}{\rho a^2}, \theta=\frac{E(T-T_0)}{RT_0^2}, \theta_a=\frac{E(T_a-T_0)}{RT_0^2}, Da=\frac{K}{a^2},$$
$$S^2=\frac{1}{Da}, G=-\frac{\partial P}{\partial x}, \delta=\frac{\alpha_1}{\rho a^2}, \alpha=\frac{bRT_0^2}{E}, Bi_1=\frac{ah_1}{k}, Bi_2=\frac{ah_2}{k}, \Omega=\frac{\beta_3\mu_0}{a^4\rho^2},$$
$$Ha^2=\frac{\sigma_0 B_0^2 a^2}{\mu_0}, Pr=\frac{\mu_0 c_p}{k}, \epsilon=\frac{RT_0}{E}, P=\frac{P'\rho a^2}{\mu_0^2}, \lambda=\left(\frac{hT_0}{vl}\right)^m \frac{QEAa^2C_0}{kRT_0^2}e^{-\frac{E}{RT_0}},$$
$$\gamma=\left(\frac{vl}{hT_0}\right)^m \frac{\mu_0^3}{QA\rho^2a^4C_0}e^{\frac{E}{RT_0}}, Gr=\frac{\rho^2 g\beta a^3 RT_0^2}{\mu_0^2 E}, N_s=\frac{E_g a^2 E}{kRT_0}, \tag{5.5}$$

where x and y are the non-dimensional axial and normal coordinates to the inclined channel, u is the non-dimensional fluid velocity, t is the non-dimensional time, θ is the non-dimensional fluid temperature, δ is the material parameter, γ is the viscous heating parameter, α is the variable viscosity parameter, Ω is the third grade fluid material parameter, λ is the Frank-Kamenetskii parameter, Ha is the Hartmann number, Pr is the Prandtl number, Gr is the Grashoff number, ϵ is the activation energy parameter, Bi_1 and Bi_2 are the Biot numbers at the left and right-hand side channel plates, respectively, G is the pressure gradient parameter, θ_a is the ambient temperature parameter, Da is the Darcy number, S is the porous medium shape parameter and N_s is the nondimensional entropy generation rate.

Substituting equation (5.5) into governing equations (5.1), (5.2) and boundary conditions (5.3), the following non-dimensional nonlinear equations

$$\frac{\partial u}{\partial t}=G-\alpha e^{-\alpha\theta}\frac{\partial\theta}{\partial y}\frac{\partial u}{\partial y}+e^{-\alpha\theta}\frac{\partial^2 u}{\partial y^2}+\delta\frac{\partial^3 u}{\partial y^2\partial t}+6\Omega\frac{\partial^2 u}{\partial y^2}\left(\frac{\partial u}{\partial y}\right)^2-(S^2e^{-\alpha\theta}+Ha^2)u+Gr\theta, \tag{5.6}$$

$$Pr\frac{\partial\theta}{\partial t} = \frac{\partial^2\theta}{\partial y^2} + \lambda\left\{(1+\epsilon\theta)^m e^{\frac{\theta}{1+\epsilon\theta}} + \gamma\left[\left(\frac{\partial u}{\partial y}\right)^2\left(e^{-\alpha\theta} + 2\Omega\left(\frac{\partial u}{\partial y}\right)^2\right)\right]\right.$$
$$\left. + \gamma(S^2u^2e^{-\alpha\theta} + Ha^2u)\right\}, \tag{5.7}$$

are obtained, with corresponding initial and boundary conditions

$$u(y,0) = 0, \quad \theta(y,0) = 0, \tag{5.8}$$

$$u(0,t) = 0, \quad \frac{\partial\theta}{\partial y}(0,t) = -Bi_1[\theta_a - \theta(0,t)], \tag{5.9}$$

$$u(1,t) = 0, \quad \frac{\partial\theta}{\partial y}(1,t) = -Bi_2[\theta(1,t) - \theta_a]. \tag{5.10}$$

5.3 Entropy Generation Analysis

The local volumetric rate of entropy generation for a viscous incompressible conducting third grade fluid in the presence of porous media will be expressed as

$$E_G = \frac{k}{T_0}\frac{\partial^2 T}{\partial y'^2} + \frac{\mu'(T)}{T_0}\left(\frac{\partial u'}{\partial y'}\right)^2\left[1 + \frac{2\beta_3}{\mu'(T)}\left(\frac{\partial u'}{\partial y'}\right)^2\right] + \frac{\mu'(T)u'^2}{T_0K} + \frac{\sigma_0 B_0^2 u'^2}{T_0}, \tag{5.11}$$

where the first term is the heat transfer irreversibility, the second term is the entropy generation due to third grade fluid viscous dissipation, and the last two terms are the irreversibility due to the presence of porous media and magnetic field respectively. Using the dimensionless quantities and parameters, as defined

in equation (5.5), the equation for the dimensionless form of (5.11) emerges as

$$N_s = \frac{\partial^2 \theta}{\partial y^2} + \lambda\gamma \left\{ \left(\frac{\partial u}{\partial y} \right)^2 \left[e^{-\alpha\theta} + 2\Omega \left(\frac{\partial u}{\partial y} \right)^2 \right] + \left(Ha^2 + S^2 e^{-\alpha\theta} \right) u^2 \right\}. \quad (5.12)$$

The dimensionless entropy generation number, N_s, is the ratio of the volumetric entropy generation rate to the characteristic entropy generation rate. We breakdown the right hand side of (5.12) into N_h, N_f, where

$$N_h = \frac{\partial^2 \theta}{\partial y^2}$$

is the irreversibility due to heat transfer, and

$$N_f = \lambda\gamma \left\{ \left(\frac{\partial u}{\partial y} \right)^2 \left[e^{-\alpha\theta} + 2\Omega \left(\frac{\partial u}{\partial y} \right)^2 \right] + \left(Ha^2 + S^2 e^{-\alpha\theta} \right) u^2 \right\}.$$

is the irreversibility due to combined effect of third grade fluid viscous dissipation, porous media and magnetic field. The Bejan number (Be) is used to evaluate the irreversibility distribution and is defined as

$$Be = \frac{N_h}{N_s} = \frac{N_h}{N_h + N_f}. \quad (5.13)$$

From equation (5.13), the Bejan number is in the range $0 \leq Be \leq 1$. When $Be = 0$, N_f dominates N_h. When $Be = 0.5$ both N_f and N_h contribute equally to the entropy generation in the flow process, i.e., $N_f = N_h$. Lastly, when $Be = 1$, N_h dominates N_f.

5.4 Numerical Method of Solution

The governing system (5.6)−(5.7) with initial and boundary conditions (5.8)−(5.10) is solved numerically following the semi-implicit finite difference scheme given in Chinyoka [164]. In Chinyoka [165; 166], implicit terms are taken at the intermediate time level $(N+\xi)$, where $0 \leq \xi \leq 1$. The discretization of the equations is based on a linear cartesian mesh and uniform grid on which finite differences are taken. Both first and second spatial derivatives are approximated by second order central differences. The governing equations corresponding to the first and the last grid points are modified to incorporate the boundary conditions. The semi-implicit scheme for both velocity and temperature components are

$$\begin{aligned}\frac{\partial}{\partial t}\left(u-\delta\frac{\partial^2 u}{\partial y^2}\right) &= G - S^2 e^{-\alpha\theta^{(N)}}u^{(N+\xi)} - Ha^2 u^{(N+\xi)} + e^{-\alpha\theta^{(N)}}\frac{\partial^2}{\partial y^2}u^{(N+\xi)} \\ &\quad -\left(\alpha e^{-\alpha\theta}\frac{\partial\theta}{\partial y}\frac{\partial u}{\partial y}\right)^{(N)} + 6\Omega\left(\frac{\partial}{\partial y}u^{(N)}\right)^2\frac{\partial^2}{\partial y^2}u^{(N+\xi)} + Gr\theta^{(N)},\end{aligned} \tag{5.14}$$

$$\begin{aligned}Pr\frac{\theta^{(N+1)}-\theta^{(N)}}{\Delta t} &= \frac{\partial^2}{\partial y^2}\theta^{(N+\xi)} + \lambda\left[(1+\epsilon\theta)^m exp\left(\frac{\theta}{1+\epsilon\theta}\right)\right]^{(N)} \\ &\quad +\lambda\gamma[Ha^2u^2 + S^2u^2e^{-\alpha\theta} + \dot{\gamma}^2(e^{-\alpha\theta} + 2\Omega\dot{\gamma}^2]^{(N)}.\end{aligned} \tag{5.15}$$

In equation 5.14, it is understood that $\frac{\partial\sharp}{\partial t} := \frac{\sharp^{(N+1)}-\sharp^{(N)}}{\Delta t}$. The equation for $u^{(N+1)}$ then becomes

$$\begin{aligned}-r_1u_{j-1}^{(N+1)} + r_2u_{j-1}^{(N+1)} - r_1u_{j+1}^{(N+1)} &= \Delta tG + (u+\delta u_{yy})^{(N)} - \alpha\Delta t(e^{-\alpha\theta}\theta_y\dot{\gamma})^{(N)} \\ -\Delta tS^2e^{-\alpha\theta^{(N)}}(1-\xi)u^{(N)} - \Delta tHa^2(1-\xi)u^{(N)} &+ \Delta t(1-\xi)(e^{-\alpha\theta}+6\gamma\dot{\gamma}^2)u_{yy}^{(N)},\end{aligned} \tag{5.16}$$

where

$$
\begin{aligned}
r_1 &= \frac{1}{\Delta y^2}\left(\delta + \xi\Delta t(\mu + 6\Omega\dot{\gamma}^2)^{(N)}\right), \\
r_2 &= (1 + \xi\Delta t S^2\mu^{(N)} + \xi\Delta t Ha^2 + 2r_1), \\
\mu &= e^{(-\alpha\theta)}, \\
\dot{\gamma} &= u_y.
\end{aligned}
$$

Similarly, the equation for $\theta^{(N+1)}$ becomes

$$
\begin{aligned}
&- r\theta_{j-1}^{(N+1)} + (Pr + 2r)\theta_j^{(N+1)} - r\theta_{j+1}^{(N+1)} = \theta^{(N)} + \Delta t(1-\xi)\theta_{yy}^{(N)} \\
&+ \lambda\Delta\left[(1+\epsilon\theta)^m exp\left(\frac{\theta}{1+\epsilon\theta}\right)\right]^{(N)} + \lambda\Omega\Delta[Ha^2u^2 + S^2u^2e^{-\alpha\theta} \\
&+ \dot{\gamma}^2(e^{-\alpha\theta} + 2\Omega\dot{\gamma}^2)]^{(N)},
\end{aligned}
\tag{5.17}
$$

where $r = \frac{\xi\Delta t}{\Delta y^2}$. The solution procedure for $u^{(N+1)}$ and $\theta^{(N+1)}$ thus reduces to inversion of tri-diagonal matrices, which is an advantage over a full implicit scheme. The scheme (5.16) and (5.17) where checked for consistency. Chinyoka [164] have $\xi = \frac{1}{2}$ which improves the accuracy in time to second order. Rundora and Makinde [163] used $\xi = 1$ so that larger time steps could be chosen but still obtain convergence to the steady solutions. In this study we use $\xi = 1$.

5.5 Results and Discussion

In the following discussion, we investigate an unsteady MHD reactive flow of a third grade fluid in a vertical channel filled with a saturated porous medium with asymmetric convective boundary conditions. The semi-implicit finite difference scheme is coded into symbolic package MAPLE for easy computation of the graphical solutions. The effects of the various parameters embedded in the flow

system on the flow velocity, temperature field, the entropy generation rate and the irreversibility ratio will be carried out with the aid of simulated graphs. The default parameter values $G = 1$, $Pr = 10$, $\delta = 0.000001$, $\lambda = 0.1$, $\gamma = 1$, $\Omega = 0.1$, $\epsilon = 0.1$, $\alpha = 0.1$, $Ha = 1$, $S = 1$, $Bi_1 = 0.1$, $Bi_2 = 1$, $m = 0.5$, $Gr = 1$ and $\theta_a = 0.1$ will be employed. Where a parameter is not varied, it will be assumed to take the stated default value.

5.5.1 Steady State Velocity and Temperature Profiles

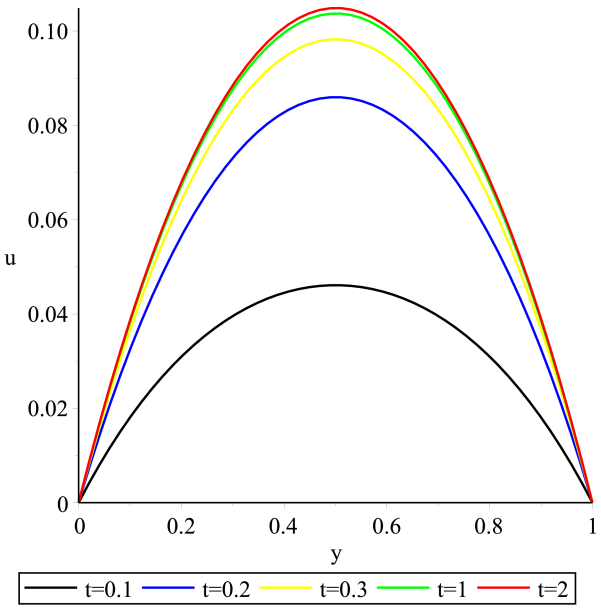

Figure 5.2: Steady state velocity profile

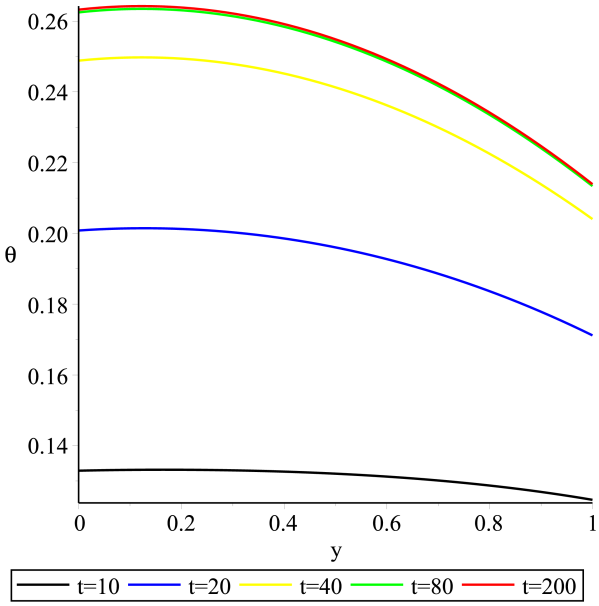

Figure 5.3: Steady state temperature profile

Figures 5.2 and 5.3 demonstrate the convergence of the solution. The figures illustrate a transient increase in the velocity and temperature profiles until steady state is attained.

5.5.2 Fluid Velocity and Temperature Profiles

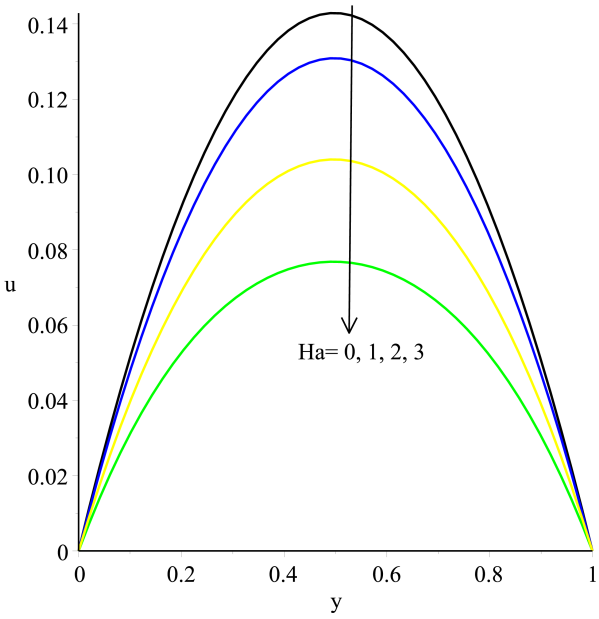

Figure 5.4: Effects of the Hartmann number on velocity profile

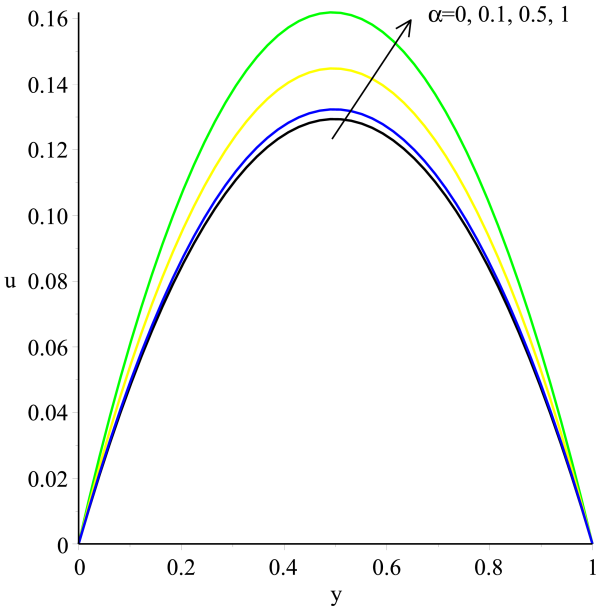

Figure 5.5: Effects of the variable viscosity parameter on velocity profile

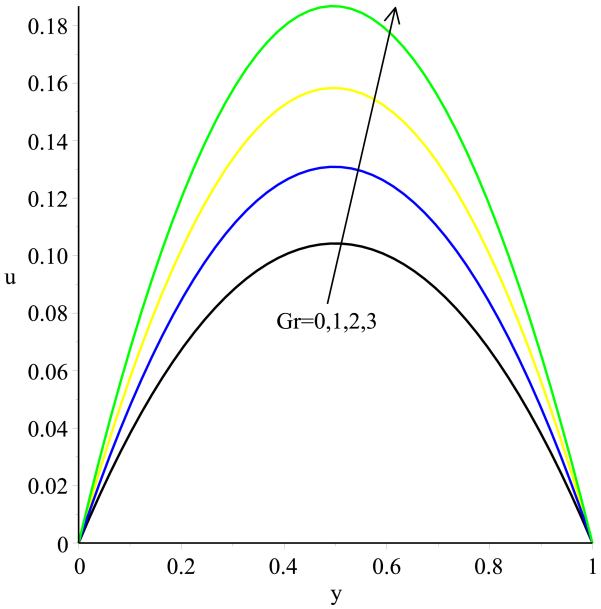

Figure 5.6: Effects of the Grashof number on velocity profile

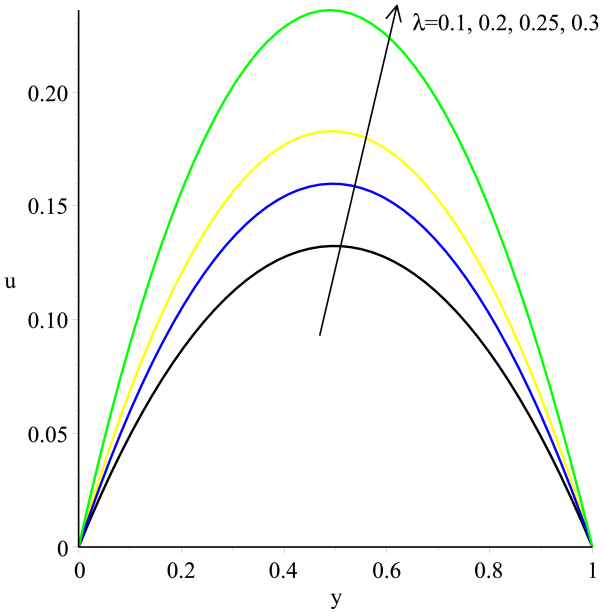

Figure 5.7: Effects of the Frank Kamenetskii parameter on velocity profile

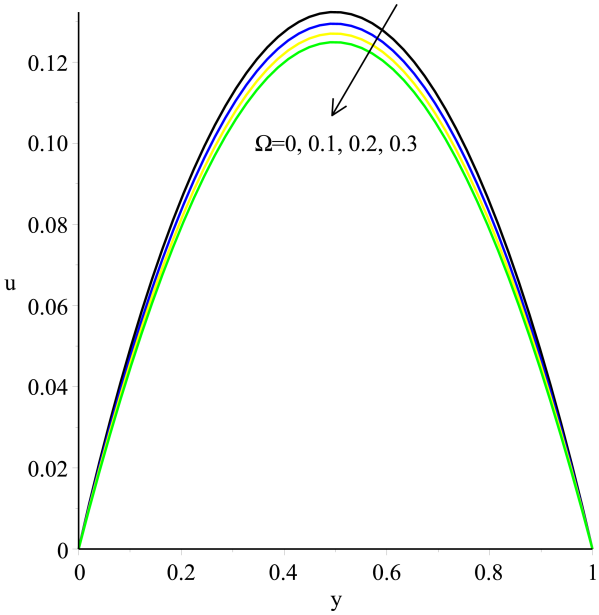

Figure 5.8: Effects of the third grade fluid material parameter on velocity profile

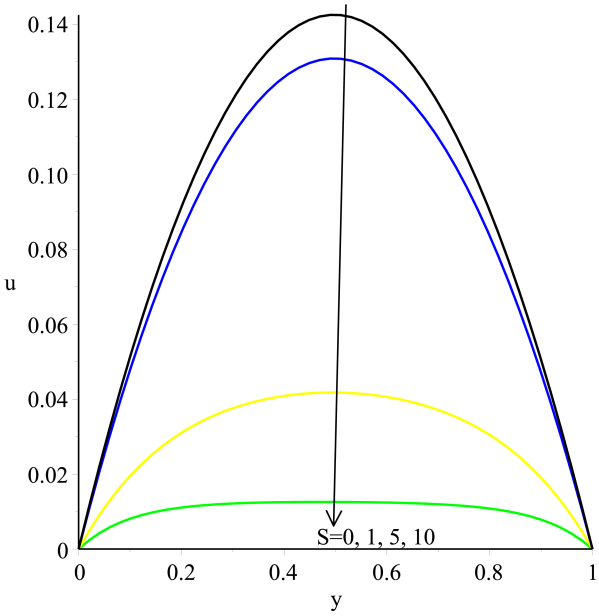

Figure 5.9: Effects of the porous medium shape parameter on velocity profile

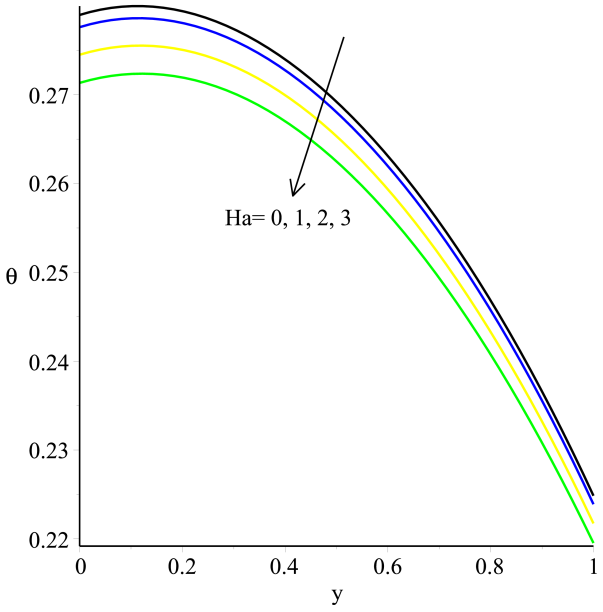

Figure 5.10: Effects of the Hartmann number on temperature profile

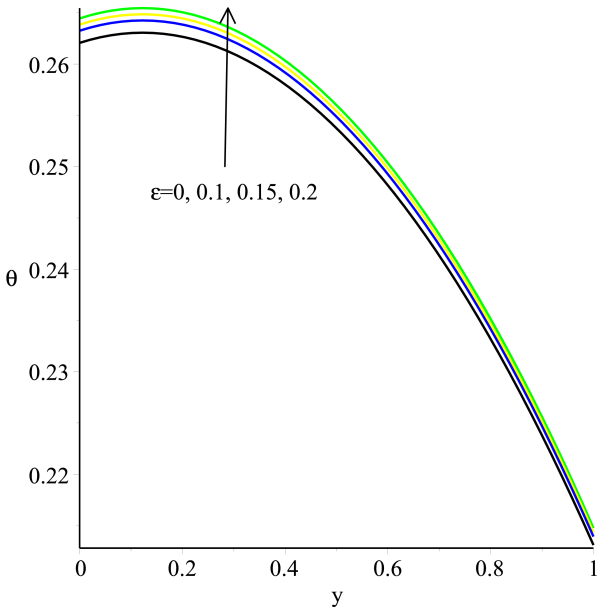

Figure 5.11: Effects of the activation energy parameter for $m = 0.5$ on temperature profile

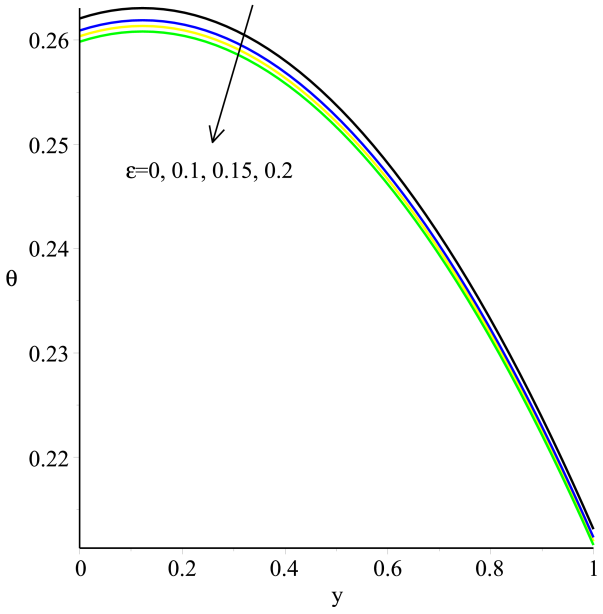

Figure 5.12: Effects of the activation energy parameter for $m = 0$ on temperature profile

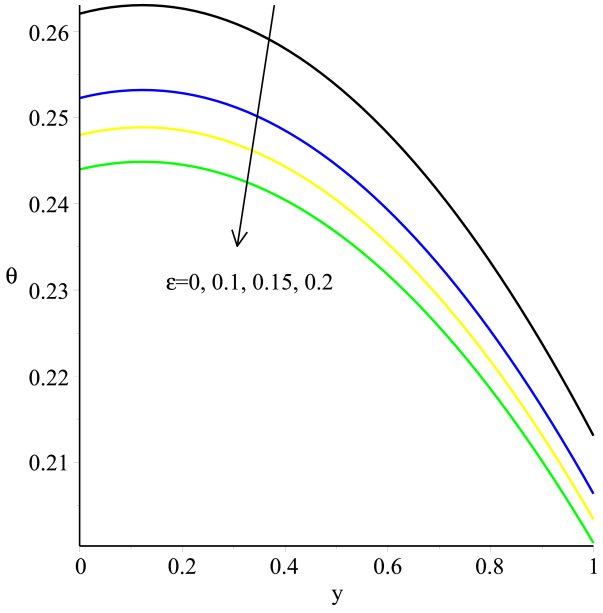

Figure 5.13: Effects of the activation energy parameter for $m = -2$ on temperature profile

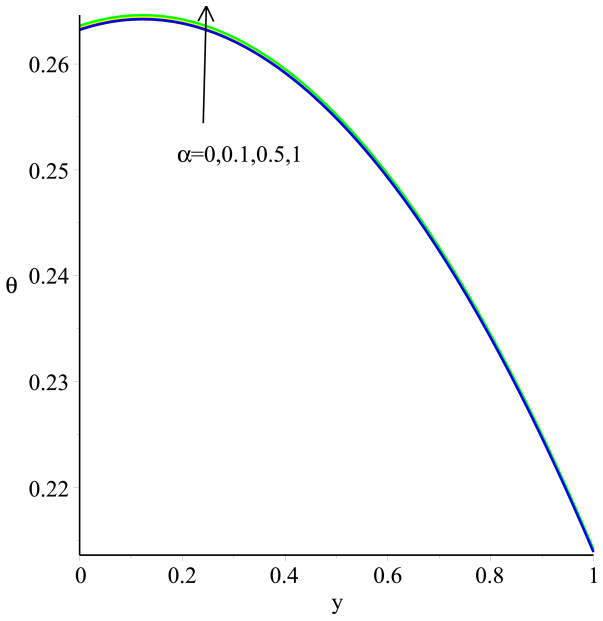

Figure 5.14: Effects of the variable viscosity parameter on temperature profile

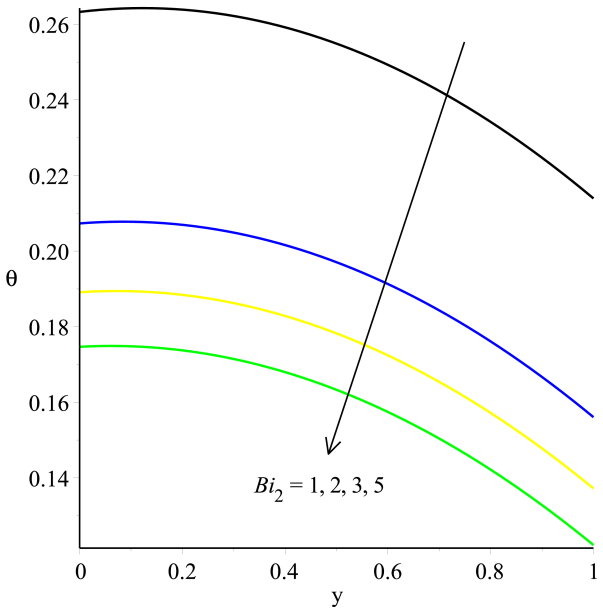

Figure 5.15: Effects of the Biot number Bi_2 on temperature profile

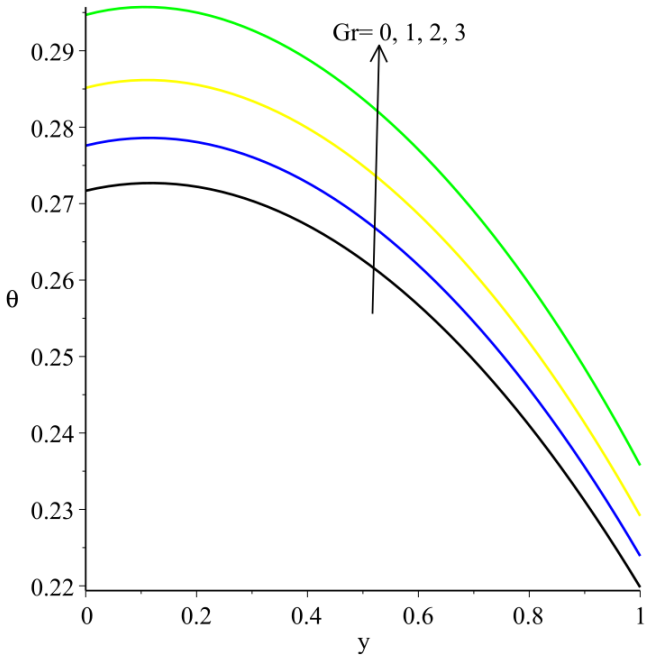

Figure 5.16: Effects of the Grashof number on temperature profile

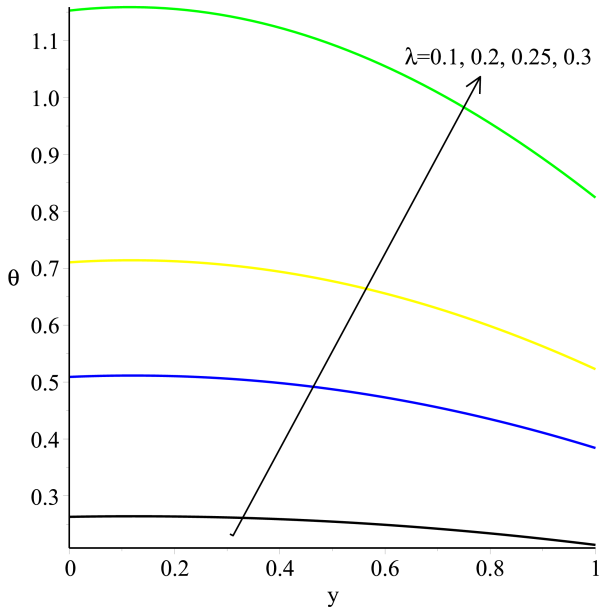

Figure 5.17: Effects of the Frank Kamenetskii parameter on temperature profile

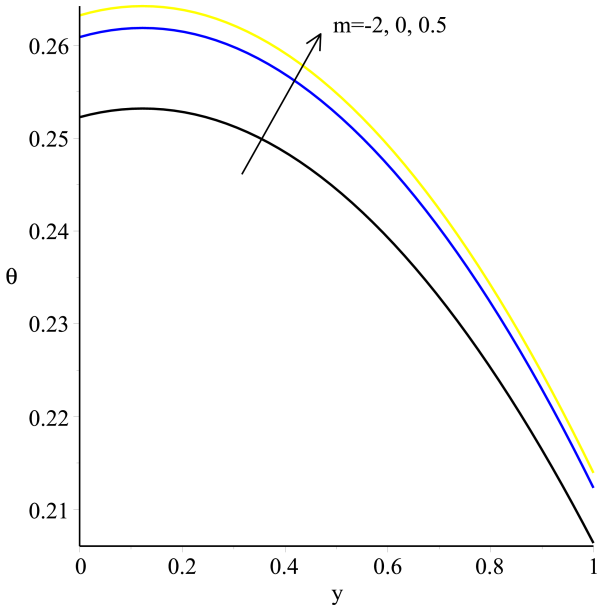

Figure 5.18: Effects of the parameter m on temperature profile

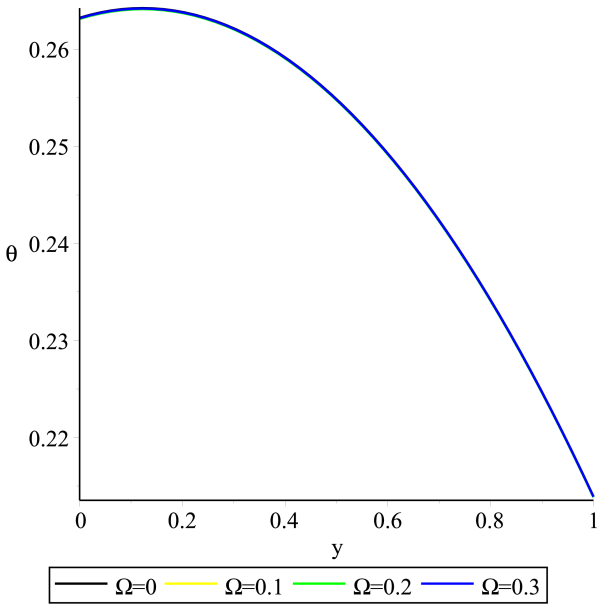

Figure 5.19: Effects of the third grade fluid material parameter on temperature profile

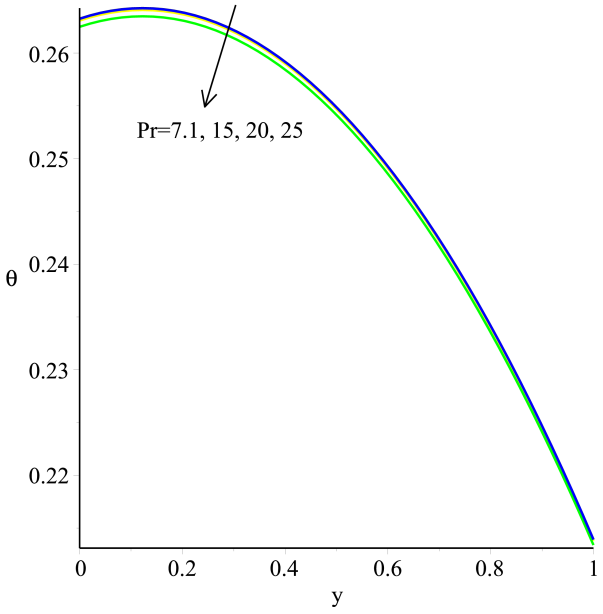

Figure 5.20: Effects of the Prandtl number on temperature profile

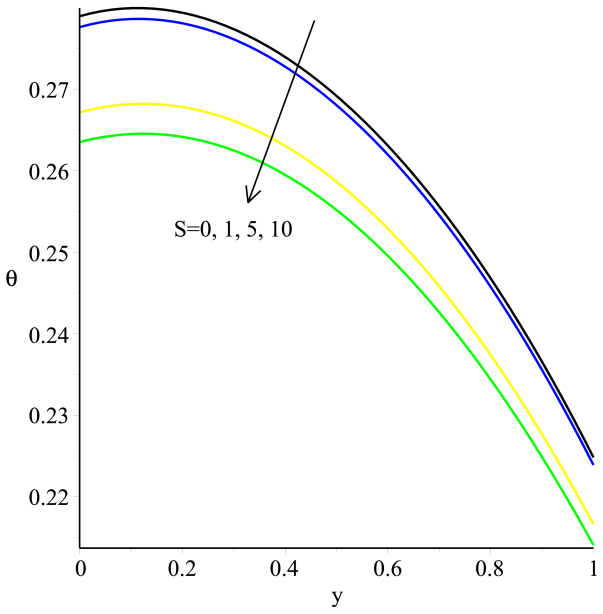

Figure 5.21: Effects of the porous medium shape parameter on temperature profile

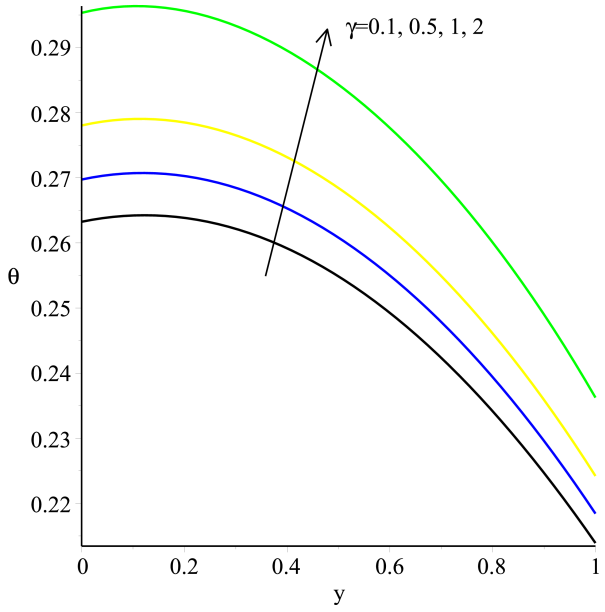

Figure 5.22: Effects of the viscous heating parameter on temperature profile

In Figs. 5.4, 5.8 and 5.9 the fluid velocity is observed to decrease with increasing values of the Hartmann number, the third grade fluid material parameter and the porous medium shape parameter, respectively. On the other hand, Figs. 5.5, 5.6 and 5.7 show the velocity profile increasing with the variable viscosity parameter, the Grashof number and the Frank Kamenetskii parameter (reaction parameter), respectively. The Hartmann number measures the effect of the externally applied magnetic field intensity on the flow system, and the effects of the porous medium are measured by the porous medium shape parameter. Figs. 5.4 and 5.9 show that as these two parameters are increased, the fluid flow is damped. Thus the magnetic field intensity and the porous matrix have a damping effect on the fluid flow. An increase in the variable viscosity parameter, α, means a reduction in the fluid viscosity. Thus, as Fig. 5.5 shows, a reduction in fluid viscosity leads to an increase in the velocity field. Figures 5.6 and 5.7 are mirror images of each other showing the flow enhancement effects of buoyancy, as measured by the Grashof number, and the reaction parameter. The Grashof number represents

the effects of the buoyancy source terms on the flow system. As Fig. 5.6 shows, an increase in the buoyancy source terms enhances the flow rate. On the other hand, Fig. 5.7, an increase in the reaction rate leads to the reduction of fluid viscosity which in turn leads to an increase in the flow velocity. An increase in the reaction rate increases the fluid temperature which in turn reduces the fluid viscosity. In this work velocity is assumed to be temperature dependent, an assumption which captures physical reality. In Fig. 5.8, an increase in the non-Newtonian properties of the third grade fluid, e.g. viscoelastic effects, renders the fluid's resistance to flow. The variation of the fluid temperature profile in response to the various flow field parameters is displayed in Figs. 5.10 to 5.22. In Fig. 5.10 an increase in the magnetic field intensity reduces the temperature of the fluid. This phenomenon can be explained by the coupling effect. The reduction in velocity due to the damping effect of the magnetic field reduces the heating source terms in the temperature equation, resulting in fluid temperature drop. In Fig. 5.11, increasing the activation energy parameter enhances the fluid temperature in the case of a bimolecular type of reaction ($m = 0.5$). This is consistent with expectation. On the other hand, in Figs. 5.12 and 5.13 the fluid temperature is retarded by the activation energy parameter for the cases $m = 0$ (the Arrhenius reaction type) and $m = -2$ (the sensitized reaction type). This is consistent with the temperature equation where the heating source terms clearly decrease as epsilon increases when m is less or equal to 0. Figure 5.14 shows the fluid temperature increasing, albeit marginally, with increasing values of the variable viscosity parameter. This behavior can be explained by the coupling effect where an increase in fluid velocity with increasing α enhances the heating source terms in the temperature equation. The significant reduction in fluid temperature due to an increase in the Biot number, Fig. 5.15, is consistent with expectation. As explained in the previous chapter, high values of the Biot

number result in increased convective heat loss from the channel wall to the ambient, leading to convective cooling at the wall and in the bulk of the fluid. In Fig. 5.16 an increase in the fluid temperature with increasing values of the Grashof number can again be explain by the coupling effect. A significant increase in the fluid temperature with an increase in the Frank-Kamenetskii parameter, λ, is consistent with expectation as well. Increasing the exothermic reaction rate obviously results in temperature rise. As the exponent m increases from $m = -2$ (sensitized reaction type) to $m = 0.5$ (bimolecular reaction type), the fluid temperature is seen to rise significantly. The internal heat generated in the fluid by a bimolecular reaction type is significantly higher than that generated under an Arrhenius or the sensitized type of reaction. In this way, the trend depicted in Fig. 5.18 cannot be surprising. Fig. 5.19 shows that the third grade material parameter has no significant effect on the fluid temperature. Figure 5.20 shows that the influence of the Prandtl number on the fluid temperature is to decrease it. A decrease in fluid temperature following an increase in the porous medium shape parameter, Fig. 5.21, is explained by the coupling effect that has been alluded to earlier on. The retardation of the flow velocity as a result of decreasing porosity also leads to a drop in temperature due to the corresponding decrease in the heating source terms. In Fig. 5.22, as expected, the viscous heating parameter increases the fluid temperature.

5.5.3 Entropy Generation Rate

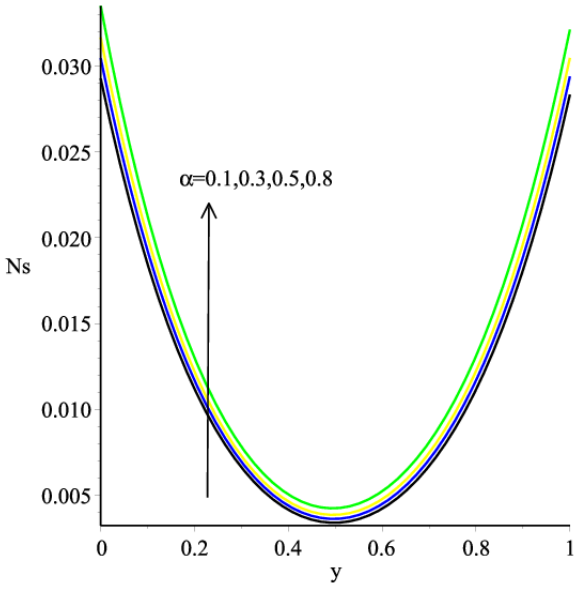

Figure 5.23: Effects of the variable viscosity parameter on entropy generation rate

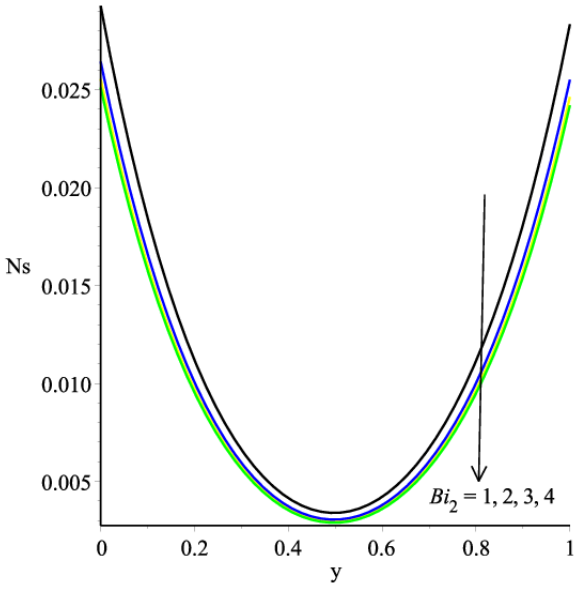

Figure 5.24: Effects of the Biot number on entropy generation rate

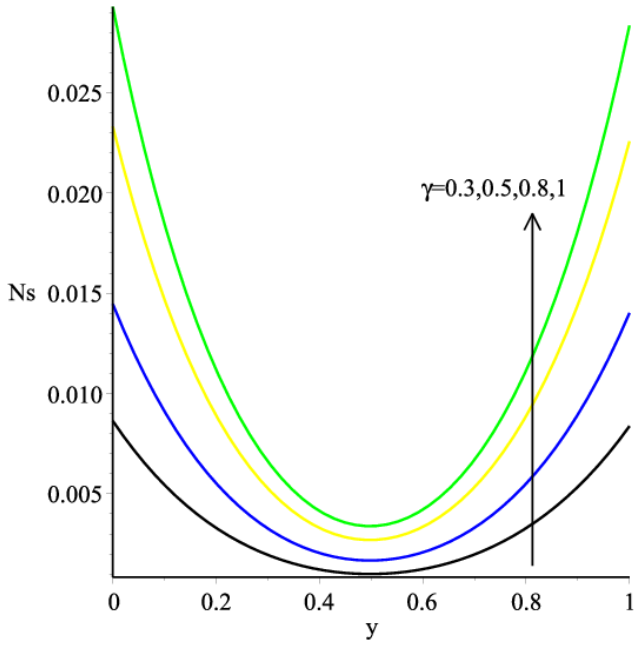

Figure 5.25: Effects of the viscous heating parameter on entropy generation rate

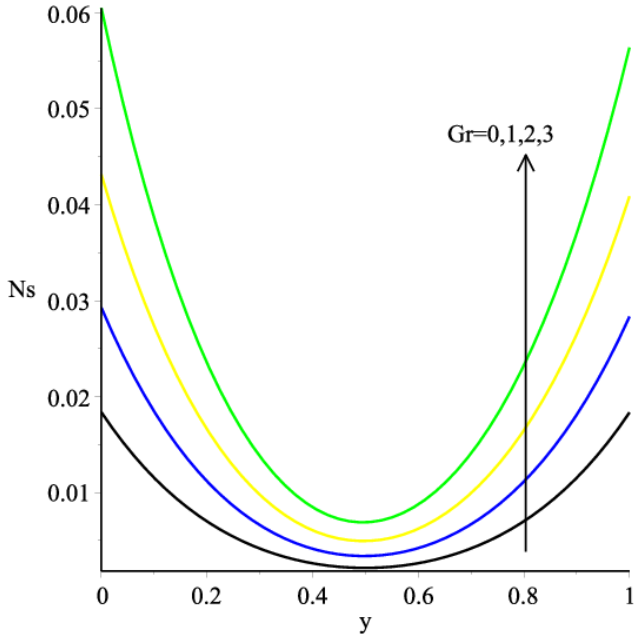

Figure 5.26: Effects of the Grashof number on entropy generation rate

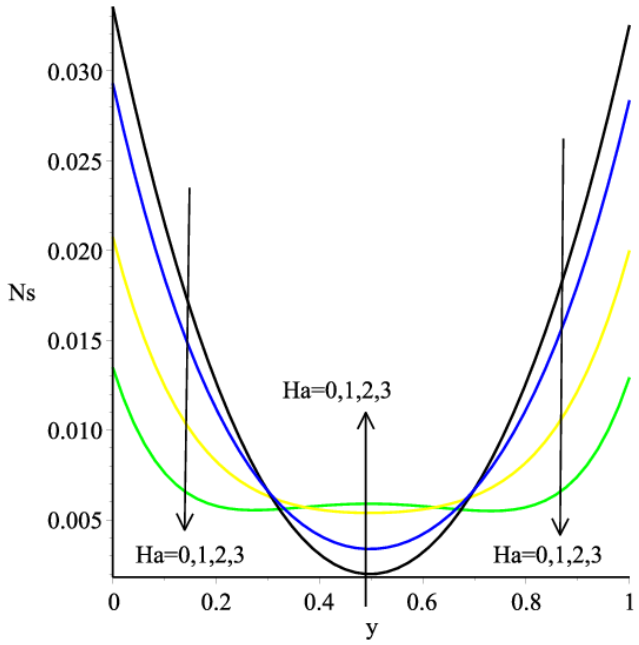

Figure 5.27: Effects of the Hartmann number on entropy generation rate

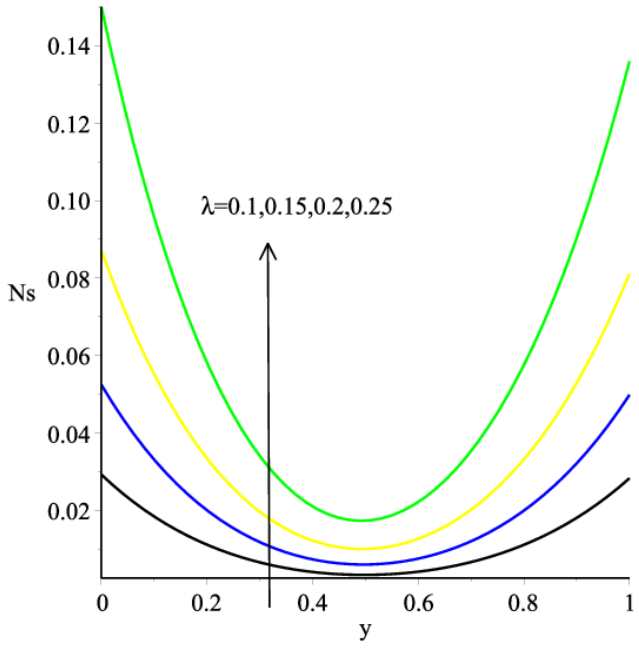

Figure 5.28: Effects of the Frank-Kameneskii parameter on entropy generation rate

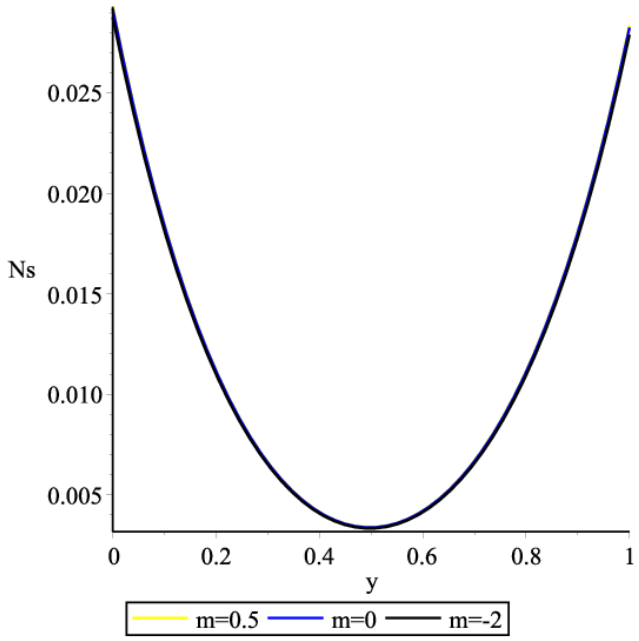

Figure 5.29: Effects of the chemical kinetics on entropy generation rate

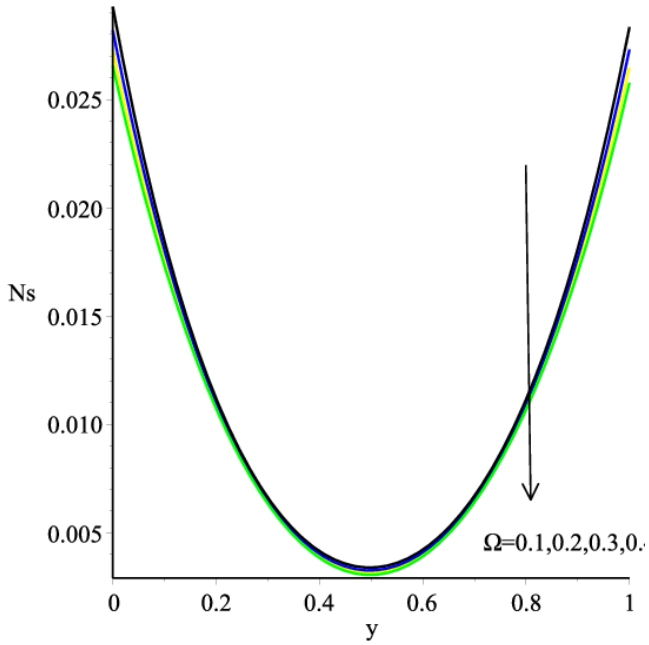

Figure 5.30: Effects of the third grade fluid material parameter on entropy generation rate

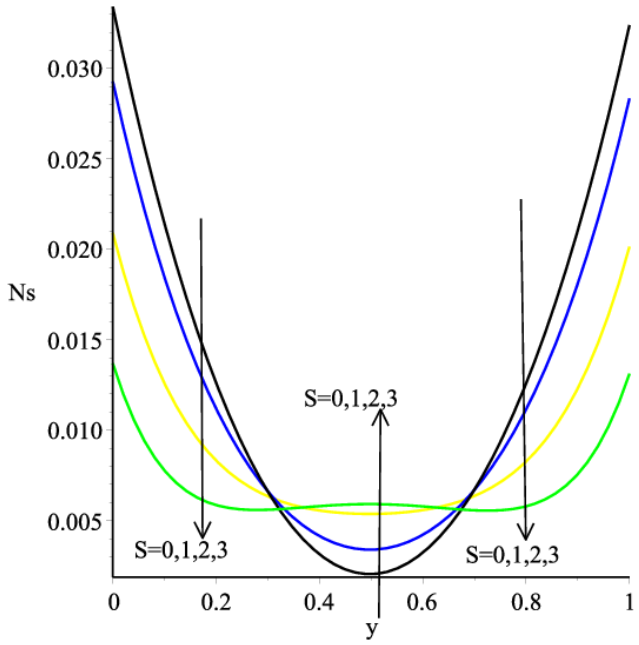

Figure 5.31: Effects of the porous medium shape parameter on entropy generation rate

The variation of the rate of entropy generation in the flow system is described in Figs. 5.23 – 5.31. Parabolic profiles are observed with minimum entropy generation rate along the core region of the channel and maximum at the channel walls. In Fig. 5.23, the rate of entropy generation is seen to increase with an increase in the variable viscosity parameter. Thus, as the fluid viscosity decreases, the entropy generation rate increases. The effect of the Biot number, Fig. 5.24, is exactly the opposite of the effect of the variable viscosity parameter. Entropy generation rate diminishes with increasing Biot number. Figure 5.25 displays the relationship between the viscous heating parameter and the entropy generation rate. The figure shows an increase in the viscous heating parameter significantly raising the rate of entropy generation. The Grashof number is observed to have the same effect as that of the viscous heating parameter (see Fig. 5.26). Thus, buoyancy has the effect of increasing the rate of entropy generation. Figures 5.27

and 5.31 depict similar variation of the entropy generation rate as the Hartmann number and the porous medium shape parameter are increased. At the channel core region, as the parameters are increased, the entropy generation rate increases from 0 and thereafter stabilizes. Towards the channel walls, the magnetic field and the porous medium retard the entropy generation rate significantly. In Fig. 5.28, the rate of exothermic chemical reaction has the same effects as the viscous heating parameter and buoyancy. The figure shows that an increase in the rate of chemical reaction significantly enhances the rate of entropy generation. Figure 5.29 shows that the entropy generation rate is not sensitive to the nature of the chemical reaction. The figure shows the entropy generation rate remaining the same regardless of whether the chemical reaction is Arrhenius, sensitized or bimolecular. In Fig. 5.30, the third grade material parameter marginally retards the entropy generation rate. Thus the non-Newtonian properties of the fluid, e.g. viscoelasticity, have the effect of marginally reducing the rate of entropy generation.

5.5.4 Irreversibility Ratio

Table 5.1 shows that the Bejan number remains unaltered at level $Be = 0$ by varying any parameter embedded in the flow system. This tells us that in this flow system the combined irreversibility due to the third grade fluid viscous dissipation, porous medium porosity and magnetic field is dominant over the heat transfer irreversibility.

Table 5.1: Variation of Bejan number in a response to the parameters

α	Bi_2	γ	Gr	Ha	λ	m	Ω	S	Be
								0	0
								1	0
								2	0
								3	0
							0.1		0
							0.2		0
							0.3		0
							0.4		0
						-2			0
						0			0
						0.5			0
					0.1				0
					0.15				0
					0.2				0
					0.25				0
				0					0
				1					0
				2					0
				3					0
			0						0
			1						0
			2						0
			3						0
		0.3							0
		0.5							0
		0.8							0
		1							0
	1								0
	2								0
	3								0
	4								0
0.1									0
0.3									0
0.5									0
0.8									0

5.6 Conclusion

In this chapter, entropy generation analysis of an unsteady flow of a reactive variable viscosity third grade fluid through a vertical channel filled with porous saturated medium and asymmetric convective boundary conditions was successfully investigated using a semi-implicit finite difference scheme. The flow was assumed to be driven by the combined effects of an axial pressure gradient and buoyancy, and was subjected to an externally applied transverse magnetic field. Graphical analysis of the response of the velocity and temperature distributions, entropy generation rate and irreversibility ratio to the various parameters embedded in the flow system was performed. The analysis revealed that the effects of the parameters on the thermo-fluid flow cannot be neglected. The flow velocity field is enhanced by the variable viscosity parameter, the Grashof number and the exothermic chemical reaction parameter, while the magnetic field, the porous medium and the third grade material parameter retard it. The variable viscosity parameter, the viscous heating parameter, the Grashof number, the exothermic chemical reaction parameter and the parameter m, where $m = -2$ represent sensitized reaction type, $m = 0$ represent the Arrhenius type of reaction and $m = 0.5$ represent the bimolecular type of reaction, increase the temperature field. On the other hand, the fluid temperature is decreased by the Biot number, the Prandtl number, the magnetic field and the porous medium. The entropy generation rate is enhanced by the variable viscosity parameter, the viscous heating parameter, the Grashof number and the exothermic chemical reaction parameter. The Biot number, the Hartmann number, the third grade material parameter and the porous medium have a retardation effect on the rate of entropy generation. It is also observed that the irreversibility ratio for this flow remained constant at $Be = 0$ irrespective of any value of any parameter. This phenomenon shows the dominance of the irreversibility due to the combined effects of the third grade fluid

viscous dissipation, the porous medium porosity and the magnetic field over the irreversibility due to heat transfer. It can also be concluded that, due to coupling, the fluid velocity and the fluid temperature increase and decrease together, and parameters that increase (decrease) the fluid velocity and the fluid temperature increase (decrease) the rate of entropy generation. These observations play an important role in the designs of thermo-fluid devices and processes that minimize entropy generation and ultimately achieving energy utilization efficiency.

Chapter 6

General Discussion, Conclusion and Recommendations

Chapter Abstract

In this chapter, a general discussion, a succinct summary of the results, recommendations and envisaged future work are outlined.

6.1 General Discussion

In this thesis, three problems focusing on second law analysis for reactive third grade fluid flow with variable properties have been studied. Different channel geometries and physical effects were considered. The semi-analytic ADM, the semi-implicit FDM and the SQLM were applied to solve the coupled nonlinear flow governing equations. The effects of the important thermophysical parameters on the flow velocity field, the temperature distribution, the entropy generation rate and the irreversibility ratio were investigated with the aid of graphical simulations.

Entropy generation analysis in a steady flow of a reactive variable exponential viscosity third grade fluid through an inclined channel filled with a saturated porous medium with Navier slip and convective boundary conditions was studied.

Combined effects of Navier slip, porous medium, variable viscosity, convective boundary conditions and constant heat flux were studied.

Inherent irreversibility analysis of an unsteady reactive hydromagnetic third grade fluid flow in a vertical channel filled with a porous medium with asymmetric convective boundary conditions was carried out. Combined effects of the porous medium, convective cooling, variable viscosity and magnetic field were investigated.

Combined effects of magnetic field, variable linear viscosity and thermal conductivity on a fully developed incompressible hydromagnetic third grade fluid flow in a horizontal channel with infinite plates was investigated.

The rate of entropy generation and Bejan number were successfully computed in all the three flow systems.

6.2 Conclusions

Some important results from the studied theoretical models can be summarized as follows:

Velocity Profiles

In the inclined channel flow with convective cooling at the lower plate and constant heat flux on the upper plate:

- Parabolic velocity profiles are observed with the maximum velocity at the channel core region.

- Closer to the lower plate the velocity is retarded by increasing values of the variable viscosity parameter and the Brinkmann number, whereas towards the upper wall the velocity is enhanced. The chemical reaction parameter has similar effects.

- The third grade material parameter and the porous medium shape parameter retard the velocity, while buoyancy effects increase the flow rate.

In the MHD flows:

- Parabolic velocity profiles are also observed with maximum velocity at the channel core region as well.
- The velocity profiles are enhanced by the variable viscosity parameter, the Brinkmann number, the Grashof number, and the exothermic chemical reaction parameter.
- The magnetic field, the porous medium and the third grade material parameter have a damping effect on the flows.

Fluid Temperature Profiles

In the inclined channel flow with convective cooling at the lower plate and constant heat flux on the upper plate:

- The temperature profiles are increased by the Grashof number, the Brinkmann number and the reaction parameter.
- The variable viscosity parameter, the porous medium and the third grade material parameter significantly decreases the fluid temperature.

In the MHD flow without porous media:

- The variable viscosity parameter, the Hartmann number, the Brinkmann number and the internal heat generation parameter enhance the fluid temperature.
- The third-grade material parameter diminishes the fluid temperature.

In the MHD flow with porous media:

- Fluid temperature is boosted by the variable viscosity parameter, the activation energy parameter, the Grashof number, the exothermic chemical reaction parameter and the reaction exponent m, where $m = -2$ represents a sensitized chemical reaction type, $m = 0$ represents an Arrhenius type of chemical reaction and $m = 0.5$ represents a bimolecular type of chemical reaction.

- The Biot number, the magnetic field and the porous media decrease the fluid temperature.

- The third grade material parameter displays no significant effect on the fluid temperature.

Entropy Generation Rate and Irreversibility Ratio

- In all the three problems, parabolic entropy generation profiles are observed where, in general, entropy is more pronounced near the channel walls and less significant along the core region of the channel.

- Entropy generation is enhanced by the Brinkmann number, the activation energy parameter, the exothermic chemical reaction parameter, the Grashof number, and the variable viscosity parameter.

- The third grade material parameter, the porous medium, the magnetic field and the Biot number retard the entropy generation rate.

- In the inclined channel flow with convective cooling at the lower plate and constant heat flux on the upper plate, the heat transfer irreversibility is dominant in the channel core region while at the centre of either half of the channel the irreversibility due to the combined effects of the third grade fluid viscous dissipation and porous medium porosity dominate.

- In the MHD flow without porous media, the irreversibility due to the combined effects of the third grade fluid viscous dissipation and the magnetic field is dominant at the core region of the channel, whereas at the centre region of each half of the channel heat transfer irreversibility is dominant. The dominance of the heat transfer irreversibility is enhanced by the Brinkmann number, the Hartmann number, the internal heat generation parameter and the pressure gradient. The third grade material parameter diminishes the dominance of the heat transfer irreversibility.

- In the MHD flow with porous media, the Bejan number is identically 0 irrespective of the value of any parameter, indicating the dominance of the irreversibility due to the combined effects of the magnetic field, the third grade fluid viscous dissipation and the porous medium porosity over the irreversibility due to heat transfer.

General Observation:

- Due to coupling, fluid velocity and fluid temperature decrease (increase) together in most situations.

- An interesting phenomenon that has been observed is that parameters that increase (decrease) the fluid velocity and the fluid temperature increase (decrease) the rate of entropy generation.

6.3 Recommendations

Sensitivity analysis of the flows has revealed that the effects of the embedded parameters on the thermo-fluid flows cannot be neglected. Thus, efficient and appropriate regulation of the parameters such as the Hartmann number, the Brinkmann number, the porous medium shape parameter, the third grade ma-

terial parameter, the variable viscosity parameter and the exothermic chemical reaction parameter, inevitably results in significant entropy generation minimization that would lead to optimal performance of thermomechanical systems.

6.4 Future Research

The future is pregnant with multiple possibilities. This work considered one dimensional laminar flow. Future work may involve:

- Modification of the studied problems to two and three dimensional laminar flow of third grade fluid or other non-Newtonian fluids like the couple stress fluid, the Casson fluid, power law fluid, and so on.
- As we have considered only Poiseuille flow, in future Couette flow can be considered.
- Application of other different solution techniques like the Hamotopy analysis method, the Finite element method, and others.

Appendix A
SQLM code

```
with(LinearAlgebra):
with(plots):
read "CHEB.txt":
Digits := 32:
Nx := 50: # Number of collocation points.
a := -1: b :=1: # eta in [0,10], domain of eta.
Leta := b-a: # Length of the domain of eta
D1 := d(Nx)[1]: # Original Chebychev differentiation matrix
x := d(Nx)[2]: # Guess Labato points
y := (1/2)*Leta*x+(a+b)*(1/2): #We transform the interval from [0,10] to [-1,1]
                        #for which we can implement spectral method
y := Transpose(y):
D1 := 2*D1/Leta:   #Scaled Chebychev differentiation matrix.
D1 := convert(D1, Matrix): # convert the vector to matrix, just for coding purpose.
D2 := MatrixPower(D1, 2): #Second derivative of the scaled Chebychev differentiation matrix
#Define the variables now
alpha:=0.1:
Omega:=0.1:
delta:=0.1:
#Gr:=0.5:
omega:=evalf(Pi/4):
G:=1:
Br:=0.5:
lambda:=0.1:
epsilon:=0.1:
beta[1]:=0.1:
beta[2]:=0.1:
Bi:=5.0:
m:=0.5:
```

```
CODE := [0.2,0.4,0.6]:
COL:=["Red", "Black", "Blue", "Green"]:
#LS := [dot, dash, dashdot, solid, longdash]:
LS := [solid, solid, solid, solid, solid]:
ones := Vector[column](Nx+1, fill = 1): #a unit column vector need during coding
ID := IdentityMatrix(Nx+1): # #Identity matrix need during coding
iterations := 10: # Number

#start the iteration
for j from 1 to nops(CODE) do
    Gr:=CODE[j]:
    ur:=y->  -(1/2)*G*y^2-G*(beta[1]+beta[2])*y/(beta[1]-beta[2]+2)
                -(1/2)*G*(4*beta[1]*beta[2]-3*beta[1]+3*beta[2]-2)/(beta[1]-beta[2]+2):
    thetar:=y-> 0:
    #Next convert the initial guesses into pointwise functions
        F[1] := Array([seq(ur(y[i]), i = 1 .. Nx+1)]):
        T[1] := Array([seq(thetar(y[i]), i = 1 .. Nx+1)]):
        F[2] := MatrixMatrixMultiply(D1, F[1]):
        F[3] := MatrixMatrixMultiply(D2, F[1]):
        T[2] := MatrixMatrixMultiply(D1, T[1]):
        T[3] := MatrixMatrixMultiply(D2, T[1]):
        for  n from 1 to iterations do
            #Define the coeffificents, i.e the alpha's
            fprev := F[1]:
            tprev := T[1]:
            p[1, n] := exp~(-alpha*T[1])+6*Omega*F[2]^~2:
            p[2, n] := 12*Omega*F[3]*~F[2]-alpha*exp~(-alpha*T[1])*~T[2]:
            p[3, n] := -delta*exp~(-alpha*T[1]):
            p[4, n] := -alpha*exp~(-alpha*T[1])*~F[2]:
```

```
                    p[5, n] := -alpha*exp~(-alpha*T[1])*~F[3]+alpha^2*exp~(-
alpha*T[1])*~F[2]*~T[2]

                        +delta*alpha*exp~(-alpha*T[1])*~F[1]+Gr*sin(omega)*ones:

                    p[6, n] := 2*Br*F[2]*~(exp~(-
alpha*T[1])+2*Omega*F[2]^~2)+4*Br*F[2]^~3*Omega:

                    p[7, n] := 2*delta*Br*exp~(-alpha*T[1])*~F[1]:

                    p[8,n]  := 1*ones:

                    p[9, n] := -Br*F[2]^~2*alpha*~exp~(-alpha*T[1]) -delta*Br*alpha*exp~(-
alpha*T[1])*~F[1]^~2

                    +exp~(T[1]/~(epsilon*T[1]+1*ones))*lambda*~((epsilon*T[1]+1*ones)^~(m-
1)*epsilon*m+(epsilon*T[1]+1*ones)^~(m-2)):


                    #Define the ODEs in pointwise form as follows

                    ODE[1]:= exp~(-alpha*T[1])*~F[3]+6*Omega*F[3]*~F[2]^~2-alpha*exp~(-
alpha*T[1])*~F[2]*~T[2]

                        -delta*exp~(-alpha*T[1])*~F[1]+Gr*T[1]*sin(omega)+G*ones:

                    ODE[2]:=T[3]+Br*F[2]^~2*~(exp~(-
alpha*T[1])+2*Omega*F[2]^~2)+delta*Br*exp~(-alpha*T[1])*~F[1]^~2

                        +lambda*(epsilon*T[1]+1*ones)^~m*~exp~(T[1]/~(epsilon*T[1]+1*ones)):


                    #Now we define the vector on the RHS's

                    RHS_F:= (p[1, n]*~F[3]+ p[2, n]*~F[2] + p[3, n]*~F[1]+ p[4, n]*~T[2] + p[5,
n]*~T[1])  - ODE[1]:


                RHS_T:= (p[6, n]*~F[2] + p[7, n]*~F[1]+ p[8, n]*~T[3] + p[9, n]*~T[1])  - ODE[2]:


                #Next we define the bigger matrix

                A11 := MatrixMatrixMultiply(DiagonalMatrix(p[1, n]), D2)

                                +MatrixMatrixMultiply(DiagonalMatrix(p[2, n]), D1)
+MatrixMatrixMultiply(DiagonalMatrix(p[3, n]), ID):

                    A12 :=  MatrixMatrixMultiply(DiagonalMatrix(p[4, n]), D1) +
MatrixMatrixMultiply(DiagonalMatrix(p[5, n]), ID):
```

```
A21 := MatrixMatrixMultiply(DiagonalMatrix(p[6, n]), D1)
+MatrixMatrixMultiply(DiagonalMatrix(p[7, n]), ID):

A22 := MatrixMatrixMultiply(DiagonalMatrix(p[8, n]), D2)
+MatrixMatrixMultiply(DiagonalMatrix(p[9, n]), ID):


#Imposing boundary conditions


A11[Nx+1 .. Nx+1, 1 .. -1] := beta[1]*exp~(-alpha*A12[Nx+1 .. Nx+1, 1 .. -
1])*~(D1[Nx+1 .. Nx+1, 1 .. -1])-ID[Nx+1 .. Nx+1, 1 .. -1]:

A12[Nx+1 .. Nx+1, 1 .. -1] := 0:

#A12[Nx+1 .. Nx+1, 1 .. -1] := -beta[1]*alpha*exp~(-alpha*A12[Nx+1 .. Nx+1, 1 ..
-1])*~(D1[Nx+1 .. Nx+1, 1 .. -1]):

RHS_F[Nx+1] := 0:


A21[Nx+1 .. Nx+1, 1 .. -1] := 0:

A22[Nx+1 .. Nx+1, 1 .. -1] := D1[Nx+1 .. Nx+1, 1 .. -1]+Bi*ID[Nx+1 .. Nx+1, 1 .. -1]:

RHS_T[Nx+1] := 0:


A11[1 .. 1, 1 .. -1] := beta[2]*exp~(-alpha*A12[1 .. 1, 1 .. -1])*~(D1[1 .. 1, 1 .. -1])-
ID[1 .. 1, 1 .. -1]:

A12[1 .. 1, 1 .. -1] := 0:

#A12[1 .. 1, 1 .. -1] := -beta[1]*alpha*exp~(-alpha*A12[1 .. 1, 1 .. -1])*~(D1[1 .. 1,
1 .. -1]):

RHS_F[1] := 0:


A21[1 .. 1, 1 .. -1] := 0:

A22[1 .. 1, 1 .. -1] := D1[1 .. 1, 1 .. -1]+Bi*ID[1 .. 1, 1 .. -1]:

RHS_T[1] := 0:


#Put all the RHS as a single column vector
```

```
                    RR := Matrix([seq(RHS_F[i], i = 1 .. Nx+1), seq(RHS_T[i], i = 1 .. Nx+1)]):
                    RR := convert(RR, Vector):
                    #Put the bigger matrix entries into it
                    AA := Matrix([[A11, A12], [A21, A22]]):
                    #Solve the system of equation AA*unknows = RR
                    SOL := LinearSolve(AA, RR):

                    #Extract the solution for the F, G,Theta and Phi
                    F[1] := Vector[column]([seq(SOL[i], i = 1 .. Nx+1)]):
                    F[2] := MatrixMatrixMultiply(D1, F[1]):
                F[3] := MatrixMatrixMultiply(D2, F[1]):

                    T[1] := Vector[column]([seq(SOL[i], i = (Nx+1)+1 .. 2*(Nx+1))]);
                    T[2] := MatrixMatrixMultiply(D1, T[1]);
                    T[3] := MatrixMatrixMultiply(D2, T[1]);
            od:#End of iteration
 NY:= [ seq(y[i],i=1..Nx+1)]:
 Vel[j]:= [ seq(F[1][i],i=1..Nx+1)]:
 VelPlot[j]:=plot(NY,Vel[j],color=COL[j],legend  = CODE[j] ,axes=box,labels=["y","u(y)"] ,linestyle=LS[j]) :
 Tem[j]:= [ seq(T[1][i],i=1..Nx+1)]:
 TemPlot[j]:=plot(NY,Tem[j],color=COL[j],legend  =CODE[j] ,axes = box,labels=["y","theta(y)"]
,linestyle=LS[j]) :
od:
display(seq(VelPlot[i], i = 1 .. nops(CODE)));
display(seq(TemPlot[i], i = 1 .. nops(CODE)));
```

Appendix B
MAPLE code

```
#Unsteady hydromagnetic flow of a reactive variable viscosity non-Newtonian fluid through a
    porous saturated medium with asymmetric
#convective boundary conditions
#model
Equation : diff(w(y,t),t) = G-Ha^2*w(y,t)-S^2*w(y,t)*exp(-b*C(y,t)) + exp(-b
    *C(y,t))*(diff(w(y,t),y$2))-b*exp(-b*C(y,t))*(diff(C(y,t),y))
*(diff(w(y,t),y)) + e1*(diff(w(y,t),y$2,t)) + 6*d1*(diff(w(y,t),y$2))*(diff(w(y,t),
    y))^2 + Gr·C(y,t),Pr*(diff(C(y,t),t)) = diff(C(y,t),y$2) +
g1*((1 + E2*C(y,t))^m*exp(C(y,t)/(1 + E2*C(y,t))) + N*(Ha^2*(w(y,t))^2 + S^2
    *(w(y,t))^2*exp(-b*C(y,t)) + (diff(w(y,t),y))^2*(exp(-b*C(y,t)) +
2*d1*(diff(w(y,t),y))^2)))



    #Initial and boundary conditions w(y, 0) = 0, C(y, 0) = 0, w(0, t) = 0,D[1](C)(0, t) = -Bi*
    (h-C(0, t)), w(1, t) = 0, D[1](C)(1, t) = -Bj*(C(1, t)-h)

    #Parameter values G:=1: Pr:=10: h:=0.1: e1:=0.000001: g1:=0.1: Bi:=0.1: Bj:=1: m:=
    0.5: E2:=0.1: b:=0.1: N:=0.1: d1:=0.0001: S:=1: Ha:=1:
#please note the following:
#w(y,t) and C(y,t) represent velocity and temperature profiles respectively


#here we examine steady state profiles

#velocity profile
with(plots):

G := 1: Pr := 10: h := 0.1: e1 := 0.1: g1 := 0.000001: Bi := 0.1: Bj := 1: m := 0.5: E2
    := 0.1: b := 0.1: N := 0.1: d1 := 0.0001: S := 1: Ha := 1: Gr := 1:
fcns := [w(y,t),C(y,t)]:
IBC := [w(y,0) = 0, C(y,0) = 0, w(0,t) = 0, D[1](C)(0,t) = -Bi*(h-C(0,t)), w(1,t) = 0,
    D[1](C)(1,t) = -Bj*(C(1,t)-h)]:

sys := [diff(w(y,t),t) = G-Ha^2*w(y,t)-S^2*w(y,t)*exp(-b*C(y,t)) + exp(-b*C(y,
    t))*(diff(w(y,t),y$2))-b*exp(-b*C(y,t))*(diff(C(y,t),y))
*(diff(w(y,t),y)) + e1*(diff(w(y,t),y$2,t)) + 6*d1*(diff(w(y,t),y$2))*(diff(w(y,t),
    y))^2 + Gr·C(y,t),Pr*(diff(C(y,t),t)) = diff(C(y,t),y$2) +
g1*((1 + E2*C(y,t))^m*exp(C(y,t)/(1 + E2*C(y,t))) + N*(Ha^2*(w(y,t))^2 + S^2
    *(w(y,t))^2*exp(-b*C(y,t)) + (diff(w(y,t),y))^2*(exp(-b*C(y,t)) +
2*d1*(diff(w(y,t),y))^2))):

pds := pdsolve(sys,IBC,fcns,numeric):

p1w := pds:-plot(w(y,t), t=0.1, y=0..1, numpoints=50, labels=["y","u"], style=line, color
    =black):
p2w := pds:-plot(w(y,t), t=0.3, y=0..1, numpoints=50, labels=["y","u"], style=line, color
    =blue):
p3w := pds:-plot(w(y,t), t=0.5, y=0..1, numpoints=50, labels=["y","u"], style=line, color
    =yellow):
p4w := pds:-plot(w(y,t), t=1, y=0..1, numpoints=50, labels=["y","u"], style=line, color
    =green):
p5w := pds:-plot(w(y,t), t=2, y=0..1, numpoints=50, labels=["y","u"], style=line, color
    =red):
plots[display]({p1w,p2w,p3w,p4w,p5w});
```

```
with(plots) :

G := 1 : Pr := 10 : h := 0.1 : e1 := 0.000001 : g1 := 0.1 : Bi := 0.1 : Bj := 1 : m := 0.5 : E2
     := 0.1 : b := 0.1 : N := 0.1 : d1 := 0.0001 : S := 1 : Ha := 1 : Gr := 1 :
fcns := [w(y,t), C(y,t)] :
IBC := [w(y,0) = 0, C(y,0) = 0, w(0,t) = 0, D[1](C)(0,t) = -Bi*(h-C(0,t)), w(1,t) = 0,
     D[1](C)(1,t) = -Bj*(C(1,t)-h)] :

sys := [diff(w(y,t),t) = G-Ha^2*w(y,t)-S^2*w(y,t)*exp(-b*C(y,t)) + exp(-b*C(y,
     t))*(diff(w(y,t),y$2))-b*exp(-b*C(y,t))*(diff(C(y,t),y))
*(diff(w(y,t),y)) + e1*(diff(w(y,t),y$2,t)) + 6*d1*(diff(w(y,t),y$2))*(diff(w(y,t),
     y))^2 + Gr·C(y,t), Pr*(diff(C(y,t),t)) = diff(C(y,t),y$2) +
g1*((1 + E2*C(y,t))^m*exp(C(y,t)/(1 + E2*C(y,t))) + N*(Ha^2*(w(y,t))^2 + S^2
     *(w(y,t))^2*exp(-b*C(y,t)) + (diff(w(y,t),y))^2*(exp(-b*C(y,t)) +
2*d1*(diff(w(y,t),y))^2))] :

pds := pdsolve(sys, IBC, fcns, numeric) :

p1C := pds:-plot(C(y,t), t = 10, y = 0..1, numpoints = 50, labels = ["y", "C"], style = line, color
     = black) :
p2C := pds:-plot(C(y,t), t = 20, y = 0..1, numpoints = 50, labels = ["y", "C"], style = line, color
     = blue) :
p3C := pds:-plot(C(y,t), t = 40, y = 0..1, numpoints = 50, labels = ["y", "C"], style = line, color
     = yellow) :
p4C := pds:-plot(C(y,t), t = 80, y = 0..1, numpoints = 50, labels = ["y", "C"], style = line, color
     = green) :
p5C := pds:-plot(C(y,t), t = 200, y = 0..1, numpoints = 50, labels = ["y", "C"], style = line, color
     = red) :
plots[display]({p1C, p2C, p3C, p4C, p5C});
```

```
#Effects of the non-Newtonian parameter (d1) on velocity

with(plots) :

G := 1 : Pr := 10 : h := 0.1 : e1 := 0.000001 : g1 := 0.1 : Bi := 0.1 : Bj := 1 : m := 0.5 : E2
     := 0.1 : b := 0.1 : N := 0.1 : d1 := 0 : S := 1 : Ha := 1 : Gr := 1 :
fcns := [w(y,t), C(y,t)] :
IBC := [w(y,0) = 0, C(y,0) = 0, w(0,t) = 0, D[1](C)(0,t) = -Bi*(h-C(0,t)), w(1,t) = 0,
     D[1](C)(1,t) = -Bj*(C(1,t)-h)] :

sys := [diff(w(y,t),t) = G-Ha^2*w(y,t)-S^2*w(y,t)*exp(-b*C(y,t)) + exp(-b*C(y,
     t))*(diff(w(y,t),y$2))-b*exp(-b*C(y,t))*(diff(C(y,t),y))
*(diff(w(y,t),y)) + e1*(diff(w(y,t),y$2,t)) + 6*d1*(diff(w(y,t),y$2))*(diff(w(y,t),
     y))^2 + Gr·C(y,t), Pr*(diff(C(y,t),t)) = diff(C(y,t),y$2) +
g1*((1 + E2*C(y,t))^m*exp(C(y,t)/(1 + E2*C(y,t))) + N*(Ha^2*(w(y,t))^2 + S^2
     *(w(y,t))^2*exp(-b*C(y,t)) + (diff(w(y,t),y))^2*(exp(-b*C(y,t)) +
2*d1*(diff(w(y,t),y))^2)))] :

pds := pdsolve(sys, IBC, fcns, numeric) :

p1w := pds:-plot(w(y,t), t = 200, y = 0..1, numpoints = 50, labels = ["y", "u"], style = line, color
     = black) :

with(plots) :

G := 1 : Pr := 10 : h := 0.1 : e1 := 0.000001 : g1 := 0.1 : Bi := 0.1 : Bj := 1 : m := 0.5 : E2
     := 0.1 : b := 0.1 : N := 0.1 : d1 := 0.1 : S := 1 : Ha := 1 : Gr := 1 :
fcns := [w(y,t), C(y,t)] :
IBC := [w(y,0) = 0, C(y,0) = 0, w(0,t) = 0, D[1](C)(0,t) = -Bi*(h-C(0,t)), w(1,t) = 0,
     D[1](C)(1,t) = -Bj*(C(1,t)-h)] :

sys := [diff(w(y,t),t) = G-Ha^2*w(y,t)-S^2*w(y,t)*exp(-b*C(y,t)) + exp(-b*C(y,
     t))*(diff(w(y,t),y$2))-b*exp(-b*C(y,t))*(diff(C(y,t),y))
*(diff(w(y,t),y)) + e1*(diff(w(y,t),y$2,t)) + 6*d1*(diff(w(y,t),y$2))*(diff(w(y,t),
     y))^2 + Gr·C(y,t), Pr*(diff(C(y,t),t)) = diff(C(y,t),y$2) +
g1*((1 + E2*C(y,t))^m*exp(C(y,t)/(1 + E2*C(y,t))) + N*(Ha^2*(w(y,t))^2 + S^2
     *(w(y,t))^2*exp(-b*C(y,t)) + (diff(w(y,t),y))^2*(exp(-b*C(y,t)) +
2*d1*(diff(w(y,t),y))^2)))] :

pds := pdsolve(sys, IBC, fcns, numeric) :
p2w := pds:-plot(w(y,t), t = 200, y = 0..1, numpoints = 50, labels = ["y", "u"], style = line, color
     = blue) :

with(plots) :

G := 1 : Pr := 10 : h := 0.1 : e1 := 0.000001 : g1 := 0.1 : Bi := 0.1 : Bj := 1 : m := 0.5 : E2
     := 0.1 : b := 0.1 : N := 0.1 : d1 := 0.2 : S := 1 : Ha := 1 : Gr := 1 :
fcns := [w(y,t), C(y,t)] :
IBC := [w(y,0) = 0, C(y,0) = 0, w(0,t) = 0, D[1](C)(0,t) = -Bi*(h-C(0,t)), w(1,t) = 0,
     D[1](C)(1,t) = -Bj*(C(1,t)-h)] :

sys := [diff(w(y,t),t) = G-Ha^2*w(y,t)-S^2*w(y,t)*exp(-b*C(y,t)) + exp(-b*C(y,
     t))*(diff(w(y,t),y$2))-b*exp(-b*C(y,t))*(diff(C(y,t),y))
*(diff(w(y,t),y)) + e1*(diff(w(y,t),y$2,t)) + 6*d1*(diff(w(y,t),y$2))*(diff(w(y,t),
     y))^2 + Gr·C(y,t), Pr*(diff(C(y,t),t)) = diff(C(y,t),y$2) +
g1*((1 + E2*C(y,t))^m*exp(C(y,t)/(1 + E2*C(y,t))) + N*(Ha^2*(w(y,t))^2 + S^2
     *(w(y,t))^2*exp(-b*C(y,t)) + (diff(w(y,t),y))^2*(exp(-b*C(y,t)) +
2*d1*(diff(w(y,t),y))^2)))] :

pds := pdsolve(sys, IBC, fcns, numeric) :
p3w := pds:-plot(w(y,t), t = 200, y = 0..1, numpoints = 50, labels = ["y", "u"], style = line, color
     = yellow) :

with(plots) :
```

```
with(plots) :

G := 1 : Pr := 10 : h := 0.1 : e1 := 0.1 : g1 := 0.1 : Bi := 0.1 : Bj := 1 : m := 0.5 : E2
     := 0.1 : b := 0.1 : N := 1 : d1 := 0.1 : S := 1 : Ha := 1 : Gr := 0 :
fcns := [w(y,t), C(y,t)] :
IBC := [w(y,0) = 0, C(y,0) = 0, w(0,t) = 0, D[1](C)(0,t) = -Bi*(h-C(0,t)), w(1,t) = 0,
     D[1](C)(1,t) = -Bj*(C(1,t)-h)] :

sys := [diff(w(y,t),t) = G-Ha^2*w(y,t)-S^2*w(y,t)*exp(-b*C(y,t)) + exp(-b*C(y,
     t))*(diff(w(y,t),y$2))-b*exp(-b*C(y,t))*(diff(C(y,t),y))
*(diff(w(y,t),y)) + e1*(diff(w(y,t),y$2,t)) + 6*d1*(diff(w(y,t),y$2))*(diff(w(y,t),
     y))^2 + Gr·C(y,t), Pr*(diff(C(y,t),t)) = diff(C(y,t),y$2) +
g1*((1 + E2*C(y,t))^m*exp(C(y,t)/(1 + E2*C(y,t))) + N*(Ha^2*(w(y,t))^2 + S^2
     *(w(y,t))^2*exp(-b*C(y,t)) + (diff(w(y,t),y))^2*(exp(-b*C(y,t)) +
2*d1*(diff(w(y,t),y))^2)))] :

pds := pdsolve(sys, IBC, fcns, numeric) :

p1C := pds:-plot(C(y,t), t = 200, y = 0..1, numpoints = 50, labels = ["y", "C"], style = line, color
     = black) :

with(plots) :

G := 1 : Pr := 10 : h := 0.1 : e1 := 0.1 : g1 := 0.1 : Bi := 0.1 : Bj := 1 : m := 0.5 : E2
     := 0.1 : b := 0.1 : N := 1 : d1 := 0.1 : S := 1 : Ha := 1 : Gr := 1 :
fcns := [w(y,t), C(y,t)] :
IBC := [w(y,0) = 0, C(y,0) = 0, w(0,t) = 0, D[1](C)(0,t) = -Bi*(h-C(0,t)), w(1,t) = 0,
     D[1](C)(1,t) = -Bj*(C(1,t)-h)] :

sys := [diff(w(y,t),t) = G-Ha^2*w(y,t)-S^2*w(y,t)*exp(-b*C(y,t)) + exp(-b*C(y,
     t))*(diff(w(y,t),y$2))-b*exp(-b*C(y,t))*(diff(C(y,t),y))
*(diff(w(y,t),y)) + e1*(diff(w(y,t),y$2,t)) + 6*d1*(diff(w(y,t),y$2))*(diff(w(y,t),
     y))^2 + Gr·C(y,t), Pr*(diff(C(y,t),t)) = diff(C(y,t),y$2) +
g1*((1 + E2*C(y,t))^m*exp(C(y,t)/(1 + E2*C(y,t))) + N*(Ha^2*(w(y,t))^2 + S^2
     *(w(y,t))^2*exp(-b*C(y,t)) + (diff(w(y,t),y))^2*(exp(-b*C(y,t)) +
2*d1*(diff(w(y,t),y))^2)))] :

pds := pdsolve(sys, IBC, fcns, numeric) :
p2C := pds:-plot(C(y,t), t = 200, y = 0..1, numpoints = 50, labels = ["y", "C"], style = line, color
     = blue) :

with(plots) :

G := 1 : Pr := 10 : h := 0.1 : e1 := 0.1 : g1 := 0.1 : Bi := 0.1 : Bj := 1 : m := 0.5 : E2
     := 0.1 : b := 0.1 : N := 1 : d1 := 0.1 : S := 1 : Ha := 1 : Gr := 2 :
fcns := [w(y,t), C(y,t)] :
IBC := [w(y,0) = 0, C(y,0) = 0, w(0,t) = 0, D[1](C)(0,t) = -Bi*(h-C(0,t)), w(1,t) = 0,
     D[1](C)(1,t) = -Bj*(C(1,t)-h)] :

sys := [diff(w(y,t),t) = G-Ha^2*w(y,t)-S^2*w(y,t)*exp(-b*C(y,t)) + exp(-b*C(y,
     t))*(diff(w(y,t),y$2))-b*exp(-b*C(y,t))*(diff(C(y,t),y))
*(diff(w(y,t),y)) + e1*(diff(w(y,t),y$2,t)) + 6*d1*(diff(w(y,t),y$2))*(diff(w(y,t),
     y))^2 + Gr·C(y,t), Pr*(diff(C(y,t),t)) = diff(C(y,t),y$2) +
g1*((1 + E2*C(y,t))^m*exp(C(y,t)/(1 + E2*C(y,t))) + N*(Ha^2*(w(y,t))^2 + S^2
     *(w(y,t))^2*exp(-b*C(y,t)) + (diff(w(y,t),y))^2*(exp(-b*C(y,t)) +
2*d1*(diff(w(y,t),y))^2)))] :

pds := pdsolve(sys, IBC, fcns, numeric) :
p3C := pds:-plot(C(y,t), t = 200, y = 0..1, numpoints = 50, labels = ["y", "C"], style = line, color
     = yellow) :

with(plots) :

G := 1 : Pr := 10 : h := 0.1 : e1 := 0.1 : g1 := 0.1 : Bi := 0.1 : Bj := 1 : m := 0.5 : E2
     := 0.1 : b := 0.1 : N := 1 : d1 := 0.1 : S := 1 : Ha := 1 : Gr := 3 :
```

```
with(plots):
G := 1: Pr := 10: h := 0.1: e1 := 0.1: g1 := 0.1: Bi := 0.1: Bj := 1: m := 0.5: E2
     := 0.1: b := 0.1: N := 1: d1 := 0.1: S := 1: Ha := 1: Gr := 1:
fcns := {w(y), C(y)}:
sys := G-Ha^2*w(y)-S^2*w(y)*exp(-b*C(y)) + exp(-b*C(y))*(diff(w(y),y$2))-b
     *exp(-b*C(y))*(diff(C(y),y))
*(diff(w(y),y)) + 6*d1*(diff(w(y),y$2))*(diff(w(y),y))^2 + Gr·C(y) = 0, diff(C(y),y
     $2) +
g1*((1 + E2*C(y))^m*exp(C(y)/(1 + E2*C(y))) + N*(Ha^2*(w(y))^2 + S^2
     *(w(y))^2*exp(-b*C(y)) + (diff(w(y),y))^2*(exp(-b*C(y)) +
2*d1*(diff(w(y),y))^2))) = 0:
p1 := dsolve({sys, w(0) = 0, w(1) = 0, D(C)(0) = -Bi*(h-C(0)), D(C)(1) = -Bj*(C(1)
     -h)}, fcns, type = numeric, method = bvp[midrich], abserr = 1e-10):
p1C1 := odeplot(p1, [y, diff(C(y),y$2) + g1·N·((diff(w(y),y))^2·(exp(-b·C(y)) + 2·d1
     ·(diff(w(y),y))^2) + (Ha^2 + S^2·exp(-b·C(y)))·(w(y))^2)], 0..1, numpoints = 50, labels
     = ["y", "Ns"], style = line, color = black):

with(plots):
G := 1: Pr := 10: h := 0.1: e1 := 0.1: g1 := 0.15: Bi := 0.1: Bj := 1: m := 0.5: E2
     := 0.1: b := 0.1: N := 1: d1 := 0.1: S := 1: Ha := 1: Gr := 1:
fcns := {w(y), C(y)}:
sys := G-Ha^2*w(y)-S^2*w(y)*exp(-b*C(y)) + exp(-b*C(y))*(diff(w(y),y$2))-b
     *exp(-b*C(y))*(diff(C(y),y))
*(diff(w(y),y)) + 6*d1*(diff(w(y),y$2))*(diff(w(y),y))^2 + Gr·C(y) = 0, diff(C(y),y
     $2) +
g1*((1 + E2*C(y))^m*exp(C(y)/(1 + E2*C(y))) + N*(Ha^2*(w(y))^2 + S^2
     *(w(y))^2*exp(-b*C(y)) + (diff(w(y),y))^2*(exp(-b*C(y)) +
2*d1*(diff(w(y),y))^2))) = 0:
p1 := dsolve({sys, w(0) = 0, w(1) = 0, D(C)(0) = -Bi*(h-C(0)), D(C)(1) = -Bj*(C(1)
     -h)}, fcns, type = numeric, method = bvp[midrich], abserr = 1e-10):
p1C2 := odeplot(p1, [y, diff(C(y),y$2) + g1·N·((diff(w(y),y))^2·(exp(-b·C(y)) + 2·d1
     ·(diff(w(y),y))^2) + (Ha^2 + S^2·exp(-b·C(y)))·(w(y))^2)], 0..1, numpoints = 50, labels
     = ["y", "Ns"], style = line, color = blue):

with(plots):
G := 1: Pr := 10: h := 0.1: e1 := 0.1: g1 := 0.2: Bi := 0.1: Bj := 1: m := 0.5: E2
     := 0.1: b := 0.1: N := 1: d1 := 0.1: S := 1: Ha := 1: Gr := 1:
fcns := {w(y), C(y)}:
sys := G-Ha^2*w(y)-S^2*w(y)*exp(-b*C(y)) + exp(-b*C(y))*(diff(w(y),y$2))-b
     *exp(-b*C(y))*(diff(C(y),y))
*(diff(w(y),y)) + 6*d1*(diff(w(y),y$2))*(diff(w(y),y))^2 + Gr·C(y) = 0, diff(C(y),y
     $2) +
g1*((1 + E2*C(y))^m*exp(C(y)/(1 + E2*C(y))) + N*(Ha^2*(w(y))^2 + S^2
     *(w(y))^2*exp(-b*C(y)) + (diff(w(y),y))^2*(exp(-b*C(y)) +
2*d1*(diff(w(y),y))^2))) = 0:
p1 := dsolve({sys, w(0) = 0, w(1) = 0, D(C)(0) = -Bi*(h-C(0)), D(C)(1) = -Bj*(C(1)
     -h)}, fcns, type = numeric, method = bvp[midrich], abserr = 1e-10):
p1C3 := odeplot(p1, [y, diff(C(y),y$2) + g1·N·((diff(w(y),y))^2·(exp(-b·C(y)) + 2·d1
     ·(diff(w(y),y))^2) + (Ha^2 + S^2·exp(-b·C(y)))·(w(y))^2)], 0..1, numpoints = 50, labels
     = ["y", "Ns"], style = line, color = yellow):

with(plots):
G := 1: Pr := 10: h := 0.1: e1 := 0.1: g1 := 0.25: Bi := 0.1: Bj := 1: m := 0.5: E2
     := 0.1: b := 0.1: N := 1: d1 := 0.1: S := 1: Ha := 1: Gr := 1:
fcns := {w(y), C(y)}:
sys := G-Ha^2*w(y)-S^2*w(y)*exp(-b*C(y)) + exp(-b*C(y))*(diff(w(y),y$2))-b
     *exp(-b*C(y))*(diff(C(y),y))
*(diff(w(y),y)) + 6*d1*(diff(w(y),y$2))*(diff(w(y),y))^2 + Gr·C(y) = 0, diff(C(y),y
     $2) +
g1*((1 + E2*C(y))^m*exp(C(y)/(1 + E2*C(y))) + N*(Ha^2*(w(y))^2 + S^2
     *(w(y))^2*exp(-b*C(y)) + (diff(w(y),y))^2*(exp(-b*C(y)) +
2*d1*(diff(w(y),y))^2))) = 0:
p1 := dsolve({sys, w(0) = 0, w(1) = 0, D(C)(0) = -Bi*(h-C(0)), D(C)(1) = -Bj*(C(1)
     -h)}, fcns, type = numeric, method = bvp[midrich], abserr = 1e-10):
```

```
with(plots) :
G := 1 : Pr := 10 : h := 0.1 : e1 := 0.1 : g1 := 0.1 : Bi := 0.1 : Bj := 1 : m := 0.5 : E2
     := 0.1 : b := 0.1 : N := 1 : d1 := 0.1 : S := 1 : Ha := 1 : Gr := 1 :
fcns := {w(y), C(y)} :
sys := G-Ha^2*w(y)-S^2*w(y)*exp(-b*C(y)) + exp(-b*C(y))*(diff(w(y),y$2))-b
     *exp(-b*C(y))*(diff(C(y),y))
*(diff(w(y),y)) + 6*d1*(diff(w(y),y$2))*(diff(w(y),y))^2 + Gr·C(y) = 0, diff(C(y),y
     $2) +
g1*((1 + E2*C(y))^m*exp(C(y)/(1 + E2*C(y))) + N*(Ha^2*(w(y))^2 + S^2
     *(w(y))^2*exp(-b*C(y)) + (diff(w(y),y))^2*(exp(-b*C(y)) +
2*d1*(diff(w(y),y))^2))) = 0 :
p1 := dsolve({sys, w(0) = 0, w(1) = 0, D(C)(0) = -Bi*(h-C(0)), D(C)(1) = -Bj*(C(1)
     -h)}, fcns, type = numeric, method = bvp[midrich], abserr = 1e-10) :
p1C1 := odeplot(p1, [y, (diff(C(y),y$2))/(diff(C(y),y$2) + g1·N·((diff(w(y),y))^2
     ·(exp(-b·C(y)) + 2·d1·(diff(w(y),y))^2) + (Ha^2 + S^2·exp(-b·C(y)))·(w(y))^2))], 0
     ..1, numpoints = 50, labels = ["y", "Ns"], style = line, color = black) :

with(plots) :
G := 1 : Pr := 10 : h := 0.1 : e1 := 0.1 : g1 := 0.1 : Bi := 0.1 : Bj := 1 : m := 0.5 : E2
     := 0.1 : b := 0.1 : N := 1 : d1 := 0.2 : S := 1 : Ha := 1 : Gr := 1 :
fcns := {w(y), C(y)} :
sys := G-Ha^2*w(y)-S^2*w(y)*exp(-b*C(y)) + exp(-b*C(y))*(diff(w(y),y$2))-b
     *exp(-b*C(y))*(diff(C(y),y))
*(diff(w(y),y)) + 6*d1*(diff(w(y),y$2))*(diff(w(y),y))^2 + Gr·C(y) = 0, diff(C(y),y
     $2) +
g1*((1 + E2*C(y))^m*exp(C(y)/(1 + E2*C(y))) + N*(Ha^2*(w(y))^2 + S^2
     *(w(y))^2*exp(-b*C(y)) + (diff(w(y),y))^2*(exp(-b*C(y)) +
2*d1*(diff(w(y),y))^2))) = 0 :
p1 := dsolve({sys, w(0) = 0, w(1) = 0, D(C)(0) = -Bi*(h-C(0)), D(C)(1) = -Bj*(C(1)
     -h)}, fcns, type = numeric, method = bvp[midrich], abserr = 1e-10) :
p1C2 := odeplot(p1, [y, (diff(C(y),y$2))/(diff(C(y),y$2) + g1·N·((diff(w(y),y))^2
     ·(exp(-b·C(y)) + 2·d1·(diff(w(y),y))^2) + (Ha^2 + S^2·exp(-b·C(y)))·(w(y))^2))], 0
     ..1, numpoints = 50, labels = ["y", "Ns"], style = line, color = blue) :

with(plots) :
G := 1 : Pr := 10 : h := 0.1 : e1 := 0.1 : g1 := 0.1 : Bi := 0.1 : Bj := 1 : m := 0.5 : E2
     := 0.1 : b := 0.1 : N := 1 : d1 := 0.3 : S := 1 : Ha := 1 : Gr := 1 :
fcns := {w(y), C(y)} :
sys := G-Ha^2*w(y)-S^2*w(y)*exp(-b*C(y)) + exp(-b*C(y))*(diff(w(y),y$2))-b
     *exp(-b*C(y))*(diff(C(y),y))
*(diff(w(y),y)) + 6*d1*(diff(w(y),y$2))*(diff(w(y),y))^2 + Gr·C(y) = 0, diff(C(y),y
     $2) +
g1*((1 + E2*C(y))^m*exp(C(y)/(1 + E2*C(y))) + N*(Ha^2*(w(y))^2 + S^2
     *(w(y))^2*exp(-b*C(y)) + (diff(w(y),y))^2*(exp(-b*C(y)) +
2*d1*(diff(w(y),y))^2))) = 0 :
p1 := dsolve({sys, w(0) = 0, w(1) = 0, D(C)(0) = -Bi*(h-C(0)), D(C)(1) = -Bj*(C(1)
     -h)}, fcns, type = numeric, method = bvp[midrich], abserr = 1e-10) :
p1C3 := odeplot(p1, [y, (diff(C(y),y$2))/(diff(C(y),y$2) + g1·N·((diff(w(y),y))^2
     ·(exp(-b·C(y)) + 2·d1·(diff(w(y),y))^2) + (Ha^2 + S^2·exp(-b·C(y)))·(w(y))^2))], 0
     ..1, numpoints = 50, labels = ["y", "Ns"], style = line, color = yellow) :

with(plots) :
G := 1 : Pr := 10 : h := 0.1 : e1 := 0.1 : g1 := 0.1 : Bi := 0.1 : Bj := 1 : m := 0.5 : E2
     := 0.1 : b := 0.1 : N := 1 : d1 := 0.4 : S := 1 : Ha := 1 : Gr := 1 :
fcns := {w(y), C(y)} :
sys := G-Ha^2*w(y)-S^2*w(y)*exp(-b*C(y)) + exp(-b*C(y))*(diff(w(y),y$2))-b
     *exp(-b*C(y))*(diff(C(y),y))
*(diff(w(y),y)) + 6*d1*(diff(w(y),y$2))*(diff(w(y),y))^2 + Gr·C(y) = 0, diff(C(y),y
     $2) +
g1*((1 + E2*C(y))^m*exp(C(y)/(1 + E2*C(y))) + N*(Ha^2*(w(y))^2 + S^2
```

References

[1] O. Levenspiel, "Non-newtonian fluids," in *Engineering Flow and Heat Exchange*, pp. 99–131, Springer, Boston, MA, 2014.

[2] H. Xu, L. Gong, C. Zhao, Y. Yang, and Z. Xu, "Analytical considerations of local thermal non-equilibrium conditions for thermal transport in metal foams," *International Journal of Thermal Sciences*, vol. 95, pp. 73–87, 2015.

[3] A. Kantzas, J. Bryan, and S. Taheri, *Fundamentals of fluid flow in porous media*. Pore size distribution, Canada, Calgary, 2012.

[4] U. Jeong, T.-J. Kim, Y. H. Kim, H. H. Son, G. H. Seo, and S. J. Kim, "Numerical evaluation of smco permanent magnet flowmeter measuring sodium flow in a low flow rate regime using fluent/mhd module," *Journal of Nuclear Science and Technology*, vol. 53, no. 2, pp. 173–183, 2016.

[5] M. A. Timmer, K. de Blok, and T. H. van der Meer, "Review on the conversion of thermoacoustic power into electricity," *The Journal of the Acoustical Society of America*, vol. 143, no. 2, pp. 841–857, 2018.

[6] O. Al-Habahbeh, M. Al-Saqqa, M. Safi, and T. A. Khater, "Review of magnetohydrodynamic pump applications," *Alexandria Engineering Journal*, vol. 55, no. 2, pp. 1347–1358, 2016.

[7] H. F. Oztop and E. Abu-Nada, "Numerical study of natural convection in

partially heated rectangular enclosures filled with nanofluids," *International journal of heat and fluid flow*, vol. 29, no. 5, pp. 1326–1336, 2008.

[8] H.-q. Xie, J.-c. Wang, T.-g. Xi, and Y. Liu, "Thermal conductivity of suspensions containing nanosized sic particles," *International Journal of Thermophysics*, vol. 23, no. 2, pp. 571–580, 2002.

[9] E. J. Shaughnessy, I. M. Katz, and J. P. Schaffer, *Introduction to fluid mechanics*, vol. 8. Oxford University Press, New York, 2005.

[10] X. Wang, X. Xu, and S. U. Choi, "Thermal conductivity of nanoparticle-fluid mixture," *Journal of thermophysics and heat transfer*, vol. 13, no. 4, pp. 474–480, 1999.

[11] M. Eckert, *The dawn of fluid dynamics: a discipline between science and technology*. John Wiley & Sons, Germany, 2007.

[12] M. Meshram and K. Sahu, "Investigation of magneto-hydrodynamic turbulence described by the space–time functional formalism," *Physica Scripta*, vol. 2013, no. T155, p. 014044, 2013.

[13] E. F. Northrup, "Some newly observed manifestations of forces in the interior of an electric conductor," *Physical Review (Series I)*, vol. 24, no. 6, p. 474, 1907.

[14] W. Yu, H. Xie, and L.-H. Liu, "A review on nanofluids: Preparation, stability mechanisms, and applications," *Journal of Nanomaterials*, vol. 2012, no. 711, p. 128, 2011.

[15] A. Dowtherm, "Heat transfer fluid." `http://samyangoil.com/new/catalog/1/2_Dow_Chemical/DOWTHERM_A_en.pdf`, accessed on 2021-03-20.

[16] W. Lipiński, E. Abbasi-Shavazi, J. Chen, J. Coventry, *et al.*, "Progress in heat transfer research for high-temperature solar thermal applications," *Applied Thermal Engineering*, p. 116137, 2020.

[17] V. Poply, "Heat transfer in a mhd nanofluid over a stretching sheet," in *Heat Transfer-Design, Experimentation and Applications*, IntechOpen, London, UK, 2020.

[18] H. Yamaguchi, "Newtonian flow," in *Engineering fluid mechanics*, pp. 279–397, Springer, Dordrecht, 2008.

[19] D. Acheson, *Elementary fluid dynamics: Oxford University Press.* Oxford, England, 1990.

[20] J. Boxall, I. Guymer, and A. Marion, "Transverse mixing in sinuous natural open channel flows," *Journal of Hydraulic Research*, vol. 41, no. 2, pp. 153–165, 2003.

[21] C. K. Batchelor and G. Batchelor, *An introduction to fluid dynamics.* Cambridge university press, United Kingdom, 2000.

[22] R. B. Bird, W. E. Stewart, and E. N. Lightfoot, *Transport phenomena*, vol. 1. John Wiley & Sons, New York, 2006.

[23] V. N. Constantinescu, *Laminar viscous flow.* Springer Science & Business Media, New York, 2012.

[24] R. Chhabra, "Fluid flow, heat, and mass transfer in non-newtonian fluids: multiphase systems," in *Advances in heat transfer*, vol. 23, pp. 187–278, Elsevier, 1993.

[25] Q. Zhao, H. Ma, Y. Liu, C. Yao, L. Yang, and G. Chen, "Hydrodynamics and mass transfer of taylor bubbles flowing in non-newtonian fluids in a microchannel," *Chemical Engineering Science*, vol. 231, p. 116299, 2021.

[26] B. R. Munson, T. H. Okiishi, W. W. Huebsch, and A. P. Rothmayer, *Fluid mechanics*. Wiley, Singapore, 2013.

[27] S. Murshed, K. Leong, and C. Yang, "A combined model for the effective thermal conductivity of nanofluids," *Applied Thermal Engineering*, vol. 29, no. 11-12, pp. 2477–2483, 2009.

[28] W. S. Janna, *Introduction to fluid mechanics*. CRC press, United States, 2020.

[29] N. S. Heshamudin, A. Katende, H. A. Rashid, I. Ismail, F. Sagala, and A. Samsuri, "Experimental investigation of the effect of drill pipe rotation on improving hole cleaning using water-based mud enriched with polypropylene beads in vertical and horizontal wellbores," *Journal of Petroleum Science and Engineering*, vol. 179, pp. 1173–1185, 2019.

[30] R. Sabersky, *Fluid Flow-A first course in fluid mechanics*. The Mac-Millan Company, New York, Printed in the USA, Card No. 64. 12865, 1964.

[31] R. Rajput, *A Textbook of Fluid Mechanics and Hydraulic Machines*. S. Chand Publishing, New Delhi, 2010.

[32] R. P. Chhabra and J. F. Richardson, *Non-Newtonian flow in the process industries: fundamentals and engineering applications*. Butterworth-Heinemann, Oxford, 1999.

[33] A. Ross, S. Wilson, and B. Duffy, "Blade coating of a power-law fluid," *Physics of Fluids*, vol. 11, no. 5, pp. 958–970, 1999.

[34] P. A. Longwell, *Mechanics of fluid flow*. McGraw-Hill, New York, 1966.

[35] G. I. Tardos, "Engineering flow and heat exchange, revised edition by octave levenspiel," *Chemical Engineering Education*, vol. 34, no. 1, pp. 89–89, 2000.

[36] T. Lodge and C. Macosko, "Rheology: Principles, measurements and applications, rheo-optics: Flow birefringence," *Weinheim: VCH Publisher, New York*, 1994.

[37] O. Makinde and T. Chinyoka, "Analysis of unsteady flow of a variable viscosity reactive fluid in a slit with wall suction or injection," *Journal of Petroleum Science and Engineering*, vol. 94, pp. 1–11, 2012.

[38] A. Costa and G. Macedonio, "Viscous heating in fluids with temperature-dependent viscosity: implications for magma flows," *Nonlinear Processes in Geophysics*, vol. 10, no. 6, pp. 545–555, 2003.

[39] H. A. Barnes, J. F. Hutton, and K. Walters, *An introduction to rheology*, vol. 3. Elsevier, Amsterdam, 1989.

[40] A. Ghaly and M. Seddeek, "Chebyshev finite difference method for the effects of chemical reaction, heat and mass transfer on laminar flow along a semi infinite horizontal plate with temperature dependent viscosity," *Chaos, Solitons & Fractals*, vol. 19, no. 1, pp. 61–70, 2004.

[41] T.-C. Yeh, R. Khaleel, and K. C. Carroll, *Flow through heterogeneous geologic media*. Cambridge University Press, United States, 2015.

[42] D. A. Nield and A. Bejan, *Convection in porous media*, vol. 3. Springer-Verlag, New York, 2006.

[43] P. Atkins, *The laws of thermodynamics: A very short introduction*. OUP, Oxford, 2010.

[44] J. A. Schetz and A. E. Fuhs, *Fundamentals of fluid mechanics*. John Wiley & Sons, New Jersey, 1999.

[45] M. I. Khan, S. Afzal, T. Hayat, M. Waqas, and A. Alsaedi, "Activation energy for the carreau-yasuda nanomaterial flow: Analysis of the entropy generation over a porous medium," *Journal of Molecular Liquids*, vol. 297, p. 111905, 2020.

[46] R. K. Shah and A. L. London, *Laminar flow forced convection in ducts: a source book for compact heat exchanger analytical data*. Academic press, United States, 2014.

[47] Ş. Kurt, M. Korkmaz, C. Özcan, T. Dündar, and M. Aktaş, "A new method in non-d destructive testing of wood: Thermal conductivity," *The Online Journal of Science and Technology-July*, vol. 7, no. 3, pp. 1–4, 2017.

[48] Y. A. Cengel and A. Ghajar, "Heat and mass transfer (a practical approach, si version)," *McGraw-670 Hill Education*, vol. 671, p. 52, 2011.

[49] A. Bejan, *Convection heat transfer*. John Wiley & Sons, New Jersey, 2013.

[50] Y. Jaluria, "Natural convection, heat and mass transfer," in *Unknown Host Publication Title*, Pergamon Press, 1980.

[51] S. J. Kim and S. W. Lee, *Air cooling technology for electronic equipment*. CRC press, United States, Florida, 2020.

[52] S. Mohsenian, A. Ramiar, and A. Ranjbar, "Numerical investigation of non-newtonian nanofluid flow in a converging microchannel," *Journal of Mechanical Science and Technology*, vol. 31, no. 1, pp. 385–391, 2017.

[53] K. Prabu, E. Elanchezhian, and S. Suresh, "Mhd combined convection flow of non-newtonian liquid with viscous dissipation and thermophoretic

effects," in *IOP Conference Series: Materials Science and Engineering*, vol. 561, p. 012076, IOP Publishing, 2019.

[54] J. Dunn and K. Rajagopal, "Fluids of differential type: critical review and thermodynamic analysis," *International Journal of Engineering Science*, vol. 33, no. 5, pp. 689–729, 1995.

[55] R. S. Rivlin, G. I. Barenblatt, and D. D. Joseph, *Collected papers of RS Rivlin*, vol. 1. Springer Science & Business Media, New York, 1997.

[56] S. Abbasbandy, T. Hayat, R. Ellahi, and S. Asghar, "Numerical results of a flow in a third grade fluid between two porous walls," *Zeitschrift für Naturforschung A*, vol. 64, no. 1-2, pp. 59–64, 2009.

[57] R. Fosdick and K. Rajagopal, "Thermodynamics and stability of fluids of third grade," *Proceedings of the Royal Society of London. A. Mathematical and Physical Sciences*, vol. 369, no. 1738, pp. 351–377, 1980.

[58] D. D. Schnack, *Lectures in magnetohydrodynamics: with an appendix on extended MHD*, vol. 780. Springer, New York, 2009.

[59] A. A. Opanuga, *Analysis of entropy generation due to magnetohydrodynamic couple stress fluid*. PhD thesis, Covenant University, 2017.

[60] J. Hartmann, *Theory of Laminar Flow of an Electrically Conductive Liquid in a Homogeneous Magnetic Field*. Hg-Dynamics, Munksgaard, Denmark, 1937.

[61] L. Rundora, *Laminar flow in a channel filled with saturated porous media*. PhD thesis, Cape Peninsula University of Technology, 2013.

[62] R. R. Parsodkar, "Magneto hydrodynamic generator," *Journal of Advance Research in Electrical & Electronics Engineering (ISSN: 2208-2395)*, vol. 2, no. 3, pp. 01–07, 2015.

[63] A. Bejan, "Entropy generation minimization: The new thermodynamics of finite-size devices and finite-time processes," *Journal of Applied Physics*, vol. 79, no. 3, pp. 1191–1218, 1996.

[64] A. Chandra and R. Chhabra, "Effect of prandtl number on natural convection heat transfer from a heated semi-circular cylinder," *International Journal of Chemical and Biological Engineering*, vol. 6, pp. 69–75, 2012.

[65] P. Coelho and F. Pinho, "A generalized brinkmann number for non-newtonian duct flows," *Journal of non-newtonian fluid mechanics*, vol. 156, no. 3, pp. 202–206, 2009.

[66] W. Calil, V. Rubio, and J. Inhasz, "Development of a program for the determination of the temperature at transformers copper bus bars by calculating their dimensionless numbers," *Journal of Energy: Energija*, vol. 61, no. 1-4, pp. 139–148, 2012.

[67] H. R. Ashorynejad and A. Zarghami, "Magnetohydrodynamics flow and heat transfer of cu-water nanofluid through a partially porous wavy channel," *International Journal of Heat and Mass Transfer*, vol. 119, pp. 247–258, 2018.

[68] R. L. Earle, *Unit operations in food processing.* Elsevier, United States, 2013.

[69] H. F. Oztop and K. Al-Salem, "A review on entropy generation in natural and mixed convection heat transfer for energy systems," *Renewable and Sustainable Energy Reviews*, vol. 16, no. 1, pp. 911–920, 2012.

[70] R. E. Bellman and R. E. Kalaba, *Quasilineariztion and Nonlinear Boundary-Value Problems*. Elsevier, New York, 1965.

[71] K. Maleknejad and E. Najafi, "Numerical solution of nonlinear volterra integral equations using the idea of quasilinearization," *Communications in Nonlinear Science and Numerical Simulation*, vol. 16, no. 1, pp. 93–100, 2011.

[72] R. Krivec and V. Mandelzweig, "Numerical investigation of quasilinearization method in quantum mechanics," *Computer Physics Communications*, vol. 138, no. 1, pp. 69–79, 2001.

[73] V. Mandelzweig, "Quasilinearization method and its verification on exactly solvable models in quantum mechanics," *Journal of Mathematical Physics*, vol. 40, no. 12, pp. 6266–6291, 1999.

[74] V. Lakshmikantham, "Further improvement of generalized quasilinearization method," *Nonlinear Analysis: Theory, Methods & Applications*, vol. 27, no. 2, pp. 223–227, 1996.

[75] S. Tuffuor and J. W. Labadie, "A nonlinear time variant rainfall-runoff model for augmenting monthly data," *Water Resources Research*, vol. 10, no. 6, pp. 1161–1166, 1974.

[76] S. S. Motsa and P. Sibanda, "On extending the quasilinearization method to higher order convergent hybrid schemes using the spectral homotopy analysis method," *Journal of Applied Mathematics*, vol. 2013, pp. 1–9, 2013.

[77] S. Motsa, V. Magagula, and P. Sibanda, "A bivariate chebyshev spectral collocation quasilinearization method for nonlinear evolution parabolic equations," *The Scientific World Journal*, vol. 2014, pp. 1–13, 2014.

[78] L. N. Trefethen, *Spectral methods in MATLAB*. SIAM, United State, 2000.

[79] K. A. Abro and I. Khan, "Analysis of the heat and mass transfer in the mhd flow of a generalized casson fluid in a porous space via non-integer order derivatives without a singular kernel," *Chinese journal of physics*, vol. 55, no. 4, pp. 1583–1595, 2017.

[80] M. I. Khan, T. Hayat, M. I. Khan, and A. Alsaedi, "A modified homogeneous-heterogeneous reactions for mhd stagnation flow with viscous dissipation and joule heating," *International Journal of Heat and Mass Transfer*, vol. 113, pp. 310–317, 2017.

[81] B. Ramandevi, J. R. Reddy, V. Sugunamma, and N. Sandeep, "Combined influence of viscous dissipation and non-uniform heat source/sink on mhd non-newtonian fluid flow with cattaneo-christov heat flux," *Alexandria Engineering Journal*, vol. 57, no. 2, pp. 1009–1018, 2018.

[82] I. Ullah, S. Shafie, and I. Khan, "Effects of slip condition and newtonian heating on mhd flow of casson fluid over a nonlinearly stretching sheet saturated in a porous medium," *Journal of King Saud University-Science*, vol. 29, no. 2, pp. 250–259, 2017.

[83] M. Alam, M. A. Khatun, M. Rahman, and K. Vajravelu, "Effects of variable fluid properties and thermophoresis on unsteady forced convective boundary layer flow along a permeable stretching/shrinking wedge with variable prandtl and schmidt numbers," *International Journal of Mechanical Sciences*, vol. 105, pp. 191–205, 2016.

[84] S. Mosayebidorcheh, O. Makinde, D. Ganji, and M. A. Chermahini, "Dtm-fdm hybrid approach to unsteady mhd couette flow and heat transfer of

dusty fluid with variable properties," *Thermal Science and Engineering Progress*, vol. 2, pp. 57–63, 2017.

[85] S. Siddiqa, N. Begum, and M. A. Hossain, "Radiation effects from an isothermal vertical wavy cone with variable fluid properties," *Applied Mathematics and Computation*, vol. 289, pp. 149–158, 2016.

[86] T. Latif, N. Alvi, Q. Hussain, and S. Asghar, "Variable properties of mhd third order fluid with peristalsis," *Results in physics*, vol. 6, pp. 963–972, 2016.

[87] M. Rashidi, S. Bagheri, E. Momoniat, and N. Freidoonimehr, "Entropy analysis of convective mhd flow of third grade non-newtonian fluid over a stretching sheet," *Ain Shams Engineering Journal*, vol. 8, no. 1, pp. 77–85, 2017.

[88] M. Imtiaz, A. Alsaedi, A. Shafiq, and T. Hayat, "Impact of chemical reaction on third grade fluid flow with cattaneo-christov heat flux," *Journal of molecular liquids*, vol. 229, pp. 501–507, 2017.

[89] T. Hayat, I. Ullah, B. Ahmed, and A. Alsaedi, "Mhd mixed convection flow of third grade liquid subject to non-linear thermal radiation and convective condition," *Results in physics*, vol. 7, pp. 2804–2811, 2017.

[90] S. O. Adesanya, "Second law analysis for third-grade fluid with variable properties," *Journal of Thermodynamics*, vol. 2014, pp. 1–8, 2014.

[91] S. O. Adesanya and J. Falade, "Thermodynamics analysis of hydromagnetic third grade fluid flow through a channel filled with porous medium," *Alexandria engineering journal*, vol. 54, no. 3, pp. 615–622, 2015.

[92] S. Kareem, S. Adesanya, and U. E. Vincent, "Second law analysis for hydromagnetic couple stress fluid flow through a porous channel," *Alexandria Engineering Journal*, vol. 55, no. 2, pp. 925–931, 2016.

[93] M. A. Mansour, S. E. Ahmed, S. S. Mohamed, *et al.*, "Entropy analysis for unsteady mhd boundary layer flow and heat transfer of casson fluid over a stretching sheet," *Walailak Journal of Science and Technology (WJST)*, vol. 14, no. 2, pp. 169–187, 2017.

[94] P. Davidson, "An introduction to magnetohydrodynamics," *An Introduction to Magnetohydrodynamics*, p. 452, 2001.

[95] I. Liu, "Flow and heat transfer of an electrically conducting fluid of second grade over a stretching sheet subject to a transverse magnetic field," *International Journal of Heat and Mass Transfer*, vol. 47, no. 19-20, pp. 4427–4437, 2004.

[96] K. Prasad, P. Datti, and K. Vajravelu, "Hydromagnetic flow and heat transfer of a non-newtonian power law fluid over a vertical stretching sheet," *International Journal of Heat and Mass Transfer*, vol. 53, no. 5-6, pp. 879–888, 2010.

[97] O. Makinde and T. Chinyoka, "Numerical study of unsteady hydromagnetic generalized couette flow of a reactive third-grade fluid with asymmetric convective cooling," *Computers & Mathematics with Applications*, vol. 61, no. 4, pp. 1167–1179, 2011.

[98] O. D. Makinde, T. Chinyoka, and L. Rundora, "Unsteady flow of a reactive variable viscosity non-newtonian fluid through a porous saturated medium with asymmetric convective boundary conditions," *Computers & Mathematics with Applications*, vol. 62, no. 9, pp. 3343–3352, 2011.

[99] C. Truesdell and W. Noll, *The non-linear field theories of mechanics*. Berlin: Springer, 1965.

[100] K. Rajagopal, *On boundary conditions for fluids of the differential type: NavierStokes Equations and Related Nonlinear Problems*. New York, USA: Plenum Press, 1995.

[101] L. Rundora and O. Makinde, "Effects of suction/injection on unsteady reactive variable viscosity non-newtonian fluid flow in a channel filled with porous medium and convective boundary conditions," *Journal of Petroleum Science and Engineering*, vol. 108, pp. 328–335, 2013.

[102] L. Rundora and O. D. Makinde, "Effects of navier slip on unsteady flow of a reactive variable viscosity non-newtonian fluid through a porous saturated medium with asymmetric convective boundary conditions," *Journal of Hydrodynamics*, vol. 27, no. 6, pp. 934–944, 2015.

[103] T. Chinyoka and O. D. Makinde, "Numerical analysis of the transient and non-isothermal channel flow of a third-grade fluid with convective cooling," *Engineering Transactions*, vol. 68, no. 4, pp. 335–351, 2020.

[104] R. Ellahi and A. Riaz, "Analytical solutions for mhd flow in a third-grade fluid with variable viscosity," *Mathematical and Computer Modelling*, vol. 52, no. 9-10, pp. 1783–1793, 2010.

[105] R. Ellahi, "A study on the convergence of series solution of non-newtonian third grade fluid with variable viscosity: by means of homotopy analysis method," *Advances in Mathematical Physics*, pp. 1–11, 2012.

[106] R. Ellahi, "The thermodynamics, stability, applications and techniques of differential type: a review," *Reviews in Theoretical Science*, vol. 2, no. 2, pp. 116–123, 2014.

[107] A. Akinshilo, "Steady flow and heat transfer analysis of third grade fluid with porous medium and heat generation," *Engineering Science and Technology, an International Journal*, vol. 20, no. 6, pp. 1602–1609, 2017.

[108] H. Branover and Y. Unger, *Metallurgical technologies, energy conversion, and magnetohydrodynamic flows*, vol. 148. Washington, D.C.: American Institute of Aeronautics and Astronautics, 1993.

[109] T. Hayat, S. Shehzad, and A. Alsaedi, "Soret and dufour effects on magnetohydrodynamic (mhd) flow of casson fluid," *Applied Mathematics and Mechanics*, vol. 33, no. 10, pp. 1301–1312, 2012.

[110] A. Idowu and J. Olabode, "Unsteady mhd poiseuille flow between two infinite parallel plates in an inclined magnetic field with heat transfer," *IOSR Journal of Mathematics*, vol. 10, no. 3, pp. 47–53, 2014.

[111] G. Bolarin, A. Yusuf, O. Emmanuel, and Y. Aiyesimi, "Magnetohydrodynamics (mhd) flow of a third grade fluid through a cylindrical pipe in an inclined plane with radiation," *Covenant Journal of Physical and Life Sciences*, vol. 7, no. 1, 2019.

[112] S. Nadeem and S. Hussain, "Analysis of mhd williamson nano fluid flow over a heated surface.," *Journal of Applied Fluid Mechanics*, vol. 9, no. 2, 2016.

[113] G. Reddy, T. Reddy, and S. Varma, "Mhd flow of a newtonian fluid through a porous medium in planer channel," *Global Journal of Pure and Applied Mathematics*, vol. 13, pp. 3811–3832, 2017.

[114] B. Purvis, Y. Mao, and D. Robinson, "Entropy and its application to urban systems," *Entropy*, vol. 21, no. 1, p. 56, 2019.

[115] A. Bejan, "Second law analysis in heat transfer," *Energy*, vol. 5, no. 8-9, pp. 720–732, 1980.

[116] A. Bejan and J. Kestin, "Entropy generation through heat and fluid flow," *JAM*, vol. 50, no. 2, p. 475, 1983.

[117] A. Bejan, "The method of entropy generation minimization," in *Energy and the Environment*, pp. 11–22, Springer, 1999.

[118] G. Ibáñez, "Entropy generation in mhd porous channel with hydrodynamic slip and convective boundary conditions," *International Journal of Heat and Mass Transfer*, vol. 80, pp. 274–280, 2015.

[119] A. Eegunjobi and O. Makinde, "Combined effect of buoyancy force and navier slip on entropy generation in a vertical porous channel," *Entropy*, vol. 14, no. 6, pp. 1028–1044, 2012.

[120] S. Adesanya, S. Kareem, J. Falade, and S. Arekete, "Entropy generation analysis for a reactive couple stress fluid flow through a channel saturated with porous material," *Energy*, vol. 93, pp. 1239–1245, 2015.

[121] T. Hayat, R. Riaz, A. Aziz, and A. Alsaedi, "Analysis of entropy generation for mhd flow of third grade nanofluid over a nonlinear stretching surface embedded in a porous medium," *Physica Scripta*, vol. 94, no. 12, p. 125703, 2019.

[122] M. I. Khan, S. A. Khan, T. Hayat, and A. Alsaedi, "Entropy optimization in magnetohydrodynamic flow of third-grade nanofluid with viscous dissipation and chemical reaction," *Iranian Journal of Science and Technology, Transactions A: Science*, vol. 43, no. 5, pp. 2679–2689, 2019.

[123] O. Makinde and A. Aziz, "Second law analysis for a variable viscosity plane poiseuille flow with asymmetric convective cooling," *Computers & Mathematics with Applications*, vol. 60, no. 11, pp. 3012–3019, 2010.

[124] T. Hayat, S. Shehzad, and S. Asghar, "Mhd flow of thixotropic fluid with variable thermal conductivity and thermal radiation," *Walailak Journal of Science and Technology (WJST)*, vol. 10, no. 1, pp. 29–42, 2013.

[125] L. Woods, *The Thermodynamics of Fluid Systems*. UK: Oxford University Press, 1975.

[126] G. Adomian, *Solving Frontier Problems Decomposition Method*. Berlin: Springer, 1994.

[127] A. Hassan, "Thermodynamics analysis of an internal heat generating fluid of a variable viscosity reactive couette flow," *Journal of King Saud University-Science*, vol. 31, no. 4, pp. 506–510, 2019.

[128] "Mhd couette-poiseuille flow of variable viscosity nanofluids in a rotating permeable channel with hall effects," *Journal of Molecular liquids*, vol. 221, pp. 778–787, 2016.

[129] A. M. Salem, "Variable viscosity and thermal conductivity effects on mhd flow and heat transfer in viscoelastic fluid over a stretching sheet," *Physics letters A*, vol. 369, no. 4, pp. 315–322, 2007.

[130] S. S. Okoya, "Computational study of thermal influence in axial annular flow of a reactive third grade fluid with non-linear viscosity," *Alexandria Engineering Journal*, vol. 58, no. 1, pp. 401–411, 2019.

[131] O. Makinde, "Irreversibility analysis of variable viscosity channel flow with

convective cooling at the walls," *Canadian Journal of Physics*, vol. 86, no. 2, pp. 383–389, 2008.

[132] O. Makinde, "Entropy-generation analysis for variable-viscosity channel flow with non-uniform wall temperature," *Applied Energy*, vol. 85, no. 5, pp. 384–393, 2008.

[133] H. Mondal, S. Mishra, P. K. Kundu, and P. Sibanda, "Entropy generation of variable viscosity and thermal radiation on magneto nanofluid flow with dusty fluid," *Journal of Applied and Computational Mechanics*, vol. 6, no. 1, pp. 171–182, 2020.

[134] M. Matthews and J. Hill, "Newtonian flow with nonlinear navier boundary condition," *Acta Mechanica*, vol. 191, no. 3, pp. 195–217, 2007.

[135] Y. Zhu and S. Granick, "Rate-dependent slip of newtonian liquid at smooth surfaces," *Physical review letters*, vol. 87, no. 9, p. 096105, 2001.

[136] L. Rundora and O. D. Makinde, "Unsteady mhd flow of non-newtonian fluid in a channel filled with a saturated porous medium with asymmetric navier slip and convective heating," vol. 12, no. 3, pp. 483–493, 2018.

[137] S. Das, R. Jana, and A. Chamkha, "Entropy generation in an unsteady mhd channel flow with navier slip and asymmetric convective cooling," *International Journal of Industrial Mathematics*, vol. 9, no. 2, pp. 149–160, 2017.

[138] S. O. Salawu and E. O. Fatunmbi, "Inherent irreversibility of hydromagnetic third-grade reactive poiseuille flow of a variable viscosity in porous media with convective cooling," *Journal of the Serbian Society for Computational Mechanics*, vol. 11, no. 1, pp. 46–58, 2017.

[139] S. O. Adesanya, J. Falade, J. Ukaegbu, and O. D. Makinde, "Adomian-hermite-pade approximation approach to thermal criticality for a reactive third grade fluid flow through porous medium," *Theoretical and Applied Mechanics*, vol. 43, no. 1, pp. 133–144, 2016.

[140] Frank-Kamenetskii and D. Al'bertovich, *Diffusion and heat transfer in chemical kinetics*. New York: Plenum Press, 1969.

[141] O. D. Makinde, "Thermal stability of a reactive viscous flow through a porous-saturated channel with convective boundary conditions," *Applied Thermal Engineering*, vol. 29, no. 8-9, pp. 1773–1777, 2009.

[142] M. VeeraKrishna and G. S. Reddy, "Unsteady mhd reactive flow of second grade fluid through porous medium in a rotating parallel plate channel," *The Journal of Analysis*, vol. 27, no. 1, pp. 103–120, 2019.

[143] S. Reza-E-Rabbi, S. Arifuzzaman, T. Sarkar, M. S. Khan, and S. F. Ahmmed, "Explicit finite difference analysis of an unsteady mhd flow of a chemically reacting casson fluid past a stretching sheet with brownian motion and thermophoresis effects," *Journal of King Saud University-Science*, vol. 32, no. 1, pp. 690–701, 2020.

[144] M. Das, G. Mahanta, S. Shaw, and S. Parida, "Unsteady mhd chemically reactive double-diffusive casson fluid past a flat plate in porous medium with heat and mass transfer," *Heat TransferAsian Research*, vol. 48, no. 5, pp. 1761–1777, 2019.

[145] S. Das, S. Sarkar, and R. Jana, "Assessment of irreversible losses of non-newtonian nanofluid flow underlying hall current, chemical reaction and thermal radiation," *World Journal of Engineering*, 2020.

[146] A. Hassan, R. Maritz, and J. Gbadeyan, "A reactive hydromagnetic heat generating fluid flow with thermal radiation within porous channel with symmetrical convective cooling," *International Journal of Thermal Sciences*, vol. 122, pp. 248–256, 2017.

[147] S. O. Adesanya, "Thermal stability analysis of reactive hydromagnetic third-grade fluid through a channel with convective cooling," *Journal of the Nigerian Mathematical Society*, vol. 32, no. 1-3, pp. 61–72, 2013.

[148] P. Vyas and N. Srivastava, "Entropy analysis of generalized mhd couette flow inside a composite duct with asymmetric convective cooling," *Arabian Journal for Science and Engineering*, vol. 40, no. 2, pp. 603–614, 2015.

[149] A. Bejan, "Notes on the history of the method of entropy generation minimization (finite time thermodynamics)," *Journal of Non Equilibrium Thermodynamics*, vol. 21, no. 3, pp. 239–242, 1996.

[150] S. O. Adesanya and O. D. Makinde, "Irreversibility analysis in a couple stress film flow along an inclined heated plate with adiabatic free surface," *Physica A: Statistical Mechanics and its Applications*, vol. 432, pp. 222–229, 2015.

[151] A. Eegunjobi, O. Makinde, M. Tshehla, and O. Franks, "Irreversibility analysis of unsteady couette flow with variable viscosity," *Journal of Hydrodynamics*, vol. 27, no. 2, pp. 304–310, 2015.

[152] J. A. Gbadeyan and A. A. Opanuga, "Inherent irreversibility analysis in a buoyancy induced magnetohydrodynamic couple stress fluid," *Journal of Mathematics and Computer Science*, vol. 18, pp. 411–422, 2018.

[153] R. Kareem, S. Salawu, and Y. Yan, "Analysis of transient rivlin-ericksen

fluid and irreversibility of exothermic reactive hydromagnetic variable viscosity," *J. Appl. Comput. Mech.*, vol. 6, no. 1, pp. 26–36, 2020.

[154] R. Ellahi, S. Z. Alamri, A. Basit, and A. Majeed, "Effects of mhd and slip on heat transfer boundary layer flow over a moving plate based on specific entropy generation," *Journal of Taibah University for Science*, vol. 12, no. 4, pp. 476–482, 2018.

[155] M. Almakki, H. Mondal, and P. Sibanda, "Entropy generation in magneto nanofluid flow with joule heating and thermal radiation," *World Journal of Engineering*, vol. 17, no. 1, pp. 1–11, 2020.

[156] M. Nayak, A. A. Hakeem, B. Ganga, M. I. Khan, M. Waqas, and O. D. Makinde, "Entropy optimized mhd 3d nanomaterial of non-newtonian fluid: a combined approach to good absorber of solar energy and intensification of heat transport," *Computer methods and programs in biomedicine*, vol. 186, p. 105131, 2020.

[157] N. Shukla, P. Rana, and O. A. Bég, "Unsteady mhd non-newtonian heat transfer nanofluids with entropy generation analysis," *Nonlinear Engineering*, vol. 8, no. 1, pp. 630–644, 2019.

[158] G. Ibáñez, A. López, I. López, J. Pantoja, J. Moreira, and O. Lastres, "Optimization of mhd nanofluid flow in a vertical microchannel with a porous medium, nonlinear radiation heat flux, slip flow and convective–radiative boundary conditions," *Journal of Thermal Analysis and Calorimetry*, vol. 135, no. 6, pp. 3401–3420, 2019.

[159] F. Yue, P. Li, and C. Zhao, "Numerical investigation of thermally developing non-darcy forced convection in a porous circular duct with asymmetric

entrance temperature under ltne condition," *Transport in Porous Media*, vol. 136, no. 2, pp. 639–655, 2021.

[160] M. VeeraKrishna, G. Subba Reddy, and A. Chamkha, "Hall effects on unsteady mhd oscillatory free convective flow of second grade fluid through porous medium between two vertical plates," *Physics of Fluids*, vol. 30, no. 2, p. 023106, 2018.

[161] S. Ahmad, M. Farooq, A. Anjum, and N. A. Mir, "Squeezing flow of convectively heated fluid in porous medium with binary chemical reaction and activation energy," *Advances in Mechanical Engineering*, vol. 11, no. 10, p. 1687814019883774, 2019.

[162] A. R. Hassan and R. Maritz, "The analysis of a reactive hydromagnetic fluid flow in a channel through porous medium with convective cooling," *UPB Sci. Bull. Series D*, vol. 78, no. 4, pp. 43–56, 2016.

[163] L. Rundora and O. Makinde, "Analysis of unsteady mhd reactive flow of non-newtonian fluid through a porous saturated medium with asymmetric boundary conditions," *Iranian Journal of Science and Technology, Transactions of Mechanical Engineering*, vol. 40, no. 3, pp. 189–201, 2016.

[164] T. Chinyoka, "Computational dynamics of a thermally decomposable viscoelastic lubricant under shear," *Journal of Fluids Engineering*, vol. 130, no. 12, pp. 1–7, 2008.

[165] T. Chinyoka, "Poiseuille flow of reactive phan–thien–tanner liquids in 1d channel flow," *Journal of Heat Transfer*, vol. 132, no. 11, pp. 1–7, 2010.

[166] T. Chinyoka, "Suction-injection control of shear banding in non-isothermal and exothermic channel flow of johnson-segalman liquids," *Journal of fluids engineering*, vol. 133, no. 7, pp. 1–12, 2011.